M 2023

U.PORTO
FEUP FACULDADE DE ENGENHARIA
UNIVERSIDADE DO PORTO

EXTRACTION OF ANTIOXIDANTS FOR FOOD SUPPLEMENTATION USING AQUEOUS TWO-PHASE SYSTEMS WITH LOW ENVIRONMENTAL IMPACT

ANA CATARINA SANTOS REBELO

MASTER THESIS IN CHEMICAL ENGINEERING
PRESENTED TO THE FACULTY OF ENGINEERING
OF THE UNIVERSITY OF PORTO

Master in Chemical Engineering

Extraction of Antioxidants for Food Supplementation Using Aqueous Two-Phase Systems with Low Environmental Impact

Master's dissertation of

Ana Catarina Santos Rebelo

Developed within the course of Dissertation (M.EQ013) and held at:



Supervisor at FEUP: **Prof. Maria Eugénia Macedo**



July 2023

Acknowledgments

First, I would like to express my gratitude to my supervisor, Professor Maria Eugénia Macedo, for the high-level scientific knowledge transmitted, for offering invaluable advice, and for the opportunity to be part of this project.

I would also like to express my deep gratitude to Pedro Velho for his support, mentoring and companionship throughout this project. His guidance and encouragement, along with the moments of shared laughter, played a crucial role in the successful completion of this dissertation. Thank you for welcoming me so helpfully at the laboratory, teaching me so much and for being available regardless of time or day. Thank you also to Leonor Barroca for her support and care. Her assistance has been immensely helpful, and I am thankful for all that she has done.

To my friends, I am truly grateful for their support throughout this entire journey. Thank you for listening, offering valuable advice, and providing help whenever I needed it. Your presence has made a significant difference in my life.

To my family, thank you for encouraging me in all of my pursuits and inspiring me to follow my dreams. I am especially grateful to my parents, who supported me emotionally and financially. Their countless sacrifices, unconditional love, support and continuous encouragement throughout my life have led me to where I am now. This accomplishment would not have been possible without them.

Also, I would like to deeply thank all of those who contributed directly or indirectly to the completion of my dissertation and have helped me overcome the challenges in the past five years.

Lastly, I thank the financial support from Project FEUP_2SMART_BILic_THERMO2, Project 2SMART – engineered Smart materials for Smart citizens (NORTE-01-0145-FEDER-000054), supported by Norte Portugal Regional Operational Programme (NORTE 2020), under the PORTUGAL 2020 Partnership Agreement, through the European Regional Development Fund (ERDF).



Abstract

Antioxidant-rich food supplements can effectively address widespread nutritional deficiencies in the human diet and simultaneously reduce the concentration of reactive oxygen species (ROS) due to the free radical scavenging activity of antioxidants, minimizing inflammation and oxidative stress.

Resveratrol (RVT), ferulic acid (FA), and gallic acid (GA) are very important antioxidants, which can be extracted from food industry by-products such as grape skins, sweet corn residues and gallnuts, contributing to a more circular economy and reducing the environmental impact of extraction processes. In this project, these phenolic compounds were successfully extracted in the Aqueous Two-Phase Systems (ATPS) {ethyl lactate (1) + Na_3Citrate or K_3Citrate or Na_2Succinate or NaKTartrate (2) + water (3)} at 298.15 K and 0.1 MPa, which provide biocompatible and sustainable extractive media.

Generally, the studied ATPS yielded partition coefficients (K) greater than one, indicating a preference for the top phase (rich in ethyl lactate), which suggests successful extraction of these phenolic compounds. Larger tie-lines generally resulted in higher K and extraction efficiency (E) values, favoring migration to the top phase. The most promising results were obtained for resveratrol, which attained maximum partition coefficients (K) of 40 ± 6 and 41 ± 9 and extraction efficiencies (E) of (98 ± 1) % and (95.0 ± 0.6) % for the longest tie-lines (77.66 and $70.73\ m\%$) in {ethyl lactate (1) + K_3Citrate (2) + water (3)} and {ethyl lactate (1) + NaKTartrate (2) + water (3)}, respectively. Additionally, the effect of pH on the UV-Vis absorbance spectra was studied for all the species to minimize errors in solute quantification, resulting in low antioxidant mass losses (< 5 %). However, the low ultraviolet-visible (UV-Vis) absorbance values of resveratrol indicated the need for an alternative analytical method, such as High-Performance Liquid Chromatography. All the studied antioxidants were found to be mostly stable at the used extractive conditions.

Moreover, a successful liquid-liquid equilibrium study was performed in the novel ATPS {polyvinylpyrrolidone (1) + NaKTartrate (2) + water (3)}, at 298.15 K and 0.1 MPa in order to assess the efficiency of this medium for the extraction of different antioxidants. The solubility curve of the ATPS was determined and fitted to the Merchuk equation, which demonstrated excellent agreement with the experimental data, indicating a significant potential working area for separation. Tie-lines, tie-line lengths (TLL), and their slopes (STL) were also determined, revealing that higher concentrations of polyvinylpyrrolidone in the feed mixtures resulted in increased TLL values and phase separation.

Lastly, the tie-line compositions were effectively described using the electrolyte non-random two-liquid (e-NRTL) model, combining the NRTL model, which accounted for short-range interactions (involving neutral molecules), with the Pitzer-Debye-Hückel (PDH) equation (for long-range interactions caused by charged species). This model was applied for the first time in the research group to a system composed of three ions and it accurately predicted the behavior of the ATPS and provided good agreement with the experimental data.

Keywords: Food supplements; Antioxidants; ATPS; Modeling; e-NRTL.

Resumo

Suplementos alimentares ricos em antioxidantes são uma ferramenta eficaz no combate de deficiências nutricionais na dieta humana e, simultaneamente, possuem a capacidade de neutralizar radicais livres, minimizando a inflamação e o *stress* oxidativo.

O resveratrol (RVT), o ácido ferúlico (FA) e o ácido gálico (GA) são antioxidantes importantes que podem ser extraídos de subprodutos da indústria alimentar, como cascas de uva, resíduos de milho doce e galhas (bugalhos), contribuindo para uma economia mais circular. Neste projeto, estes compostos fenólicos foram extraídos com sucesso em diferentes sistemas aquosos bifásicos (SAB) {lactato de etilo (1) + Na_3Citrato ou K_3Citrato ou Na_2Succinato ou NaKTartrato (2) + água (3)} a 298,15 K e 0,1 MPa, que proporcionam um meio extrativo biocompatível e sustentável.

Em geral, os SAB estudados apresentaram coeficientes de partição (*K*) superiores a 1, indicando uma preferência pela fase superior (rica em lactato de etilo), o que sugere uma extração bem-sucedida destes compostos fenólicos. Linhas de equilíbrio mais longas resultaram em valores de *K* mais elevados, bem como em eficiências de extração (*E)* superiores, favorecendo a migração para a fase de topo. O resveratrol obteve os resultados mais promissores, com coeficientes de partição de 40 ± 6 e 41 ± 9 e eficiências de extração de 98 ± 1 e $95{,}0 \pm 0{,}6$ para as linhas de equilíbrio mais longas ($77{,}66$ e $70{,}73\ m\%$) nos sistemas com K_3Citrato e NaKTartrato, respetivamente. Além disso, o efeito do pH nos espetros de absorvância ultravioleta-visível (UV-Vis) foi estudado para todos os antioxidantes, a fim de minimizar erros na quantificação dos solutos. Os antioxidantes mostraram-se geralmente estáveis nas condições de extração utilizadas, resultando em baixas perdas de massa na quantificação (< 5 %). No entanto, os baixos valores de absorvância UV-Vis do resveratrol indicaram a necessidade de recorrer a um método analítico alternativo, como a Cromatografia Líquida de Alta Eficiência.

Além disso, determinou-se, com sucesso, o equilíbrio líquido-líquido do SAB {polivinilpirrolidona (1) + NaKTartrato (2) + água (3)} a 298,15 K e 0,1 MPa, apresentando resultados promissores para a eficiente extração de diferentes antioxidantes. A curva de solubilidade deste SAB foi determinada pelo método de *cloud-point* e ajustada pela equação de Merchuk, apresentando excelente concordância com os dados experimentais e indicando uma significativa área de trabalho para potenciais extrações. As linhas de equilíbrio também foram estudadas, revelando que maiores concentrações de polivinilpirrolidona na mistura inicial resultaram em maior comprimento das linhas de equilíbrio e mais distinta composição de fases.

Por fim, os sistemas ternários estudados foram descritos de forma satisfatória pelo modelo e-NRTL (*electrolyte non-random two-liquid*). Este modelo combina o modelo NRTL, que tem em consideração as interações de curto alcance (que envolvem moléculas neutras), com a equação de Pitzer-Debye-Hückel (PDH), para interações de longo alcance (causadas por espécies carregadas). Este modelo foi aplicado pela primeira vez no grupo de investigação a um SAB com um sal composto por três iões, apresentando uma ótima concordância com os dados experimentais.

Palavras-chave: Suplementos alimentares; Antioxidantes; SAB; Modelação; e-NRTL.

Declaration

I hereby declare under word of honor that this work is original and that all non-original contributions were properly referenced with source identification.

Ana Catarina Santos Rebelo

3rd July 2023

Index

1 Introduction 1

1.1 Problem statement 1

1.2 LSRE-LCM and ALiCE 2

1.3 Author's contribution 3

1.4 Document's structure 3

2 State of the art 5

2.1 Extraction of antioxidants 5

2.2 Aqueous Two-Phase Systems 7

2.3 Thermodynamic models 8

2.3.1 Non-Random Two-Liquid model 9

2.3.2 Electrolyte-Non-Random Two-Liquid model 10

2.4 Bondi method 13

3 Materials and methods 15

3.1 Materials 15

3.2 Apparatus 16

3.3 Methods 16

3.3.1 Solubility curve 16

3.3.2 Tie-lines 17

3.3.3 pH study 20

3.3.4 UV-Vis absorbance calibration curves 22

3.3.5 Liquid-liquid extraction 22

3.3.6 Thermodynamic modeling 24

4 Results and discussion 26

4.1.1 Liquid-liquid equilibria 26

4.1.2 pH study 30

4.1.3 Calibration curves 33

4.1.4 Liquid-liquid extraction 35

4.1.5 Thermodynamic modeling 40

5 Conclusion 42

6 Project assessment 44

6.1 Degree of completion 44

6.2 Additional work 44

6.3 Future work 45

6.4 Final assessment 45

7 References 46

Annex A - Physicochemical properties 52

Annex B - Liquid-liquid equilibria 54

Annex C - Pure compound parameters 55

Appendix A. Experimental apparatus 56

Appendix B. Liquid-liquid equilibria 58

Appendix C. pH study 63

Appendix D. Calibration curves 72

Appendix E. Extraction of antioxidants 74

Appendix F. Thermodynamic modeling 87

References 95

List of Figures

Fig. 1 *- Possible feedstocks for the extraction of ferulic acid, gallic acid and resveratrol. 6*

Fig. 2 *- Procedure taken for the cloud-point titration method. 17*

Fig. 3 *- Solubility curve and homogeneous zone feed compositions for {PVP (1) + NaKTartrate (2) + Water (3)} at 298.15 K and 0.1 MPa. 18*

Fig. 4 *- Scheme of the procedure of the pH stability study. 21*

Fig. 5 *- Procedure of the liquid-liquid extraction of antioxidants. 24*

Fig. 6 *– Algorithm for the optimization of τ_{ij} and x_{ij} using the e-NRTL model. 25*

Fig. 7 *– Representation of the polynomial expressions for density (a) and conductivity (b) as function of composition for {PVP (1) + NaKTartrate (2) + Water (3)} at 298.15 K and 0.1 MPa. 28*

Fig. 8 *- Solubility curve and corresponding tie-lines for the ternary system {PVP (1) + NakTartrate (2) + water (3)} at 298.15 K and 0.1 MPa. 29*

Fig. 9 *- Calculated mean electrical charge (q) for resveratrol (triangles), ferulic acid (squares) and gallic acid (circles), expressed in terms of the elementary charge (e). 31*

Fig. 10 *- Influence of pH on the UV-Vis absorbance spectra of resveratrol at 298.15 K and 0.1 MPa (left). Study of UV-Vis absorbance spectra stability for resveratrol in the moment of preparation and after 3 days of settling for the pH of the ATPS (~ 6.5-7.5) at 298.15 K and 0.1 MPa (right). 31*

Fig. 11 *- Influence of pH on the UV-Vis absorbance spectra of ferulic acid at 298.15 K and 0.1 MPa (left). Study of UV-Vis absorbance spectra stability for ferulic acid in the moment of preparation and after 3 days of settling for the pH of the ATPS (~ 6.5-7.5) at 298.15 K and 0.1 MPa (right). 32*

Fig. 12 *- Influence of pH on the UV-Vis absorbance spectra of gallic acid at 298.15 K and 0.1 MPa (left). Study of UV-Vis absorbance spectra stability for gallic acid in the moment of preparation and after 3 days of settling for the pH of the ATPS (~ 6.5-7.5) at 298.15 K and 0.1 MPa (right). 33*

Fig. 13 *- UV-Vis absorbance calibration curves for ferulic acid, gallic acid and resveratrol at pH ~ 7, 298.15 K and 0.1 MPa. 34*

Fig. 14 *- Chemical structures of the three studied antioxidants – resveratrol (a), ferulic acid (b) and gallic acid (c) – at the pH of the system (pH ~ 7). 36*

Fig. 15 *- Relation between the tie-line lengths (TLL) and the natural logarithms of the experimental partition coefficients (K) (left) and extraction efficiencies (E) (right) for resveratrol (RVT) in the ATPS containing ethyl lactate, water and salts (K_3Citrate, Na_3Citrate, Na_2Succinate and NaKTartrate) at 298.15 K and 0.1 MPa. 36*

Fig. 16 *- Relation between the tie-line lengths (TLL) and the natural logarithms of the experimental partition coefficients (K) (left) and extraction efficiencies (E) (right) for ferulic acid (FA) in the ATPS*

containing ethyl lactate, water and salts (K_3Citrate, Na_3Citrate, Na_2Succinate and NaKTartrate) at 298.15 K and 0.1 MPa. 37

***Fig. 17** – Chemical structure of the salts K_3Citrate (a), Na_3Citrate (b), Na_2Succinate (c) and NaKTartrate (d). 39*

***Fig. 18** - Relation between the tie-line lengths (TLL) and the natural logarithms of the experimental partition coefficients (K) (left) and extraction efficiencies (E) (right) for gallic acid (GA) in the ATPS containing ethyl lactate, water and salts (K_3Citrate, Na_3Citrate, Na_2Succinate or NaKTartrate) at 298.15 K and 0.1 MPa. 38*

***Fig. 19** - Effect of the tie-line compositions in the calculated stage fractions of the antioxidant stages of ferulic acid (FA) in the ATPS containing ethyl lactate, water and different salts (K_3Citrate, Na_3Citrate, Na_2Succinate and NaKTartrate) at 298.15 K and 0.1 MPa. 40*

***Fig. 20** - Effect of the tie-line compositions in the calculated stage fractions of the antioxidant stages of gallic acid (GA) in the ATPS containing ethyl lactate, water and different salts (K_3Citrate, Na_3Citrate, Na_2Succinate and NaKTartrate) at 298.15 K and 0.1 MPa. 40*

***Fig. 21** - Comparison of predicted and experimental liquid-liquid equilibrium data of ATPS containing ethyl lactate, water and different salts (a) K_3Citrate, (b) Na_3Citrate, (c) Na_2Succinate and (d) NaKTartrate at 298.15 K and 0.1 MPa. 41*

***Fig. A.1** – Stock solutions of gallic acid at different pH values in the moment of preparation (left) and after 3 days of settling (right). 56*

***Fig. A.2** - Stock solutions of resveratrol at different pH values in the moment of preparation (left) and after 3 days of settling (right). 56*

***Fig. A.3** – Blanks and partition of ferulic acid (FA) for ATPS {EL (1) + NaKTartrate (2) + Water (3)} while stirring (left) and after settling for one minute (right). 57*

***Fig. B.1** – Cloud-point data and solubility curve fitting data according to Han's equation[91]. 58*

***Fig. B.2** - Cloud-point data and solubility curve fitting data according to Merchuk's equation[92]. 58*

***Fig. B.3** - Cloud-point data and solubility curve fitting data according to Hu's equation[93]. 59*

***Fig. B.4** - Cloud-point data and solubility curve fitting data according to Jayapal's equation[94]. 59*

***Fig. C.1** - Study of UV-Vis absorbance spectra stability for resveratrol in the moment of preparation and after 3 days of settling for pH = 9.3 at 298.15 K and 0.1 MPa. 63*

***Fig. C.2** - Study of UV-Vis absorbance spectra stability for resveratrol in the moment of preparation and after 3 days of settling for pH = 10.0 at 298.15 K and 0.1 MPa. 63*

***Fig. C.3** - Study of UV-Vis absorbance spectra stability for resveratrol in the moment of preparation and after 3 days of settling for pH = 10.9 at 298.15 K and 0.1 MPa. 64*

***Fig. C.4** - Study of UV-Vis absorbance spectra stability for resveratrol in the moment of preparation and after 3 days of settling for pH = 4.3 at 298.15 K and 0.1 MPa. 64*

Fig. C.5 *- Study of UV-Vis absorbance spectra stability for ferulic acid in the moment of preparation and after 3 days of settling for pH = 3.0 at 298.15 K and 0.1 MPa..... 65*

Fig. C.6 *- Study of UV-Vis absorbance spectra stability for ferulic acid in the moment of preparation and after 3 days of settling for pH = 4.1 at 298.15 K and 0.1 MPa..... 65*

Fig. C.7 *- Study of UV-Vis absorbance spectra stability for ferulic acid in the moment of preparation and after 3 days of settling for pH = 10.6 at 298.15 K and 0.1 MPa. 66*

Fig. C.8 *- Study of UV-Vis absorbance spectra stability for ferulic acid in the moment of preparation and after 3 days of settling for pH = 12.2 at 298.15 K and 0.1 MPa. 66*

Fig. C.9 *- Study of UV-Vis absorbance spectra stability for gallic acid in the moment of preparation and after 3 days of settling for pH = 3.6 at 298.15 K and 0.1 MPa..... 67*

Fig. C.10 *- Study of UV-Vis absorbance spectra stability for gallic acid in the moment of preparation and after 3 days of settling for pH = 4.8 at 298.15 K and 0.1 MPa..... 67*

Fig. C.11 *- Study of UV-Vis absorbance spectra stability for gallic acid in the moment of preparation and after 3 days of settling for pH = 10.5 at 298.15 K and 0.1 MPa. 68*

Fig. C.12 *- Study of UV-Vis absorbance spectra stability for gallic acid in the moment of preparation and after 3 days of settling for pH = 12.5 at 298.15 K and 0.1 MPa. 68*

Fig. E.1. *- Relation between the natural logarithms of the experimental partition coefficients (K) and the tie-line lengths (TLL) for ferulic acid (FA), gallic acid (GA) and resveratrol (RVT) in the ATPS {ethyl lactate (1) + K_3Citrate (2) + water (3)} at 298.15 K and 0.1 MPa..... 74*

Fig. E.2 *- Relation between the natural logarithms of the experimental partition coefficients (K) and the tie-line lengths (TLL) for ferulic acid (FA), gallic acid (GA) and resveratrol (RVT) in the ATPS {ethyl lactate (1) + Na_3Citrate (2) + water (3)} at 298.15 K and 0.1 MPa. 74*

Fig. E.3 *- Relation between the natural logarithms of the experimental partition coefficients (K) and the tie-line lengths (TLL) for ferulic acid (FA), gallic acid (GA) and resveratrol (RVT) in the ATPS {ethyl lactate (1) + Na_2Succinate (2) + water (3)} at 298.15 K and 0.1 MPa. 75*

Fig. E.4 *- Relation between the natural logarithms of the experimental partition coefficients (K) and the tie-line lengths (TLL) for ferulic acid (FA), gallic acid (GA) and resveratrol (RVT) in the ATPS {ethyl lactate (1) + NaKTartrate (2) + water (3)} at 298.15 K and 0.1 MPa..... 75*

Fig. E.5 *- Relation between the extraction efficiencies (E) and the tie-line lengths (TLL) for ferulic acid (FA) gallic acid (GA) and resveratrol (RVT) in the ATPS {ethyl lactate (1) + K_3Citrate (2) and water (3)} at 298.15 K and 0.1 MPa. 76*

Fig. E.6 *- Relation between the extraction efficiencies (E) and the tie-line lengths (TLL) for ferulic acid (FA) gallic acid (GA) and resveratrol (RVT) in the ATPS {ethyl lactate (1) + Na_3Citrate (2) and water (3)} at 298.15 K and 0.1 MPa. 76*

Fig. E.7 *- Relation between the extraction efficiencies (E) and the tie-line lengths (TLL) for ferulic acid (FA) gallic acid (GA) and resveratrol (RVT) in the ATPS {ethyl lactate (1) + Na_2Succinate (2) and water (3)} at 298.15 K and 0.1 MPa. 77*

Fig. E.8 *- Relation between the extraction efficiencies (E) and the tie-line lengths (TLL) for ferulic acid (FA), gallic acid (GA) and resveratrol (RVT) in the ATPS {ethyl lactate (1) + NaKTartrate (2) and water (3)} at 298.15 K and 0.1 MPa. 77*

Fig. E.9 *- Effect of the tie-line compositions in the calculated stage fractions of the antioxidant stages of resveratrol (RVT) in the ATPS containing ethyl lactate, water and different salts (K_3Citrate, Na_3Citrate, Na_2Succinate and NaKTartrate) at 298.15 K and 0.1 MPa. 78*

List of Tables

Table 1 *- List of chemicals used and their respective suppliers, purities, CAS numbers and abbreviations. 15*

Table 2 - *Values of* pK_a *of the studied antioxidants: gallic acid, ferulic acid and resveratrol. 20*

Table 3 - *Solubility curve data for the ternary systems {PVP (1) + NaKTartrate (2) + Water (3)} determined experimentally at 298.15 K and 0.1 MPa. 26*

Table 4 - *Fitting parameters obtained with equations proposed by Han et al.[91], Merchuk et al.[92], Hu et al.[93] and Jayapal et al.[94] and standard deviation for the experimental solubility curves data..... 27*

Table 5 - *Polynomial expressions for density and conductivity as function of the composition for {PVP (1) + NaKTartrate (2) + Water (3)} at 298.15 K and 0.1 MPa..... 27*

Table 6 - *Tie-line equilibria data in the top and bottom phases for the ternary system {PVP (1) + NaKTartrate (2) + Water (3)} at 298.15 K and 0.1 MPa..... 28*

Table 7 - *Parameters obtained using Othmer-Tobias[96] and Brancroft[97] equations with the respective correlation coefficients. 29*

Table 8 - *Stability of the UV-Vis absorbance spectra of ferulic acid (FA), gallic acid (GA) and resveratrol (RVT) after settling for 3 days at 298.15 K and 0.1 MPa. 33*

Table 9 - *Calibration curves data for the studied antioxidants resveratrol, ferulic acid and gallic acid determined at 298.15 K and 0.1 MPa. 34*

Table AA.1 *- Physicochemical properties of the compounds used in the liquid-liquid equilibria study and in the extraction of antioxidants. 52*

Table BB.1 *- Liquid-liquid equilibria data for the ternary systems containing ethyl lactate, water and different salts ($Na_3Citrate$[89], $K_3Citrate$[89], NaKTartrate[18], $Na_2Succinate$[62]), at 298.15 K and 0.1 MPa. .. 54*

Table CC.1 *- Molar density, molecular mass and dielectric constants of the solvents, ethyl lactate (EL) and water (H_2O) of the ATPS with different salts ($K_3Citrate$, $Na_3Citrate$, $Na_2Succinate$ and NaKTartrate). 55*

Table CC.2 *- Molecular mass, charge, radius, van de Waals radius and volume of the sodium and potassium ions. 55*

Table CC.3 *- Molecular mass and charge of ions present in the studied with different salts ($K_3Citrate$, $Na_3Citrate$, $Na_2Succinate$ and NaKTartrate). 55*

Table B.1 *- Cloud-point compositions for the ATPS {PVP (1) + NaKTartrate (2) + Water (3)} and calculated PVP mass fraction using fitting equations Han[91], Merchuk[92], Hu[93] and Jayapal[94]..... 60*

Table B.2 *- Density and conductivity obtained experimentally and calculated through the fitting equation for different compositions of salt and PVP in the homogeneous zone for the ATPS {PVP (1) + NaKTartrate (2) + Water (3)}. 61*

Table B.3 *– F-test results for the isolines of two physical properties – density and conductivity..... 62*

Table C.1 *– Calculated stage fraction of each antioxidant and mean electrical charge (q) at different pH values for gallic acid (GA). 69*

Table C.2 *- Calculated stage fraction of each antioxidant and mean electrical charge (q) at different pH values for ferulic acid (FA). 70*

Table C.3 - *Calculated stage fraction of each antioxidant and mean electrical charge (q) at different pH values for resveratrol (RVT)..... 71*

Table D.1 *- Parameters of validation of the calibration curve for gallic acid. 72*

Table D.2 *– Parameters of validation of the calibration curve for ferulic acid..... 72*

Table D.3 *- Parameters of validation of the calibration curve for resveratrol. 73*

Table D.4 *– Parameters of the calibration curves for ferulic acid, gallic acid and resveratrol..... 73*

Table E.1 *- Experimental phase mass, antioxidant mass losses, antioxidant concentration, phase density and phase pH for the top and bottom phases in the extraction of gallic acid, ferulic acid and resveratrol in the ATPS {ethyl lactate (1) + trisodium citrate (2) + water (3)} at 298.15 K and 0.1 MPa. 79*

Table E.2 *- Experimental phase mass, antioxidant mass losses, antioxidant concentration, phase density and phase pH for the top and bottom phases in the extraction of gallic acid, ferulic acid and resveratrol in the ATPS {ethyl lactate (1) + tripotassium citrate (2) + water (3)} at 298.15 K and 0.1 MPa. 80*

Table E.3 *- Experimental phase mass, antioxidant mass losses, antioxidant concentration, phase density and phase pH for the top and bottom phases in the extraction of gallic acid, ferulic acid and resveratrol in the ATPS {ethyl lactate (1) + disodium succinate (2) + water (3)} at 298.15 K and 0.1 MPa. 81*

Table E.4 *- Experimental phase mass, antioxidant mass losses, antioxidant concentration, phase density and phase pH for the top and bottom phases in the extraction of gallic acid, ferulic acid and resveratrol in the ATPS {ethyl lactate (1) + sodium potassium tartrate (2) + water (3)} at 298.15 K and 0.1 MPa. 82*

Table E.5 *- Calculated solute losses, extraction efficiency (E) intervals, partition coefficients (K) and literature-based tie-line lengths (TLL) for the extraction of gallic acid, ferulic acid and resveratrol in the ATPS {ethyl lactate (1) + trisodium citrate (2) + water (3)} at 298.15 K and 0.1 MPa. 83*

Table E.6 *- Calculated solute losses, extraction efficiency (E) intervals, partition coefficients (K) and literature-based tie-line lengths (TLL) for the extraction of gallic acid, ferulic acid and resveratrol in the ATPS {ethyl lactate (1) + tripotassium citrate (2) + water (3)} at 298.15 K and 0.1 MPa..... 84*

Table E.7 *- Calculated solute losses, extraction efficiency (E) intervals, partition coefficients (K) and literature-based tie-line lengths (TLL) for the extraction of gallic acid, ferulic acid and resveratrol in the ATPS {ethyl lactate (1) + disodium succinate (2) + water (3)} at 298.15 K and 0.1 MPa. 85*

Table E.8 *- Calculated solute losses, extraction efficiency (E) intervals, partition coefficients (K) and literature-based tie-line lengths (TLL) for the extraction of gallic acid, ferulic acid and resveratrol in the ATPS {ethyl lactate (1) + sodium potassium tartrate (2) + water (3)} at 298.15 K and 0.1 MPa. ... 86*

Table F.1 *– Calculated values of radii for the ions presented in the systems. 87*

Table F.2 *– Calculated values of van der Waals radii for ions presented in the systems using the Bondi method[85]. 87*

Table F.3 *- Values of non-randomness parameter, standard deviation and optimized τij values obtained for the ATPS {EL (1) + $Na_3Citrate$ (2) + H_2O (3)}. 87*

Table F.4 *- Initial values of each component in each phase in molar fraction of the ATPS {EL (1) + $Na_3Citrate$ (2) + H_2O (3)}. 88*

Table F.5 *- Calculated values of the ionic strength, Debye-Hückel parameter and the closest approach parameter for the ATPS {EL (1) + $Na_3Citrate$ (2) + H_2O (3)}. 88*

Table F.6 *- Calculated values of each component in each phase in molar fraction of the ATPS {EL (1) + $Na_3Citrate$ (2) + H_2O (3)}. 89*

Table F.7 *- Values of non-randomness parameter, standard deviation and optimized τij values obtained for the ATPS {EL (1) + $K_3Citrate$ (2) + H_2O (3)}. 89*

Table F.8 *- Initial values of each component in each phase in molar fraction of the ATPS {EL (1) + $K_3Citrate$ (2) + H_2O (3)}. 90*

Table F.9 *- Calculated values of the ionic strength, Debye-Hückel parameter and the closest approach parameter for the ATPS {EL (1) + $K_3Citrate$ (2) + H_2O (3)}. 90*

Table F.10 *- Calculated values of each component in each phase in molar fraction of the ATPS {EL (1) + $K_3Citrate$ (2) + H_2O (3)}. 91*

Table F.11 *- Values of non-randomness parameter, standard deviation and optimized τij values obtained for the ATPS {EL (1) + $Na_2Succinate$ (2) + H_2O (3)}. 91*

Table F.12 *- Initial values of each component in each phase in molar fraction of the ATPS {EL (1) + $Na_2Succinate$ (2) + H_2O (3)}. 91*

Table F.13 *- Calculated values of the ionic strength, Debye-Hückel parameter and the closest approach parameter for the ATPS {EL (1) + $Na_2Succinate$ (2) + H_2O (3)}. 92*

Table F.14 *- Calculated values of each component in each phase in molar fraction of the ATPS {EL (1) + $Na_2Succinate$ (2) + H_2O (3)}. 92*

Table F.15 *- Values of non-randomness parameter, standard deviation and optimized τij values obtained for the ATPS {EL (1) + NaKTartrate (2) + H_2O (3)}. 92*

Table F.16 *- Initial values of each component in each phase in molar fraction of the ATPS {EL (1) + NaKTartrate (2) + H_2O (3)}. 93*

Table F.17 *- Calculated values of the ionic strength, Debye-Hückel parameter and the closest approach parameter for the ATPS {EL (1) + NaKTartrate (2) + H_2O (3)}. 93*

Table F.18 *- Calculated values of each component in each phase in molar fraction of the ATPS {EL (1) + NaKTartrate (2) + H_2O (3)}..... 93*

Notation and Glossary

$A_{\mathrm{DH},x}$	Debye-Hückel parameter	
A	UV-Vis absorbance	
A'	Normalized UV-Vis absorbance	
A_{ij}	Polynomial adjustable parameters	
$\left[\mathrm{A}^{q_0-i+1}\right]$	Mole concentration of the antioxidant species with electrical charges equal to $(q_0 - i + 1)$ e	$\mathrm{mol \cdot m^{-3}}$
$\left[\mathrm{A}^{q_0-i}\right]$	Mole concentration of the antioxidant species with electrical charges equal to $(q_0 - i)$ e	$\mathrm{mol \cdot m^{-3}}$
a	Hard-core collision diameter	m
c	Stoichiometric coefficients	
C	Concentration	$\mathrm{kg \cdot m^{-3}}$
e	Elementary electrical charge of an electron	C
E	Extraction efficiencies	%
$\mathrm{G^E}$	Excess Gibbs free energy	J
G	Gibbs energy of the solution	J
$\mathrm{G^{ideal}}$	Gibbs energy for an ideal solution	J
g_{ij}	Interaction energy parameter	J
$\mathrm{H^{\bullet}}$	Radical proton	
I_x	Ionic strength	$\mathrm{C^2}$
I_x^0	Ionic strength of the pure salt	$\mathrm{C^2}$
$I_{x,\mathrm{ca}}^0$	Ionic strength of the pure liquid electrolyte ca	$\mathrm{C^2}$
k_{B}	Boltzmann constant	$\mathrm{J \cdot K^{-1}}$
k	Number of data points	
K_1, n	Othmer-Tobias equation parameters	
K_2, r	Brancroft equation parameters	
K	Partition coefficients	
L_{m}	Mass losses	%
m_i	Mass of species i	Kg
m	Degree of the polynomial	
M	Number of components in the mixture	
M_{ms}	Molecular mass of the mixed solvent	$\mathrm{kg \cdot mol^{-1}}$
M_i	Molecular mass of species i	$\mathrm{kg \cdot mol^{-1}}$
n	Number of components of the ternary mixtures	
N_{A}	Avogradro's constant	$\mathrm{mol^{-1}}$

N_i	Number of groups i	
N	Number of equilibria points of the top and bottom phases	
N_{species}	Number of species	
$\text{p}K_\text{a}$	Acid dissociation constant	
Q'	General physical property	
q	Mean electrical charge	C
q_0	Initial electrical charge at pH = 0	C
R_g	Ideal gas constant	$\text{J} \cdot \text{K}^{-1} \cdot \text{mol}^{-1}$
R	Relative molecular volume	
r_w	van der Waals radius	m
R^2	Correlation coefficient	
S_β	Variance of the y-intercept of the calibration curve	
T	Temperature	K
V_w	van der Waals volume	$\text{m}^3 \cdot \text{mol}^{-1}$
x	Molar fraction	
w	Mass fraction	
z_i	Electrical charge of species i	C

Greek Letters

α_{ij}	Non-randomness parameter	
α	Slope of the calibration curve	$\text{m}^{-3} \cdot \text{kg}^{-1}$
β	y-intercept of the calibration curve	
γ_i	Activity coefficients of component i	
${\gamma_i}^{\text{NRTL}}$	Activity coefficient of species i calculated from the NRTL model	
${\gamma_i}^{\text{PDH}}$	Activity coefficient of species i calculated from the PDH equation	
ε_0	Vacuum permittivity	$\text{F} \cdot \text{m}^{-1}$
ε_i	Dielectric constant of species i	
ε_ms	Dielectric constant of the mixed solvent	
μ_i	Conductivity of species i	$\text{S} \cdot \text{m}^{-1}$
ρ	Closest approach parameter	
ρ_i	Density of species i	$\text{kg} \cdot \text{m}^{-3}$
$\rho_{i,x}$	Molar density of species i	$\text{mol} \cdot \text{m}^{-3}$
$\rho_{\text{ms},x}$	Molar density of the mixed solvent	$\text{mol} \cdot \text{m}^{-3}$
τ_{ij}	Binary interaction energy parameter of NRTL model between species i and j	

Indexes

i	Index or counter
j	Index or counter
k	Index or counter
l	Index or counter
ms	Mixed solvent
top	Top phase
bot	Bottom phase
M	Cation or anion
M	Mass
phases	Phase
feed	Feed
C	Cation
A	Anion
Ca	Cation-anion
G	Gas
s	Neutral solvent
0	Pure species

List of Acronyms

ABS	Aqueous biphasic systems
AcOH	Acetic acid
AH	Antioxidant
API	Active pharmaceutical ingredient
ATPS	Aqueous two-phase systems
CAS	Chemical abstracts service
DNA	Deoxyribonucleic acid
EL	Ethyl lactate
EtOH	Ethanol
FA	Ferulic acid
GA	Gallic acid
HPLC	High-performance liquid chromatography
K_3Citrate	Tripotassium citrate
MATLAB	MATrix LABoratory
MS	Mostly stable
Na_3Citrate	Trisodium citrate

NaKTartrate	Potassium sodium tartrate
Na_2Succinate	Disodium succinate
NRTL	Non-Random Two-Liquid
PDH	Pitzer-Debye-Hückel
PVP	Polyvinylpyrrolidone
$R^{\bullet}$	Free radical
RNA	Ribonucleic acid
ROS	Reactive oxygen species
RVT	Resveratrol
S	Stable
STL	Tie-line slope
TL	Tie-line
TLL	Tie-line length
UNIFAC	UNIversal Functional Activity Coefficients
UNIQUAC	UNIversal QUAsi-Chemical
US	Unstable
UV	Ultraviolet

1 Introduction

Malnutrition remains a critical issue in developing countries, being the most important risk factor for illness and death worldwide, as a consequence of a poor diet, resulting in about 300 000 deaths per year[1]. Food supplements can play a crucial role in addressing this issue by providing essential nutrients to those in need. While they alone cannot solve the problem entirely, dietary supplementation can complement efforts to alleviate undernourishment[2].

One of the reasons why food supplements are important is the nutrient enrichment, since these prescriptions are rich in vital nutrients such as proteins, vitamins, minerals and antioxidants, which are essential for the healthy growth and development of individuals[3,4]. In times of crises like natural disasters, conflicts, or famines, these play a crucial role in the emergency relief by supplying a rapid and concentrated source of essential nutrients to meet immediate needs[2,5]. Besides, these are relatively affordable, easy to distribute and can quickly provide nutrients to large populations in need, making them a practical solution in resource-constrained environments[3].

The recovery of these antioxidants from by-products of the food industry is a promising approach to the circular economy model, which focuses on sustainable use of resources and minimizes waste generation, in order to reduce the environmental impact of industrial processes[6-8]. Furthermore, the use of Aqueous Two-Phase Systems (ATPS), or Aqueous Biphasic Systems (ABS), is a more sustainable alternative for the efficient extraction, recovery and purification of these species, given their favorable physicochemical properties[9,10]. Moreover, this technique is environmentally friendly, due to its high water-content and biocompatible extractive media[11,12].

1.1 Problem statement

Although Aqueous Two-Phase Systems (ATPS) present a sustainable alternative for the efficient extraction of antioxidants, the liquid-liquid equilibria data related to these systems is relatively scarce in literature, in particular for systems using environmentally benign solvents, such as ethyl lactate (EL), and green polymers, such as polyvinylpyrrolidone (PVP)[13-15]. The use of these systems with organic salts, such as citrates, tartrates and succinates, has a proven lower impact on the environment than inorganic salts since the former are biodegradable and can be used as food additives[16]. However, there are no sufficient data available in literature, so it is crucial to investigate the solubility curve and tie-line data referent to sustainable aqueous two-phase systems, in order to use them on the extraction of important antioxidants, vitamins and other biomolecules to be implemented in food supplements.

Furthermore, the pH of the system may significantly affect the quantification of biomolecules, due to the presence of differently charged chemical structures. However, this variable is not usually taken into account in the literature[17,18]. Therefore, a study of the pH stability of each species must be performed before carrying out a partition, in order to ensure the validity of the obtained results.

During the last years, there have been numerous studies, both experimental and theoretical, on the thermodynamic properties of electrolyte solutions. Therefore, accurate computer thermodynamic modeling and process simulation of electrolyte systems are now being pursued actively, in order to avoid the difficult and expensive experimental procedures to predict the liquid-liquid behavior of ATPS[19-21].

The electrolyte non-random two-liquid model (e-NRTL) couples the Pitzer–Debye–Hückel theory for long-range ion-ion electrostatic interactions and the NRTL theory for three types of short-range interaction: molecule-molecule, molecule-ion and ion-ion[22]. This model can be easily extended to mixtures with multiple electrolytes and mixed solvents. Also, the eNRTL model is simple and capable of correctly describing the short and long-range interactions over the entire range of concentrations and system's temperatures[20]. This gives the model a strong basis for reliable extrapolation and decreases the chances of overfitting a specific data set[22]. Nonetheless, other models that are not adequate for electrolytes are still being incorrectly used to predict the behavior of liquid-liquid equilibria of ATPS including these species, such as UNIversal QUAse-Chemical (UNIQUAC) and NRTL. Moreover, the research on the use of this model in systems with double salts (composed of more than two types of cations or anions) is still scarce, so a deeper look at this topic is vital.

1.2 LSRE-LCM and ALiCE

This project was developed at the Laboratory of Separation and Reaction Engineering – Laboratory of Catalysis and Materials (LSRE-LCM), which is comprised of 4 research groups: Thermodynamics and Environment, Cyclic Adsorption Reaction Processes, Product Engineering, and Catalysis and Carbon Materials, and based at *Faculdade de Engenharia da Universidade do Porto* (FEUP), Portugal.

This laboratory is part of the largest Portuguese associate laboratory in the field of Chemical Engineering, the Associate Laboratory in Chemical Engineering (ALiCE). This group integrates three older research and development units, LSRE-LCM, Laboratory for Process Engineering, Environment, Biotechnology and Energy (LEPABE) and Transport Phenomena Research Center (CEFT), focused on 5 research lines: Chemical Industry, BioIndustry, Materials, Energy and Environment.

1.3 Author's contribution

All the work presented in this document was performed by the author, under the guidance and assessment of the supervisor and team. Both laboratory experiments and MatLab code were developed from scratch by the author. In addition to the author's own work, the used preexisting materials developed by others were properly cited.

1.4 Document's structure

This dissertation is comprised of seven chapters.

The first chapter corresponds to the **Introduction**, which includes a general framing of the issue and a study overview.

The Chapter 2, **State of the Art**, introduces the importance and properties of antioxidants and their use in food supplements. The studied antioxidants and solvents are presented as well as the concepts related to aqueous two-phase systems. In addition, a review of the thermodynamic models is given with emphasis in the electrolyte Non-Random Two-Liquid model, used to model the considered systems.

During Chapter 3, **Materials and Methods**, information about the materials and equipment used in the project, as well as the followed procedures, are described.

Then, in Chapter 4, **Results and Discussion**, the outcomes of this work are summarized and discussed. The challenges and potential difficulties are also mentioned.

Following, in Chapter 5, **Conclusion**, the main findings, discussions and final remarks of this project are assessed.

Next, in Chapter 6, **Project assessment**, the dissertation's limitations, the objectives' completion and suggestions for future work are presented.

Lastly, the **References**, **Annexes** and **Appendices** sections contain supplementary information on certain contents.

2 State of the art

Throughout this chapter, a literature review will be performed, exploring the most important concepts related to the extraction of antioxidants using Aqueous Two-Phase Systems and the prediction of liquid-liquid equilibria through thermodynamic modeling.

2.1 Extraction of antioxidants

One of the major global challenges is to provide healthy and nutritious food for all population while ensuring a sustainable food production[5]. While some individuals have access to the minimum calorie requirements, they lack essential nutrients, such as vitamins and antioxidants, in their diet, which leads to a large range of diseases and to higher rates of child and maternal mortality, in developing countries[2,3,5].

This insufficiency may lead to higher oxidative stress, characterized by an excessive production of reactive oxygen species (ROS)[23,24]. ROS are free radicals, *i.e.*, reactive chemicals with an unpaired electron, which are produced when humans are exposed to microbial infections, extensive exercise, ultraviolet radiations, or to pollutants and toxins[25]. This unbalance between the oxidant species and the antioxidant defense system may alter the deoxyribonucleic acid (DNA), ribonucleic acid (RNA), lipids and protein structure, resulting in the generation of mutagen compounds, inflammation, over-expression of oncogenes, and causing health issues such as cancer, neurodegeneration, cardiovascular diseases, diabetes and premature aging[26-28].

The consumption of antioxidants-,vitamins-, and minerals-rich dietary supplements, has been increasing, aiming to tackle this issue by correcting the inefficiencies of these components in the human diet. Food supplements contain antioxidants, which are substances that, when present at low concentrations, delay or prevent oxidative damage of the substrate by donating hydrogen radicals ($H^{\bullet}$), neutralizing the reactive oxygen species by breaking the reactions' chain and balancing the generation and depletion of ROS, as shown by equation (1)[23,25,29].

$$AH + R^{\bullet} \rightarrow A^{\bullet} + RH \quad (1)$$

where AH is the antioxidant and $R^{\bullet}$ is the free radical.

Food supplements may contain various antioxidants, such as vitamin A, C and E and polyphenols. Polyphenols are the most abundant and widely distributed group of antioxidants, and play a key role in the prevention of diabetes, cancer, and cardiovascular and neurodegenerative diseases[30,31]. Moreover, they present strong antioxidant, antimicrobial, anti-inflammatory, antimutagenic and anticancer properties[32].

Gallic acid (3,4,5-trihydroxybenzoic acid) is a polyphenol found in gallnuts, berries, grapes, mangos, hazelnuts, tea and wine, and is used in the cosmetics, pharmaceutical, leather (as a chelating agent) and in the food (as a preservative) industries[32,33]. This benzoic acid has been successfully extracted using, for example, ethanol and ionic liquids[34]. The methods used to quantify gallic acid (GA) include capillary electrophoresis, chromatography, mass spectrometry and UV-Vis spectroscopy[34,35].

Ferulic acid ((2E)-3-(4-hydroxy-3-methoxyphenyl)prop-2-enoic acid) is a phenolic acid of low toxicity that can be found in fruits and vegetables, such as sweet corn, tomatoes, beans, oats, coffee seeds, nuts and rice bran[36]. Moreover, it is used in cosmetic lotions for photoprotection since it has radical scavenging capacity, which allows to suppress radiation-induced oxidative reactions, protecting cells exposed to ultraviolet radiation[36-38]. Although there are techniques used to obtain this antioxidant, such as alkaline, enzymatic or acidic extractions, these generally fail to preserve the bioactivity of ferulic acid, so new approaches have to be developed[39].

Resveratrol (trans-3,4′,5-trihydroxystilbene) is a polyphenol that occurs naturally in some plants, for which it is present in mulberries, peanuts, grape skins and red wine, and has been proven to play an important role in the prevention of human cardiovascular diseases[40-42]. Moreover, it has the capacity to modulate the metabolism of lipids and possesses neuroprotective abilities[40,42,43]. Even though several simple and intuitive methods of extraction of this antioxidant have been experimented, such as heating under reflux with ethanol and supercritical fluid extraction, these are time-consuming and expensive[44].

The recovery of these antioxidants from by-products of the food industry is a promising approach to the circular economy model, which focuses on sustainable use of resources and minimizes waste generation, in order to reduce the environmental impact of the processes[6-8]. Some examples of feedstocks for the extraction of ferulic acid (FA), gallic acid (GA) and resveratrol (RVT) are shown in Fig. 1.

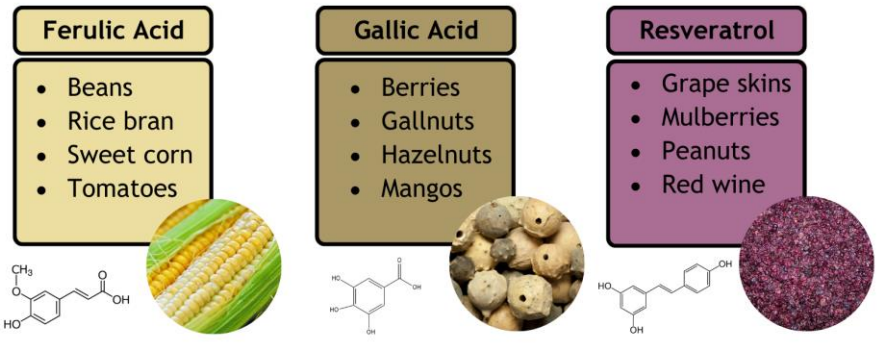


Fig. 1 - Possible feedstocks for the extraction of ferulic acid, gallic acid and resveratrol.

In order to extract antioxidants in a way that is environmentally friendly, there has been a growing interest in replacing conventional extraction procedures, such as maceration, percolation, digestion and heat-assisted extraction, that have shown disadvantages namely long extraction time, high raw material and solvent consumption, and low antioxidants yield. Therefore, some modern techniques have been studied, including supercritical fluid, microwave-assisted, ultrasound-assisted, accelerated solvent, pulse electrical field extraction, high-voltage electrical discharge, pressurized liquid and enzyme-assisted extraction[45-49].

2.2 Aqueous Two-Phase Systems

Liquid-liquid extraction is still the most commonly used extraction procedure, mainly because of its simplicity, efficiency and wide-ranging applicability. However, there are some disadvantages pointed out to this method, such as the use of large volumes of conventional solvents, such as alcohols, that are not biocompatible. Moreover, the residues of the solvents may remain in the final product, obligating to undergo expensive purification procedures[9,50]. In addition, there is usually the need to perform multiple extractions over a long extraction time and operation conditions with high temperatures and pressures, which may modify the properties of the antioxidants[51-53].

The use of Aqueous Two-Phase Systems (ATPS), or Aqueous Biphasic Systems (ABS), is a more sustainable alternative for the efficient extraction of biomolecules, such as proteins, antioxidants, vitamins, pigments and active pharmaceutical ingredients (APIs), such as Ibuprofen[9,10]. These liquid-liquid separations have shown great potential for the extraction, recovery and purification of a variety of biological compounds, given their favorable physicochemical properties. This technique has a good scale-up potential, provides non-toxic and biocompatible extractive media, has a low cost, is environmentally friendly (due to its high water-content) and preserves the bioactivity of the separated molecules[9-12,54-56].

ATPS are formed when the concentrations of two water-soluble components, such as polymers, salts and ionic liquids, reach a specific level, causing the mixture to spontaneously form two immiscible phases: the top (lower density) and the bottom (higher density) phases[10,11]. The migration of each component to the top or bottom phase is ruled by properties such as electrical charge, polarity, molecular mass, density, hydrophobicity and viscosity[11,55-60].

Nowadays, there has been an increasing demand for environmentally benign alternatives with application in ATPS, including green solvents (such as ethyl lactate) and green polymers (such as polyvinylpyrrolidone). These alternatives are bio-renewable, biodegradable, non-flammable and present low toxicity towards humans and animals, besides being economically viable[15,61,62].

Ethyl lactate can be produced from bio-renewable sources such as biomass fermentation or by the esterification reaction between ethanol and lactic acid. Additionally to the use of EL as a food additive and flavoring agent, this monobasic ester is also being used to extract biomolecules, such as vitamins, antibiotics, proteins, amino acids and antioxidants, exhibiting effectiveness similar to petroleum-based solvents[15,63]. Likewise, polyvinylpyrrolidone (PVP) is a hydrophilic polymer synthesized by free-radical polymerization of N-vinylpyrrolidone in water or alcohols and it is also inexpensive, stable and has great potential for extraction of biomolecules in ATPS. Moreover, it has found application in paints, adhesives and as an additive in the food industry[13,14,16].

Despite this, liquid-liquid equilibria data of ATPS containing EL and PVP are relatively scarce in literature, so more comprehensive studies are needed[14]. Nevertheless, it is known that both these solvents form ATPS with some organic salts, such as citrates, tartrates and succinates, which have been shown to have a lower impact on the environment than inorganic salts. Furthermore, these organic salts are biodegradable components that can be used as food additives, acidity regulators, flavor enhancers, pH controllers and preservatives[62,64,65].

2.3 Thermodynamic models

Thermodynamic models are mathematical representations used to describe and analyze the thermodynamic properties and processes, through simplified representation of the system by making certain assumptions and approximations. These models are based on fundamental thermodynamic principles and laws, such as the law of conservation of energy, entropy and the ideal gas law[66-68].

To accurately design separation processes, reliable thermodynamic data are required, in order to predict the behavior of physical systems. The most used ones include phase equilibria and properties of pure components and mixtures over a wide range of temperature, pressure and composition, such as liquid density and vapor pressure[66-69].

There are two different approaches in thermodynamic modeling: the equations of state, mathematical equations which relate state variables of a system, and the models based on activity coefficients[66,70,71]. The activity coefficients models are widely used to represent the non-ideal behavior of mixtures in the liquid phase[68]. These models are based on the prediction of the excess Gibbs free energy, which is the fraction of the enthalpy available for chemical reactions occurring within a fluid and the involving transfer from one phase to another. The excess Gibbs energy is defined as the difference between its actual value for a solution and that of an ideal solution at the same temperature, pressure and composition, as represented in equation (2)[67,68].

$$G^{\mathrm{E}} = G - G^{\mathrm{ideal}} \quad (2)$$

An example of an activity coefficients model is the van Laar model[72], derived from the van der Waals equation for regular solutions[19]. This simple model assumes that the interactions between the molecules in a mixture can be described by a function of the mole fraction of each component, and yields acceptable fittings for engineering applications. However, the parameters of this model are not temperature-dependent and the form of the equation dictates that the excess Gibbs energy can never be negative[73].

The Wilson equation[74] includes both the energetic and entropic effects of the binary liquid mixtures and takes into account the concept of local composition, which states that the composition around a molecule in solution may be different than its bulk composition in the mixture, *i.e.*, it refers to the arrangement and distribution of atoms or molecules in a specific region of a material[75].

In the UNIversal QUAsi-Chemical (UNIQUAC) model[76], the molecules are characterized by the relative volume of the molecule – the volume parameter (R) – and the relative surface area – the surface parameter (Q). Therefore, it recognizes that the non-ideality of a liquid is influenced by the size and shape of the molecules and by the energetic interactions between the molecules, and assumes that the deviations from ideal behavior are due to the non-random distribution of molecules[75].

Later, Fredenslund *et al.*[77] developed an extension to this model, known as UNIversal Functional Activity Coefficients (UNIFAC), in which a mixture of compounds is replaced by a mixture of groups, taking into account the functional groups and the bounds of the molecule[75].

2.3.1 Non-Random Two-Liquid model

The Non-Random Two-Liquid (NRTL) model was developed in 1968 by Renon and Prausnitz[78] and takes into account the non-randomness of the interactions. It is based on the idea that the interactions between different molecules in the mixture can be modeled as a combination of two types of interactions: the interactions between molecules of the same type and the interactions between molecules of different types[19,75].

In this way, the NRTL model requires three parameters for a binary system: two interaction parameters and the non-randomness parameter (α_{ij})[68]. According to this model, the excess Gibbs free energy is given by equation (3)[19,68,79].

$$\frac{G^{\mathrm{E}}}{R_{\mathrm{g}}T} = \sum_{i}^{M} x_i \frac{\sum_{j}^{M} \tau_{ji} G_{ji} x_j}{\sum_{k}^{N} G_{ki} x_k} \quad (3)$$

where M is the number of components in the mixture, x_i and x_j are the mole fractions of species i and j and G_{ij} is described as followed:

$$G_{ij} = \exp\left(-\alpha_{ij} \cdot \tau_{ij}\right) \quad (4)$$

$$\tau_{ij} = \frac{g_{ij} - g_{ii}}{R_g T} \quad (5)$$

where τ_{ij} represents the differences between the interaction energies, g_{ij} and g_{ii} are the interaction energy parameters, which refer to the $i-j$ and $i-i$ interactions, and α_{ij} is an adjustable parameter that describes the non-randomness, determined by fitting the model to experimental data (liquid-liquid equilibria data, for example)[68].

The activity coefficients are calculated using[79]:

$$\ln \gamma_i = \frac{\sum_j^M \tau_{ji} G_{ji} x_j}{\sum_k^M G_{ki} x_k} + \sum_k^M \frac{G_{ij} x_j}{\sum_k^M G_{kj} x_k} \left(\tau_{ij} - \frac{\sum_l^M \tau_{li} G_{li} x_l}{\sum_k^M G_{ki} x_k} \right) \quad (6)$$

where γ_i is the activity coefficient of component, x refer to the mole fractions, τ_{ij} and τ_{li} are the interaction parameters, and G_{ij}, G_{ji}, G_{ki} and G_{li} are the Gibbs energies of the solution.

2.3.2 Electrolyte-Non-Random Two-Liquid model

Electrolytes are substances that dissociate into cations and anions when in solution. Some examples include salts, acids and bases. Strong electrolytes dissociate completely into their ions, while weak electrolytes only partially dissociate[19].

The Electrolytic-Non-Random Two-Liquid (e-NRTL) model, proposed by Chen[22], is one of the mostly applied methods for the description of electrolytic systems by means of thermodynamic properties, such as the activity coefficients and free Gibbs energy, related to the estimation of flows, compositions, and phase stability for those systems, and enthalpy, required for the energy balances[68]. E-NRTL allows the study of the contributions of the effects of each of these thermodynamic properties in a separate way and the calculation of the activity coefficient of each component in the mixture[68].

The e-NRTL model is based on the same assumptions as the NRTL model, which considers that the non-ideality of the mixture arises from the differences in the molecular size, shapes, and polarity of the components. However, the e-NRTL model introduces an additional parameter that accounts for the effect of temperature on the non-randomness of the mixture[19].

Moreover, for solutions with electrolytes, the short-range electrostatic interactions between the ions and water or other solvents must be taken into consideration. These are described by the NRTL model, and the long-range electrostatic forces, that are dominant, are described by the Pitzer-Debye-Hückel equation (PDH). The PDH equation includes several parameters, such as the ion radii, electrical charge and polarizability[19,80].

Combining the NRTL model with PDH equation, the activity coefficient of species i (γ_i) is calculated according to:

$$\ln \gamma_i = \ln {\gamma_i}^{\mathrm{NRTL}} + \ln {\gamma_i}^{\mathrm{PDH}} \tag{8}$$

where ${\gamma_i}^{\mathrm{NRTL}}$ and ${\gamma_i}^{\mathrm{PDH}}$ refer to the activity coefficients from the NRTL model and from the PDH equation, respectively.

Then, the long-range electrostatic contribution to the activity coefficient (${\gamma_i}^{\mathrm{PDH}}$) is calculated by:

$$\frac{g^{\mathrm{E,PDH}}}{RT} = -\frac{4A_{\mathrm{DH},x}I_x}{\rho}\ln\left(\frac{1+\rho I_x^{1/2}}{1+\rho (I_x^0)^{1/2}}\right) \tag{9}$$

where $A_{\mathrm{DH},x}$ is the Debye-Hückel parameter, ρ is the closest approach parameter, I_x is the ionic strength and I_x^0 is the ionic strength of the pure salt.

By the differentiation of the excess Gibbs energy, equation (9), the activity coefficient for the infinitely dilute reference state (unsymmetric convention) can be calculated by:

$$\ln {\gamma_i}^{*\,\mathrm{PDH}} = -z_i^2 A_{\mathrm{DH},x}\left[\frac{2}{\rho}\ln\left(1+\rho\sqrt{I_x}\right)\right] + \sqrt{I_x}\frac{1-2\frac{I_x}{z_i^2}}{\rho\sqrt{I_x}} \tag{10}$$

where z_i refers to the electrical charge of species i.

Given that NRTL is in the symmetrical convention, it is necessary to convert the PDH equation shown in equation (10) to the chosen reference state, as equation (11) shows.

$$\ln {\gamma_i}^{\mathrm{PDH}} = -z_i^2 A_{\mathrm{DH},x}\left[\frac{2}{\rho}\ln\left(\frac{1+\rho\sqrt{I_x}}{1+\rho\sqrt{\frac{z_i^2}{2}}}\right) + \sqrt{I_x}\frac{1-2\frac{I_x}{z_i^2}}{1+\rho\sqrt{I_x}}\right] \tag{11}$$

where the ionic strength on a mole fraction basis (I_x) is calculated by:

$$I_x = \frac{1}{2}\sum_{i=1} z_i^2\, x_i \tag{12}$$

where x_i is the mole fraction of species i.

However, this approach does not take into account salts with more than one cation or anion, known as double salts. According to Pitzer[81], in these cases, ${\gamma_i}^{\mathrm{PDH}}$ can be calculated for each cation or anion M as shown in equation (13). It is important to note that in case of M being an anion, the subscripts a changes to c and vice-versa.

$$\ln {\gamma_{\mathrm{M}}}^{\mathrm{PDH}} = -\frac{2A_{\mathrm{DH},x}}{\sum x_i|z_i|}\sum_{\mathrm{a}} x_{\mathrm{a}}|z_{\mathrm{a}}|\left\{z_{\mathrm{M}}(z_{\mathrm{M}}+|z_{\mathrm{a}}|)Y_{\mathrm{Ma}} + \sum_{\mathrm{c}} x_{\mathrm{c}}z_{\mathrm{c}}(z_{\mathrm{c}}+|z_{\mathrm{a}}|)\left[\frac{{z_{\mathrm{M}}}^2 - 2I_x}{4{I_x}^{1/2}(1+\rho {I_x}^{1/2})} - \frac{z_{\mathrm{M}}Y_{\mathrm{ca}}}{\sum x_i|z_i|}\right]\right\} \tag{13}$$

where the ionic strength on a mole fraction basis (I_x) is calculated by:

$$I_x = \sum_{\mathrm{c}} \sum_{\mathrm{a}} x_{\mathrm{c}} z_{\mathrm{c}} x_{\mathrm{a}} |z_{\mathrm{a}}| \, (z_{\mathrm{c}} + |z_{\mathrm{a}}|) \Big/ \sum_i x_i |z_i| \tag{14}$$

where c and a refer to the cations and anions, respectively, z is the electrical charge and x is the mole fraction.

Y_{ca} is a function of ρ and I_x calculated according to:

$$Y_{\mathrm{ca}} = \frac{1}{\rho_{\mathrm{ca}}} \ln \left[\frac{1 + \rho {I_x}^{1/2}}{1 + \rho ({I_{x,\mathrm{ca}}^0}^{1/2})} \right] \tag{15}$$

where the ionic strength of pure liquid electrolyte ca ($I_{\mathrm{x,ca}}^0$) is calculated by:

$$I_{x,\mathrm{ca}}^0 = \frac{c_{\mathrm{a}}}{c_{\mathrm{a}} + c_{\mathrm{c}}} {z_{\mathrm{c}}}^2 + \frac{c_{\mathrm{c}}}{c_{\mathrm{a}} + c_{\mathrm{c}}} {z_{\mathrm{a}}}^2 \tag{16}$$

where c_{a} and c_{c} are the stoichiometric coefficients of the anion and cation, respectively.

For a neutral solvent, in the case of double salts, the calculation of ${\gamma_i}^{\mathrm{PDH}}$ is performed using:

$$\ln {\gamma_{\mathrm{S}}}^{\mathrm{PDH}} = \frac{2A_x}{\sum x_i |z_i|} \sum_{\mathrm{c}} \sum_{\mathrm{a}} \frac{x_{\mathrm{c}} z_{\mathrm{c}} x_{\mathrm{a}} |z_{\mathrm{a}}| (z_{\mathrm{c}} + |z_{\mathrm{a}}|) {I_x}^{1/2}}{1 + \rho_{\mathrm{ca}} {I_x}^{1/2}} \tag{17}$$

$A_{\mathrm{DH},x}$ is the Debye-Hückel parameter, which can be determined by equation (18).

$$A_{\mathrm{DH},x} = \frac{1}{3} \sqrt{2\pi \frac{N_{\mathrm{A}} \rho_{\mathrm{ms},x}}{M_{\mathrm{ms}}}} \left(\frac{e^2}{4\pi \varepsilon_0 \varepsilon_{\mathrm{ms}} k_{\mathrm{B}} T} \right)^{3/2} \tag{18}$$

where N_{A} represents the Avogradro's constant, M_{ms} is the molecular mass of the mixed solvent, $\rho_{\mathrm{ms},x}$ is the molar density of the mixed solvent, e refers to the electrical charge of an electron, ε_0 is the vacuum permittivity, $\varepsilon_{\mathrm{ms}}$ represents the dielectric constant of the mixed solvent, k_{B} is the Boltzmann constant and T is the absolute temperature.

Molar density ($\rho_{\mathrm{ms},x}$) and the molecular mass (M_{ms}) of the mixed solvent were determined by the weighted arithmetic means given by equations (19) and (20), respectively.

$$\frac{1}{\rho_{\mathrm{ms},x}} = \sum_i \frac{x_i'}{\rho_{i,x}} \tag{19}$$

$$M_{\mathrm{ms}} = \sum_i x_i' M_i \tag{20}$$

where x_i' refers to the salt-free mole fraction, $\rho_{i,x}$ is the molar density and M_i is the molar mass. Salt-free nomenclature only considers the molecules of the solvent in the mixture, disregarding any salt molecules.

In addition, the dielectric constant of the mixed solvent ($\varepsilon_{\mathrm{ms}}$) can also be determined using a similar approach based on a weighted arithmetic mean, taking into account the mole fraction of each component. However, in this study, Oster's mixing rule[82], equation (21), was applied since it is a more common approach.

$$\varepsilon_{\mathrm{ms}} = \varepsilon_1 + \left(\frac{(\varepsilon_2 - 1)(2\varepsilon_2 - 1)}{2\varepsilon_2} - (\varepsilon_1 - 1)\right)\frac{x_2'}{\rho_{2,x}}\rho_{\mathrm{ms},x} \tag{21}$$

where ε_1 and ε_2 are the dielectric constants of the neutral species 1 and 2, x_2' refers to the salt-free mole fraction of neutral species 2, ρ_{ms} is the density of the mixed solvent and $\rho_{2,x}$ is the molar density of neutral species 2.

The closest approach parameter (ρ) is related to the minimum distance between the centers of the cation and anion of the salt. It is influenced by temperature and pressure, and by molecular properties such as size, shape and polarity[83]. To ensure the physical meaning of the parameter, this study resorted to the equation proposed by Pitzer and Simonson[84], based on the success of previous works in the prediction of the tie-lines for ATPS[83], as shown in:

$$\rho = a\left(\frac{2e^2 N_{\mathrm{A}}\rho_{\mathrm{ms}}}{M_{\mathrm{ms}}\varepsilon_0\varepsilon_{\mathrm{ms}}k_{\mathrm{B}}T}\right)^{0.5} \tag{22}$$

where a is the hard-core collision diameter, which is calculated by sum of the radii of the cation and anion without solvation, calculated by:

$$a = r_{\mathrm{c}} + r_{\mathrm{a}} \tag{23}$$

where r_{c} and r_{a} are the radii of the cation and of the anion, respectively.

The radii of the cation and anion can be estimated by their corresponding van der Waals radii (r_{w}), which can be determined by their van der Waals volume (V_{w}), supposing spherical shape. This volume represents the space taken up by an atom or molecule that cannot be penetrated by other atoms or molecules, according to equation (24).

$$V_w = \frac{4}{3}\pi \cdot {r_{\mathrm{w}}}^3 \tag{24}$$

V_w was correlated with the relative van der Waals molecular volume (R_i) using:

$$V_w = R_i \cdot 15.17 \cdot 10^6 \tag{25}$$

2.4 Bondi method

One of the most common methods to calculate the van der Waals molecular volume is the group contribution theory developed by Bondi[85] and first introduced in 1964. It is based on the idea that the properties of a substance can be predicted based on the properties of its constituent groups or functional units[69,85]. By assigning a set of empirical parameters to each

group, the contribution of each group to the overall properties of the substance can be calculated and combined to give an overall prediction.

The Bondi's group contribution method is a simple approach for calculating the van der Waals volume based on the bond distances, bond angles, atomic shapes, and intermolecular van der Waals radii. This method also provides the van der Waals surface area. However, it assumes that atoms have spherical shapes and a constant van der Waals radius, regardless of the mixture's chemical nature or phase state[69,85]. Moreover, it is not recommended for light atoms such as hydrogen or fluorine.

The method relies on knowing the contribution of individual groups to the relative molecular surface area, q, and relative molecular volume, r, calculated according to equations (26) and (27). Then, all the contributions of the molecule's constituent groups must be summed[69,85].

$$q = \sum_i N_i Q_i \tag{26}$$

$$r = \sum_i N_i R_i \tag{27}$$

where q is the relative van der Waals molecular surface area, N_i is the number of groups i, Q_i is the i group's relative van der Waals molecular surface area contribution, r is the relative van der Waals molecular radius and R_i is the i group's relative van der Waals molecular volume contribution.

In this work, the Electrolyte-Nonrandom Two-Liquid model was applied to estimate the liquid-liquid equilibria (LLE) of systems with ethyl lactate, water and different salts, using MATrix LABoratory (MATLAB). Moreover, the extraction of three antioxidants (ferulic acid, gallic acid and resveratrol) was evaluated in some of these systems, after studying their stability at different pH values. Finally, a novel LLE {Polyvinylpyrrolidone(1) + Water (2) + NaKTartrate (3)} was determined to be applied in the partition of antioxidants.

3 Materials and methods

In this chapter, the used materials and the experimental procedure will be presented, and the developed modeling procedure in MATLAB will be explained.

3.1 Materials

The list of chemicals used in this work and their respective suppliers, purities, Chemical Abstracts Service (CAS) numbers and abbreviations are shown in Table 1. No further pre-treatments or purification steps were carried out. The properties of the used chemicals are described in Table AA.1.

Table 1 - List of chemicals used and their respective suppliers, purities, CAS numbers and abbreviations.

Chemical	Supplier	Purity / *m*%	CAS	Abbreviation
Acetic Acid (CH_3COOH)	Merck	> 99	64-19-7	AcOH
Ethanol (CH_3CH_2OH)	Sigma-Aldrich	> 99	64-17-5	EtOH
(-)-ethyl L-lactate ($C_5H_{10}O_3$)	Sigma-Aldrich	> 98	97-64-3	EL
Ferulic acid ($C_{10}H_{10}O_4$)	Sigma-Aldrich	> 99	537-98-4	FA
Gallic acid ($C_7H_6O_5$)	Sigma-Aldrich	> 98	149-91-7	GA
Polyvinylpyrrolidone 29 000 $(C_6H_9NO)_n$	Thermo Scientific	-	9003-39-8	PVP
Tripotassium citrate monohydrate ($C_6H_5K_3O_7 \cdot H_2O$)	Sigma-Aldrich	> 99	6100-05-6	K_3Citrate
Potassium sodium tartrate tetra-hydrate ($C_4H_4O_6KNa \cdot 4H_2O$)	Sigma-Aldrich	> 99	6381-59-5	NaKTartrate
Purified water (H_2O)	VWR Chemicals	-	7732-18-5	W
Resveratrol ($C_{14}H_{12}O_3$)	Tokyo Chemical Industry	> 99	501-36-0	RVT
Sodium hydroxide (NaOH)	Merck	> 99	1310-73-2	NaOH
Trisodium citrate tribasic dihydrate ($C_6H_5Na_3O_7 \cdot 2H_2O$)	Sigma-Aldrich	> 99	6132-04-3	Na_3Citrate
Disodium succinate hexahydrate ($C_4H_4Na_2O_4 \cdot 6H_2O$)	Tokyo Chemical Industry	> 95	6106-24-7	Na_2Succinate

3.2 Apparatus

Concerning the used apparatus, aqueous solutions were prepared by weighing using an ADAM AAA 250 L balance with standard measurement uncertainty of 10^{-4} g, pH was assessed with a VWR pH 1100 L with standard uncertainties of 0.001 in the measurement of pH and $0.1\ \mathrm{K}$ in the measurement of temperature, and with a Crison pH meter Basic 20 with standard measurement uncertainties of 0.01 in pH and $0.1\ \mathrm{K}$ in temperature. A UV-Vis Thermo Scientific Varioskan Flash spectrophotometer with standard measurement uncertainty of 10^{-4} was used to determine UV-Vis absorbance (*A*). Further, the equilibrium temperature (*T*) was kept at 298.15 K with an uncertainty of 0.1 K using a thermoregulated bath Bath OvanTherm MultiMix BHM5E, and density (ρ) was assessed using an Anton Paar DSA-4500M densimeter with standard measurement uncertainties of $5 \cdot 10^{-5}\ \mathrm{g \cdot cm^{-3}}$ in density and 0.01 K in temperature. Liquid volumes were measured with an Eppendorf Multipipette E3x electronic pipette with an uncertainty of 0.5 μL when using the 200 μL tips. A VWR vortex VV3 and an IKA RO 10 P magnetic stirrer were used to stir the samples.

3.3 Methods

3.3.1 Solubility curve

Phase diagrams show the potential working area of Aqueous Two-Phase Systems (ATPS) and provide information on the concentration of components for two phase formation and on their concentration in the top and bottom phases. These diagrams show the solubility curve, which allows to denote the condition and concentrations at which the system forms two immiscible aqueous phases and a fully mixed phase[86].

Since the PVP29k is miscible in water, the addition of a third component, in this case, NaKTartrate, is essential to obtain the phase splitting. The solubility curve of the ternary system {Polyvinylpyrrolidone (1) + water (2) + potassium sodium tartrate (3)} was determined by the cloud-point titration method, which is a visual method, at constant temperature, 298.15 K, and 0.1 MPa[62,87,88]. Drops of the salt were added to the mixture of known composition until the turbidity in the sample was observed, known as the cloud-point. The cloudy (turbid) mixture was, then, weighted and the composition was determined. Afterwards, a specific amount of pure water was added until a clear homogeneous mixture was achieved. This procedure was repeated until enough data were obtained to cover the whole solubility curve. In order to ensure that the whole range of composition was covered, the inverse procedure was done, *i.e.*, a known amount of NaKTartrate was titrated with PVP 29k[18,62,89,90], as shown in Fig. 2.

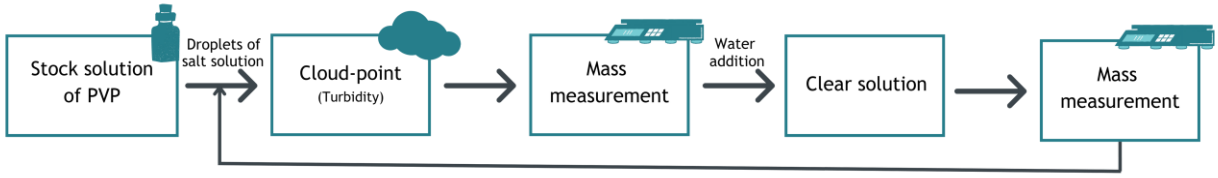


Fig. 2 - Procedure taken for the cloud-point titration method.

Experimental data of the solubility curve of {PVP (1) + NaKTartrate (2) + water (3)} were fitted using equations (28), (29), (30) and (31) proposed by Han *et al.*[91], Merchuk *et al.*[92], Hu *et al.*[93] and Jayapal *et al.*[94], respectively.

$$w_{\mathrm{PVP}} = \exp(A + Bw_{\mathrm{salt}} + Cw_{\mathrm{salt}}{}^2 + Dw_{\mathrm{salt}}{}^3) \tag{28}$$

$$w_{\mathrm{PVP}} = A \cdot \exp(Bw_{\mathrm{salt}}{}^{0.5} - Cw_{\mathrm{salt}}{}^3) \tag{29}$$

$$w_{\mathrm{PVP}} = A + Bw_{\mathrm{salt}} + Cw_{\mathrm{salt}}{}^2 + Dw_{\mathrm{salt}}{}^3 \tag{30}$$

$$w_{\mathrm{PVP}} = A + Bw_{\mathrm{salt}}{}^{0.5} + Cw_{\mathrm{salt}} \tag{31}$$

where $\mathrm{w_{PVP}}$ and $\mathrm{w_{salt}}$ are the compositions of PVP and salt in mass fraction, and *A*, *B*, *C* and *D* are adjustable parameters obtained by the regression of the experimental cloud-point data.

The standard deviation (σ) of each fitting alternative for the experimental solubility curve data was calculated using equation (32).

$$\sigma = \left\{ \sum_{\mathrm{i}}^{n_{\mathrm{data}}} (z - z_{\mathrm{cal}})^2 / n_{\mathrm{data}} \right\}^{1/2} \tag{32}$$

where n_{data} is the number of points and z and z_{cal} are the experimental and calculated values, respectively.

3.3.2 Tie-lines

Tie-lines are lines that connect two nodes which lie on the solubility curve, and show the compositions of two immiscible phases in equilibrium at a specific composition.

Previous to the estimation of the tie-lines compositions, different ternary mixtures with known composition within the homogeneous region of the diagram were prepared, ensuring enough points distributed through all the miscible region so as to best characterize the ternary system, as shown in Fig. 3[62,89]. Then, experimental data of density (ρ_i) and conductivity (μ_i) of the samples were measured and fitted to a polynomial equation, equation (33) [89].

$$Q' = \sum_{i=1}^{n} \sum_{j=1}^{m} A_{ij} w_i^m \tag{33}$$

where Q' refers to the physical property (density, ρ_i, or conductivity, μ_i), n is the number of components of the ternary mixtures, m is the degree of the polynomial, w_i is the mass fraction of component i, and A_{ij} are the adjustable parameters.

The error given by equation (34) was minimized using Microsoft Excel Solver.

$$E = \sqrt{\sum_{i}^{k} (Q' - Q)/k} \tag{34}$$

where E is the error, Q' is the calculated physical property (ρ_i or μ_i) and k is the number of data points obtained.

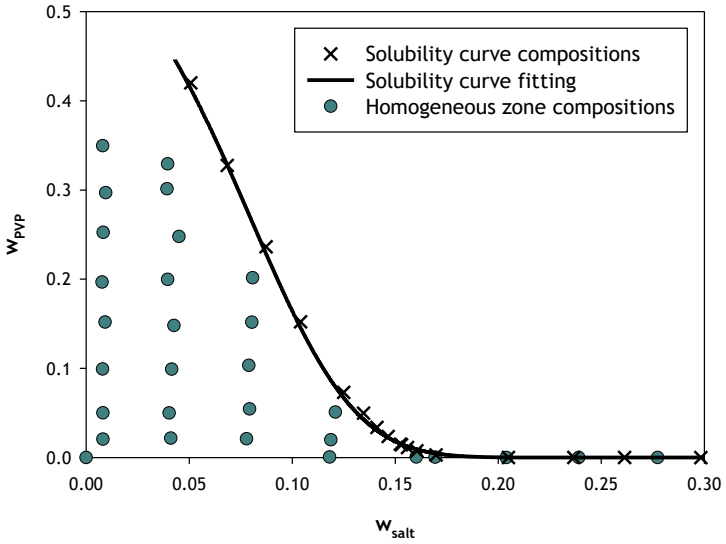


Fig. 3 - Solubility curve and homogeneous zone feed compositions for {PVP (1) + NaKTartrate (2) + Water (3)} at 298.15 K and 0.1 MPa.

For the determination of phase separation, ternary mixtures with known compositions within the immiscible region were weighted in vials and sealed with parafilm, to avoid losses by evaporation and contamination of the sample. Then, the samples were stirred in the vortex for 1 minute and placed into a thermostatic bath at 298.15 K where these were left to stir for 6 h to allow an intimate contact between the two phases. Later, they were left to settle overnight (~12 h) to ensure the achievement of the equilibrium and an adequate phase splitting. After the phase separation, samples of top and bottom phases were taken with pipettes. By crossing the correlations previously obtained for ρ_i' and μ_i', it was possible to estimate the values of mass fraction of PVP and salt in the samples[89,95].

However, the mass balance must be verified, so 4 equations were taken into account to calculate the mass fractions of each component:

$$\begin{cases} w_{\mathrm{PVP}} + w_{\mathrm{salt}} + w_{\mathrm{water}} - 1 = 0 \\ \rho_i - \mathrm{f}(w) = 0 \\ \mu_i - \mathrm{g}(w) = 0 \\ m_{\mathrm{feed}} \cdot w_{\mathrm{feed}} - m_{\mathrm{top}} \cdot w_{\mathrm{top}} - m_{\mathrm{bottom}} \cdot w_{\mathrm{bottom}} = 0 \end{cases} \quad (35)$$

where ρ and μ are the measured density and conductivity, respectively, and $\mathrm{f}(w)$ and $\mathrm{g}(w)$ are the fitted polynomial equations of the properties density and conductivity, respectively.

Once the tie-line compositions were determined, the lengths of the tie-lines (TLL) were calculated using equation (36). The tie-line length gives relevant information on the broadness of the two-phase region in the phase diagram: the longer the tie-line the more uneven the distribution of the phases. It characterizes the relative amounts of the two phases[62,89,90].

$$\mathrm{TLL} = \sqrt{(w_{\mathrm{PVP}}^{\mathrm{top}} - w_{\mathrm{PVP}}^{\mathrm{bot}})^2 + (w_{\mathrm{salt}}^{\mathrm{top}} - w_{\mathrm{salt}}^{\mathrm{bot}})^2} \times 100\% \quad (36)$$

where the subscripts PVP and salt refer to compositions of PVP and salt in mass fraction, respectively, and the superscripts top and bot refer to the top and bottom phases, respectively.

Another important characteristic is the tie-lines slope (STL), calculated according to equation (37), which provides information about the relative solubilities of the components in the two liquid phases[62,89,90]. Moreover, it is known that the highest the slope, the larger the difference in the distribution of components between the phases[62,89,90].

$$\mathrm{STL} = (w_{\mathrm{PVP}}^{\mathrm{top}} - w_{\mathrm{PVP}}^{\mathrm{bot}})/(w_{\mathrm{salt}}^{\mathrm{top}} - w_{\mathrm{salt}}^{\mathrm{bot}}) \quad (37)$$

where the subscripts PVP and salt refer to compositions of PVP and salt in mass fraction, respectively, and the superscripts top and bot refer to the top and bottom phases, respectively.

Moreover, the relation between the equilibrium compositions of the ternary systems was tested using the equations (38) and (39), proposed by Othmer-Tobias[96] and Brancroft[97], respectively,[88]. These equations are used to obtain tie-line interpolations, by adjusting the parameters K_1 and n, for the Othmer-Tobias equation, and K_2 and r, for the Brancroft equation[88]. These equations provide a means to interpolate tie-lines and avoid the time-consuming experimental procedure.

$$\log\left[\frac{1 - w_{\mathrm{PVP}}^{\mathrm{top}}}{w_{\mathrm{PVP}}^{\mathrm{top}}}\right] = K_1 + n \cdot \log\left[\frac{1 - w_{\mathrm{salt}}^{\mathrm{bot}}}{\mathrm{w}_{\mathrm{salt}}^{\mathrm{bot}}}\right] \quad (38)$$

$$\log\left[\frac{w_{\mathrm{water}}^{\mathrm{bot}}}{w_{\mathrm{salt}}^{\mathrm{bot}}}\right] = K_2 + r \cdot \log\left[\frac{w_{\mathrm{water}}^{\mathrm{top}}}{w_{\mathrm{salt}}^{\mathrm{top}}}\right] \quad (39)$$

where $w_{\mathrm{PVP}}, w_{\mathrm{water}}$ and w_{salt} are the mass fraction of PVP, water and salt, respectively, and the superscripts top and bot denote top and bottom phases, respectively.

3.3.3 pH study

The pH of an ATPS can influence the partitioning of biomolecules by the alteration of the electrical charge and surface properties of the solute[9]. To investigate how pH impacts the ultraviolet-visible (UV-Vis) absorbance spectra of resveratrol (RVT), ferulic acid (FA) and gallic acid (GA), the mean electrical charge (q) of each antioxidant was calculated as a function of pH, using the negative base-10 logarithm of their acid dissociation constants ($\mathrm{p}K_\mathrm{a}$).

The acid dissociation constant (K_a) of the reaction of an acid in water is calculated according to[98]:

$$K_\mathrm{a} = \frac{[\mathrm{A}^-][\mathrm{H_3O}^+]}{[\mathrm{HA}][\mathrm{H_2O}]} \tag{40}$$

where $[\mathrm{HA}]$, $[\mathrm{H_2O}]$, $[\mathrm{A}^-]$ and $[\mathrm{H_3O}^+]$ refer to the concentrations of the species in solution of a generic acid, water and their ionized species, respectively.

Considering constant the concentration of water and taking the negative logarithm of both terms, the negative base-10 logarithm of their acid dissociation constants ($\mathrm{p}K_\mathrm{a}$), can be calculated according to equation (41). The values of $\mathrm{p}K_\mathrm{a}$ for GA, FA and RVT, taken from literature, are shown in Table 2.

$$\mathrm{p}K_\mathrm{a} = \log\left(\frac{[\mathrm{HA}]}{[\mathrm{A}^-]}\right) + \mathrm{pH} \tag{41}$$

Table 2 - Values of pK_a of the studied antioxidants: gallic acid, ferulic acid and resveratrol.

Antioxidant	$\mathrm{p}K_\mathrm{a}$ values
Gallic acid	4.28, 8.62, 11.90[99], >13[100]
Ferulic acid	4.50, 8.92[101]
Resveratrol	8.73, 9.56, 10.88[102]

Given that these specific phenolic compounds may present acidic behavior under certain pH conditions, the relative abundance of a certain acidic stage with respect to its conjugate base was calculated according to[64]:

$$\frac{\left[\mathrm{A}^{q_0-i+1}\right]}{\left[\mathrm{A}^{q_0-i}\right]} = 10^{\mathrm{pH_{phase}} - \mathrm{p}K_\mathrm{a}^i} \tag{42}$$

where q_0 is the initial electrical charge (at pH = 0), i is the number of the dissociation constant ($\mathrm{p}K_\mathrm{a}^i$) under observation, $\mathrm{pH_{phase}}$ is the pH of the phase, and $\left[\mathrm{A}^{q_0-i+1}\right]$ and $\left[\mathrm{A}^{q_0-i}\right]$ are the mole concentrations of the antioxidant species with electrical charges equal to $(q_0 - i + 1)\,\mathrm{e}$ and $(q_0 - i)\,\mathrm{e}$, respectively, and e stands for the elementary charge $\left(1.602 \cdot 10^{-19}\ \mathrm{C}\right)$.

After calculating the relative abundances for each conjugate acid-base pair, the mole fraction of each antioxidant species with an electrical charge equal to $(q_0 - i + 1)\,\mathrm{e}$ was determined using equation (43)[64].

$$x_{\mathrm{A}^{q_0-i+1}} = \frac{[\mathrm{A}^{q_0-i+1}]}{[\mathrm{A}^{q_0-i}]} \Bigg/ \left(\frac{[\mathrm{A}^{q_0}]}{[\mathrm{A}^{q_0-1}]} + 1 + \sum_{j=2}^{i_{\max}} \left[\prod_{k=2}^{j} \frac{[\mathrm{A}^{q_0-k}]}{[\mathrm{A}^{q_0-(k-1)}]} \right] \right) \tag{43}$$

where i is the number of the dissociation constant under observation and $i_{\max}$ is the maximum number of radicals the antioxidant can donate.

Next, the mean electrical charge of the antioxidant in solution (q) was calculated using the weighted arithmetic mean, as follows:

$$q = \sum_{i=1}^{i_{\max}} \left[x_{\mathrm{A}^{q_0-i+1}} \cdot (q_0 - i + 1) \right] + \left[\sum_{i=1}^{i_{\max}} \left(x_{\mathrm{A}^{q_0-i+1}} \right) \right] \cdot (q_0 - i_{\max}) \tag{44}$$

Afterwards, five stock solutions of GA (~ $2.00 \cdot 10^{-4}\ \mathrm{g \cdot mL^{-1}}$), FA (~ $1.22 \cdot 10^{-4}\ \mathrm{g \cdot mL^{-1}}$) and RVT (~ $6.57 \cdot 10^{-5}\ \mathrm{g \cdot mL^{-1}}$) were prepared close to maximum solubility, according to the measurement range of the spectrophotometer at 298.15 K and at pH conditions near the known pH values of the applied ATPS.

When required, the pH of the solutions was adjusted by gradualllly adding droplets of either a 0.5 M sodium hydroxide (NaOH) solution to increase pH or 0.5 M acetic acid (CH_3COOH) solution to decrease pH. Each addition was followed by 30 min of mixing in the magnetic stirrer. Then, the antioxidant concentrations were recalculated considering the added quantity of the pH adjusters. Afterwards, an UV-Vis absorbance scan was carried out from 200 to 600 nm, with temperature stabilization of the 200 μL samples at 298.15 K.

Lastly, to assess the stability of the UV-Vis absorbance spectra, the prepared solutions were allowed to settle for a period of 3 days without any special protection from daylight, and the absorbance scan was repeated following the same procedure, after stirring the solutions for 30 min, as represented in Fig. 4.

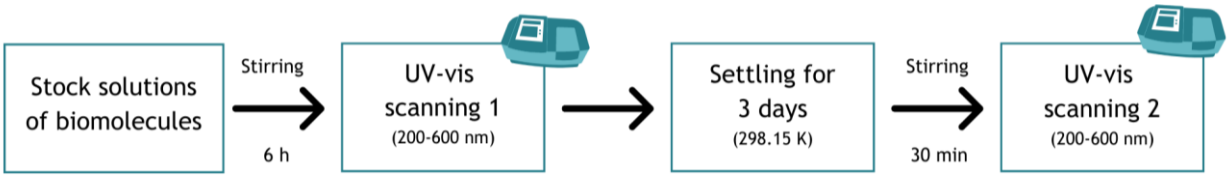


Fig. 4 - Scheme of the procedure of the pH stability study.

The concentrations were normalized to reduce the effect of dilution by the pH adjusters' addition (NaOH or CH_3COOH) on the absorbance spectra using[64]:

$$A' = A \cdot \frac{C_{\mathrm{pH}=7}}{C_{\mathrm{pH}=k}} \tag{45}$$

where A' is the normalized absorbance, A refers to the experimental UV-Vis absorbance for a given wavelength (λ), $C_{\mathrm{pH}=7}$ is the reference concentration at pH = 7.5 and $C_{\mathrm{pH}=k}$ is the concentration of the stock solution of species at pH = k.

3.3.4 UV-Vis absorbance calibration curves

In order to determine the concentration of the antioxidants in an unknown sample, first a calibration curve with standard samples of known concentration had to be prepared.

To determine the UV-Vis absorbance calibration curves, mixtures with a volume of 2 mL were prepared by diluting aqueous solutions of antioxidants (~ $2.00 \cdot 10^{-4}\ \mathrm{g \cdot mL^{-1}}$ for GA, ~ $1.22 \cdot 10^{-4}\ \mathrm{g \cdot mL^{-1}}$ for FA and ~ $6.57 \cdot 10^{-5}\ \mathrm{g \cdot mL^{-1}}$ for RVT), at a pH value of ~ 7. The prepared solutions were placed in vials, which were then tightly sealed with parafilm to prevent evaporation, and vigorously stirred in a vortex for about 1 min. Afterwards, $200\ \mu\mathrm{L}$ samples were taken from each vial and analyzed using the UV-Vis spectrophotometer. An absorbance scan was conducted in the wavelength from 200 to 600 nm. Lastly, the calibration curves were prepared by plotting the antioxidants' concentrations and the respective UV-vis absorbances at the chosen wavelengths. Then, the absorbances of the blanks (purified water and plate) were subtracted to the experimental data and fitted to a first-degree equation, as shown in equation (46). The chosen wavelengths were 260, 310 and 306 nm for GA, FA and RVT, respectively, and represented local UV-Vis absorbance maxima.

$$\mathrm{A} = \alpha \mathrm{C} + \beta \tag{46}$$

where A is UV-Vis absorbance, α is the slope of the calibration curve, C is the antioxidant concentration (in $\mathrm{g \cdot mL^{-1}}$) and β is the y-intercept.

3.3.5 Liquid-liquid extraction

Due to the availability of the liquid-liquid equilibria (LLE) in previous works[18,62,89], the solubility curve and tie-lines' compositions were not determined in this work, and the partitioning of the phenolic compounds was conducted at 298.15 K and 0.1 MPa in the previously reported tie-lines of the systems {EL (1) + Na_3Citrate (2) + Water (3)}[89], {EL (1) + K_3Citrate (2) + Water (3)}[89], {EL (1) + NaKTartrate (2) + Water (3)}[18] and {EL (1) + Na_2Succinate (2) + Water (3)}[62], which can be observed in Table BB.1.

In order to subtract the absorbance of the samples with only ethyl lactate, salt and water to the ones with the presence of each antioxidant, first blank samples were prepared for all the studied systems. For each established tie-line, blanks were determined following the procedure: ternary mixtures were prepared with EL, salt and water, and left to settle overnight

(~12 h) after being stirred for 6 h, at 298.15 K and 0.1 MPa. After the separation of phases, each phase was taken to vials, weighted and some properties were measured, such as mass, pH, absorbance and density.

Aqueous solutions of each antioxidant, with compositions of $\sim 2.00 \cdot 10^{-4}\ \mathrm{g \cdot mL^{-1}}$, $\sim 1.22 \cdot 10^{-4}\ \mathrm{g \cdot mL^{-1}}$ and $\sim 9.16 \cdot 10^{-5}\ \mathrm{g \cdot mL^{-1}}$ for GA, FA and RVT, respectively, were prepared by weighing. These compositions corresponded to the maximum solubility of the phenolic compounds that can be measured by the equipment at 298.15 K and 0.1 MPa.

Then, feed compositions of the tie-lines of each ternary system with 10 g of solution were gravimetrically prepared in glass cells. Then, to maintain the same composition of the tie-lines, 1 mL of water was substituted by 1 mL of stock solution of the antioxidants being studied. Following, all vials were capped, sealed with parafilm and stirred for at least 6 h and left still overnight in a bath at 298.15 K, to allow complete phase equilibrium. After the separation of phases, samples from the two phases were pipetted and weighed.

To evaluate the performed phase separation, the mass losses (L_{m}) were determined using:

$$L_{\mathrm{m}}\ /\ \% = \frac{m_{\mathrm{phases}} - m_{\mathrm{feed}}}{m_{\mathrm{feed}}} \cdot 100 \tag{47}$$

where m_{feed} is the feed mass and m_{phases} is the sum of masses of the two separated phases.

The concentrations of the antioxidants in each phase were quantified using UV-Vis spectroscopy, at wavelengths of 260 nm for GA, 310 nm for FA and 306 nm for RVT and using the calibration curves previously established. To minimize potential interferences from salt or EL on the absorbance values of mixtures, all samples were analyzed against blanks, *i.e.*, the same phase of each tie-line but lacking the presence of the specific antioxidant being analyzed. Interferences of the other components in the sample, were found to be negligible.

Partition coefficients (K), that describe the concentration ratio of the antioxidants between two phases at equilibrium with each other, were calculated using equation (48)[89,103].

$$K = [\mathrm{antioxidant}]_{\mathrm{top}} / [\mathrm{antioxidant}]_{\mathrm{bot}} \tag{48}$$

where [antioxidant] is the concentration of antioxidants in g·mL^{-1} and the subscripts top and bot indicate top and bottom phases, respectively.

The extraction efficiencies (E) were calculated for each tie-line using:

$$E = m^{\mathrm{top}}_{\mathrm{antioxidant}} / m^{\mathrm{bot}}_{\mathrm{antioxidant}} \tag{49}$$

$m_{\mathrm{antioxidant}}$ refer to the mass of antioxidants in the indicated phase, and the subscripts top and bot indicate top and bottom phases, respectively, on both equations.

In equation (41), the concentration of antioxidants is given in $\mathrm{g \cdot mL^{-1}}$; therefore to calculate the mass of antioxidant in each phase (equation (42)), it is necessary to know the volume of each phase. Since both phases were weighted, the total mass of each phase is known and one can convert it to volume, by dividing the mass by density.

Additionally, to ensure the accuracy and reliability of the experimental results, mass balance calculations were carried out. Furthermore, pH values of samples from all phases were measured at 298.15 K and 0.1 MPa. The procedure is represented in Fig. 5. Some pictures taken during the experimental procedures are shown in Appendix A.

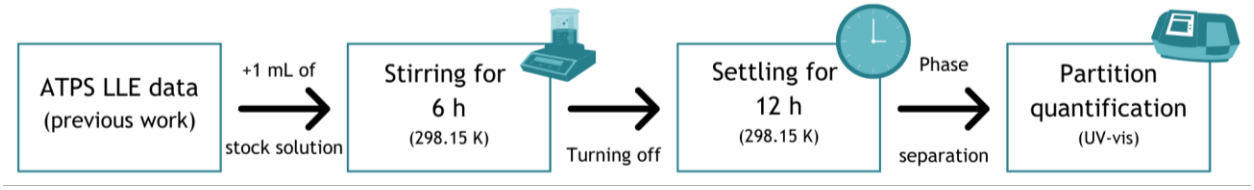


Fig. 5 - Procedure of the liquid-liquid extraction of antioxidants.

3.3.6 Thermodynamic modeling

Thermodynamic modeling is fundamental to predict the behavior of both phases of an ATPS and to its future application in industry, since it is time consuming to experimentally study the phase separation in every condition[89]. So far, there is a lack of modeling studies considering ionized species, so, for this reason, the electrolyte non-random two-liquid (e-NRTL) thermodynamic model was used in this work to describe the liquid-liquid equilibrium phase diagrams, as explained in Sections 2.4 and 2.5[19,68].

In order to perform the modeling, some initial variables of each component are required such as the temperature (T) and pressure (P) of the studied system, the electrical charges of each ion of the salt (z_i), the molecular masses of all species (M_i), as well as the compositions of the three species (EL, salt and water) in each phase (w_i) and the mass density (ρ_i) and dielectric constants (ε_i) of the neutral species. Lastly, the van der Walls volume (V_{w}) of the anions were calculated according to the Bondi method, and the radii of the cation was calculated using the van der Waals radii (r_{w_i}) by means of equation (19). Then, these data were exported from an Excel file to MatLab, where the modeling was performed, since this tool is capable of performing complicated calculations without being too time-consuming[19,66].

Initially, since it is assumed that the salt dissociates, *i.e.*, it divides into its constituent ions, the compositions of the three species were calculated for the new matrix of four species. Further, two adjustments were performed: one intended to find optimized values of τ_{ij}, so an initial guess is given, as well as a lower and upper bound; then, knowing the values of τ_{ij} another optimization is made, and the values of composition of each species in the top and bottom phases are determined.

The general phase equilibrium condition used to calculate liquid-liquid equilibrium is the equality of activity coefficients - isoactivity criterion (I.C.) - between the top and bottom phases, which is represented by equation (50). This approach calculates the difference in activities between the two liquid phases and is strongly dependent on the initial estimates[71,104].

$$\text{I. C.} = \frac{\sum_{i=1}^{N_{\text{species}}} \sum_{j=1}^{N} (x_{ij}^{\text{T}} \gamma_{ij}^{\text{T}} - x_{ij}^{\text{B}} \gamma_{ij}^{\text{B}})}{N} = 0 \tag{50}$$

where N is the number of equilibria points of the top and bottom phases, N_{species} is the number of species, x_{ij}^{T} and x_{ij}^{B} refer to the mole fraction of species i for the j LLE point for the top and bottom phases, respectively, and γ_{ij}^{T} and γ_{ij}^{B} to the activity coefficients of species i for the j LLE point for the top and bottom phases, respectively.

In order to verify the isoactivity criterion (I.C. = 0), the MATLAB code arbitrated the values of τ_{ij} and applied the PDH+NRTL model and recalculated the IC value until it reached zero. Later, the code recalculated the molar fraction of each component in the top and bottom phases, presenting these results to the user. The algorithm is represented in Fig. 6.

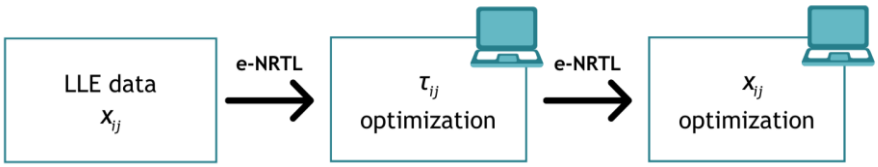


Fig. 6 – Algorithm for the optimization of τ_{ij} and x_{ij} using the e-NRTL model.

4 Results and discussion

In this chapter, the solubility curve and the corresponding tie-lines of the ATPS {polyvinylpyrrolidone (1) + sodium potassium tartrate (2) + water (3)} were determined. Additionally, the influence of pH on the absorbance spectra of resveratrol, gallic acid and ferulic acid was studied and the results of the partitions of these antioxidants in ATPS containing ethyl lactate, water and different salts were discussed. Lastly, the experimental outcomes were compared to the values obtained by the electrolyte non-random two-liquid (e-NRTL) model.

4.1.1 Liquid-liquid equilibria

In this work, the solubility curve of the aqueous two-phase system (ATPS) {polyvinylpyrrolidone 29k (1) + sodium potassium tartrate (2) + water (3)} was experimentally evaluated at 298.15 K and 0.1 MPa. Therefore, experimental cloud-points for this ternary mixture were determined and the mass fraction referent to each point was determined, as described in Section 3.3.1 and shown in Table 3.

Table 3 - Solubility curve data (mass fraction, w_i) for the ternary systems {PVP (1) + NaKTartrate (2) + Water (3)} determined experimentally at 298.15 K and 0.1 MPa.

{PVP (1) + NaKTartrate (2) + Water (3)}					
w_{PVP}	$w_{\mathrm{NaKTartrate}}$	w_{PVP}	$w_{\mathrm{NaKTartrate}}$	w_{PVP}	$w_{\mathrm{NaKTartrate}}$
0.4137	0.0507	0.0325	0.1411	0.0014	0.1698
0.3291	0.0684	0.0183	0.1456	0.0010	0.2050
0.2251	0.0872	0.0104	0.1525	0.0010	0.2367
0.1447	0.1040	0.0098	0.1530	0.0009	0.2613
0.0740	0.1249	0.0054	0.1560	0.0008	0.2983
0.0516	0.1346	0.0028	0.1606	-	-

These data points were fitted to the equations (28), (29), (30) and (31), proposed by Han *et al.*[91], Merchuk *et al.*[92], Hu *et al.*[93] and Jayapal *et al.*[94], respectively. The calculated adjustable parameters are shown in Table 4, as well as the standard deviation values for each equation. The solubility curve fitting values according to each equation are shown in Table B.1 and graphically represented in Figs. B.1-B.4, in Appendix B.

The lowest value of standard deviation (σ) was obtained for the Merchuk equation, so it can be inferred that it more adequately represented the experimental values of the solubility curve.

Table 4 - Fitting parameters obtained with equations proposed by Han *et al.*[91], Merchuk *et al.*[92], Hu *et al.*[93] and Jayapal *et al.*[94] and standard deviation for the experimental solubility curves data.

Equation	*A*	*B*	*C*	*D*	σ
Han *et al.*[91]	-0.13	-20.84	200.15	-1575.67	$1.43 \cdot 10^{-2}$
Merchuk *et al.*[92]	0.69	-1.79	874.35	-	$5.09 \cdot 10^{-11}$
Hu *et al.*[93]	0.93	-12.13	51.21	-70.04	$3.10 \cdot 10^{-2}$
Jayapal *et al.*[94]	1.68	-7.27	7.77	-	$2.04 \cdot 10^{-4}$

The tie lines' mass compositions were calculated by crossing two isolines of the physical properties density (ρ_i) and conductivity (μ_i). These experimental data were fitted to a polynomial expression, using equation (51). The adjustable parameters of the polynomial expressions for each physical property are presented in Table 5.

Table 5 - Polynomial expressions for density and conductivity as function of the composition for {PVP (1) + NaKTartrate (2) + Water (3)} at 298.15 K and 0.1 MPa.

{PVP (1) + NaKTartrate (2) + Water (3)}
$\rho = 1.9733w_{\mathrm{salt}} - 0.1364{w_{\mathrm{salt}}}^2 + 0.7963{w_{\mathrm{salt}}}^3 + 1.4667w_{\mathrm{PVP}} + 0.2275{w_{\mathrm{PVP}}}^2$ $-0.3590{w_{\mathrm{PVP}}}^3 + 0.2871w_{\mathrm{water}} + 1.1434{w_{\mathrm{water}}}^2 - 0.4336{w_{\mathrm{water}}}^3$
$\mu = -201.01w_{\mathrm{salt}} + 117.17{w_{\mathrm{salt}}}^2 - 3883.37{w_{\mathrm{salt}}}^3 - 871.73w_{\mathrm{PVP}} + 762.40{w_{\mathrm{PVP}}}^2$ $-47.87{w_{\mathrm{PVP}}}^3 + 1111.51w_{\mathrm{water}} - 1374.25{w_{\mathrm{water}}}^2 + 265.02{w_{\mathrm{water}}}^3$

The polynomial expressions were represented graphically in the studied range of mass fraction of PVP, salt and water, as shown in Fig. 7. The experimental and calculated values of the two physical properties (density and conductivity) and the performed *F*-test results (used to validate the fitted data) for each isoline are shown in Tables B.2 and B.3, respectively.

Experimental feed and tie-lines' compositions are shown in Table 6, along with their respective calculated lengths (TLL) and slopes (STL). The results are represented graphically in Fig. 8. TLL and STL were calculated from tie-lines compositions, according to equation (36) and equation (37), respectively. Moreover, as pH plays a critical role in determining the partitioning behavior of biomolecules, the pH values of both phases were evaluated. Different pH values may alter the charge and surface properties of the solute, which affects the partition of antioxidants. The pH of both phases is similar and approximately equal to 6.5, so the stock

solutions with antioxidants studied in this ATPS must be close to this value, in order to assure that the obtained values are valid.

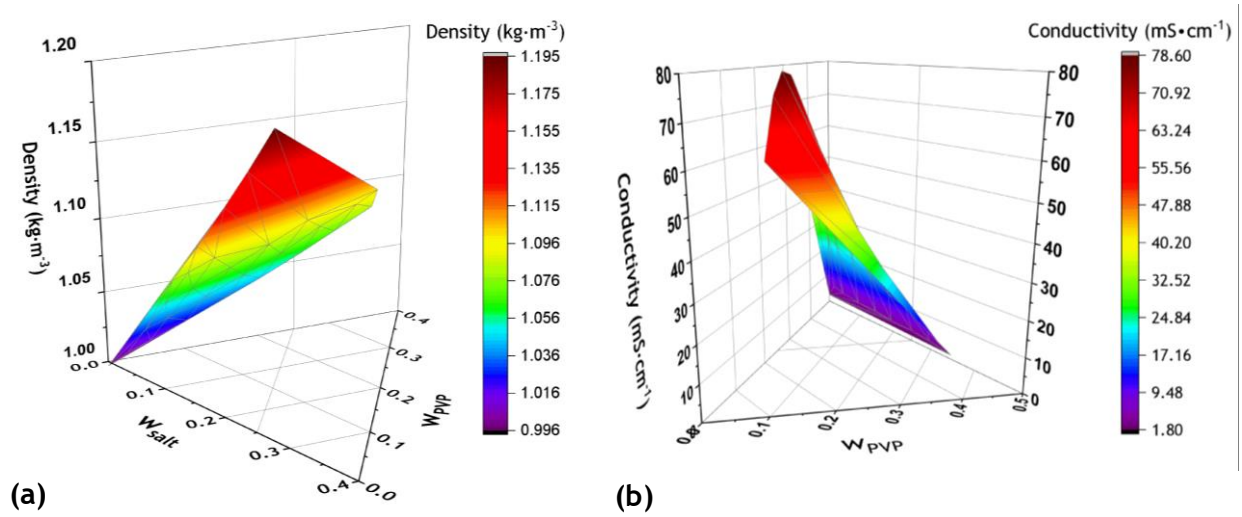


Fig. 7 – Representation of the polynomial expressions for density (a) and conductivity (b) as function of composition for {PVP (1) + NaKTartrate (2) + Water (3)} at 298.15 K and 0.1 MPa.

Table 6 - Tie-line equilibria data in the top and bottom phases for the ternary system {PVP (1) + NaKTartrate (2) + Water (3)} at 298.15 K and 0.1 MPa.

No. TL	Feed		Top phase			Bottom phase			TLL / *m*%	STL
	$w_{PVP,\ feed}$	$w_{salt,\ feed}$	$w_{PVP,\ top}$	$w_{salt,\ top}$	pH	$w_{PVP,\ bot}$	$w_{salt,\ bot}$	pH		
TL1	0.0551	0.1625	0.3547	0.0603	6.61	0.0014	0.1824	6.43	37.39	2.89
TL2	0.0751	0.1624	0.3722	0.0575	6.60	0	0.1896	6.34	39.50	2.82
TL3	0.0951	0.1626	0.3857	0.0531	6.46	0	0.1985	6.29	41.22	2.65
TL4	0.1148	0.1627	0.3973	0.0486	6.57	0	0.2080	6.50	42.81	2.49
Tl5	0.1349	0.1623	0.4119	0.0443	6.73	0	0.2222	6.63	44.87	2.32
TL6	0.1545	0.1626	0.4262	0.0403	6.83	0	0.2332	6.68	46.79	2.21

Higher TLL values indicate a greater extent of separation, *i.e.*, larger differences between the compositions of top and bottom phases. As it can be inferred, a higher composition of PVP in the feed resulted in higher values of tie-line lengths and, consequently, the top phase became enriched with PVP, while the bottom phase became enriched with salt. Therefore, the top phase is the PVP-rich phase and the bottom phase is the salt-rich phase for the studied ATPS. Regarding the slope of the tie-lines, these are not perfectly parallel, as indicated by the slight different in the STL values. It is important to note that the concentration of PVP in the bottom phase is almost negligible and constant, which means that the PVP migrates towards

the top phase. This can be explained by the fact that this polymer is nonpolar, therefore, it is repelled by the salt (a polar chemical structure), migrating to the top phase.

In Fig. 8, the good fit of the Merchuk equation to the experimental data for the ternary system studied in this work can be checked, together with the experimental feed points used to describe the homogeneous zone of the diagram. As shown in this figure, six tie-lines were obtained, which, in general, is considered the minimum number of equally spaced tie-lines required to cover the complete LLE region. Since the cloud-point method depends on the visual perception of the observer, it is not a rigorous technique, therefore, it implies that the obtained solubility curve is actually a band of values that separates the homogeneous and immiscible zone.

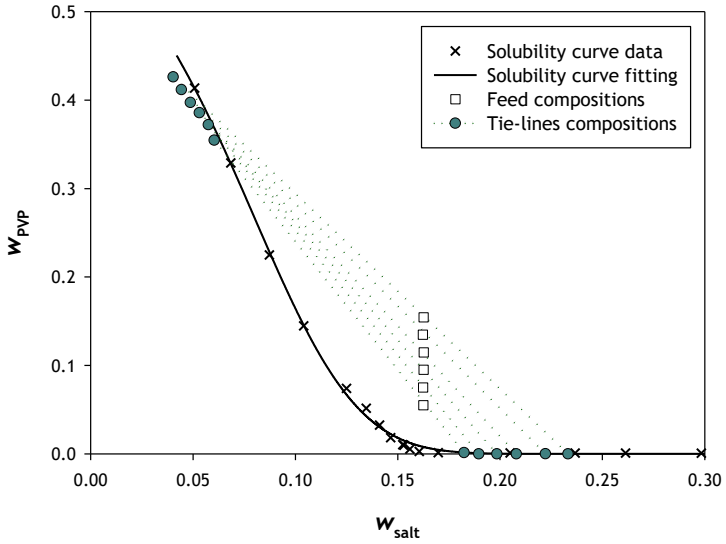


Fig. 8 - Solubility curve and corresponding tie-lines for the ternary system {PVP (1) + NakTartrate (2) + water (3)} at 298.15 K and 0.1 MPa. (□) feed compositions, (x) solubility curve, (-) fit of the solubility curve and (o) experimental tie-lines compositions.

To attain tie-line interpolation, the Othmer-Tobias[96] and Brancroft[97] equations, equation (38) and (39), respectively, were used to obtain the adjustable parameters plotting the logarithmic graph. These are shown in Table 7, as well as the correlation coefficients (R^2).

Table 7 - Parameters obtained using Othmer-Tobias[96] and Brancroft[97] equations with the respective correlation coefficients (R^2).

Othmer-Tobias			**Brancroft**		
K_1	n	R^2	K_2	r	R^2
0.237	0.106	0.992	0.222	0.395	0.976

Hence, in order to interpolate more tie-line compositions, equations (52) and (53) should be applied.

$$\log\left[\frac{1-w_{\mathrm{PVP}}^{\mathrm{top}}}{w_{\mathrm{PVP}}^{\mathrm{top}}}\right] = 0.237 + 0.106 \cdot \log\left[\frac{1-w_{\mathrm{salt}}^{\mathrm{bot}}}{\mathrm{w}_{\mathrm{salt}}^{\mathrm{bot}}}\right] \quad (52)$$

$$\log\left[\frac{w_{\mathrm{water}}^{\mathrm{bot}}}{w_{\mathrm{salt}}^{\mathrm{bot}}}\right] = 0.222 + 0.395 \cdot \log\left[\frac{w_{\mathrm{water}}^{\mathrm{top}}}{w_{\mathrm{salt}}^{\mathrm{top}}}\right] \quad (53)$$

4.1.2 pH study

In order to evaluate the solubility and stability of the antioxidants with different charges, it is crucial to study the mean electrical charge (q) of biomolecules since different $\mathrm{p}K_{\mathrm{a}}$ values correspond to the donation of a hydrogen proton and, therefore, to the formation of differently charged chemical structures, known as the biomolecules stages, which affect the UV-Vis absorbance spectra[17]. These stages show different affinities to the ATPS phases since different electrical charges may affect the dielectric constant, the ionic strength, the viscosity and reactivity of the solution[17]. Therefore, this evaluation is essential to understand if the used ATPS are suitable to extract the antioxidants without affecting their structures and to determine the pH of the stock solution that should be used.

The reported $\mathrm{p}K_{\mathrm{a}}$ values of the studied antioxidants are 8.73, 9.56 and 10.88 for resveratrol (RVT)[102], 4.50 and 8.92 for ferulic acid (FA)[101] and 4.28, 8.62, 11.90 and >13[99,100] for gallic acid (GA). Moreover, using equation (44), the mean electrical charge (q) of these antioxidants was calculated as a function of pH, as shown in Tables C.1-C.3, in Appendix C, and represented in Fig. 9, as well as the chemical structures of the studied antioxidants with the order of donated protons (H^+).

Resveratrol is a weak acid constituted by three hydroxyl groups attached to the benzoic acid ring that, when are deprotonated, result in different acidic dissociation constants[105,106]. This antioxidant is reasonably stable in acidic media since it has two phenols joined together by a double bond. However, at pH higher than 7, it starts to ionize quickly, as observed in Figs. C.1-C4, in Appendix C. Both ferulic acid and gallic acid contain a carboxyl group, which is more acid than the phenolic -OH groups, therefore, these protons are the first ones to be donated[107]. Since the $\mathrm{p}K_{\mathrm{a}}$ values of ferulic acid and gallic acid are similar, their mean electrical charges are alike until pH = 10. However, gallic acid presents more hydroxyl groups, resulting in an additional altered charge, *i.e.*, the donation of more protons (H^+), and, therefore, an extra value of $\mathrm{p}K_{\mathrm{a}}$. Furthermore, the effect of pH (acidic, neutral and basic conditions) on the UV-Vis absorbance spectra was assessed by preparing concentrations of each antioxidant at different pH values and measuring their absorbance spectra, as shown in Figs. C.5-C12, in Appendix C.

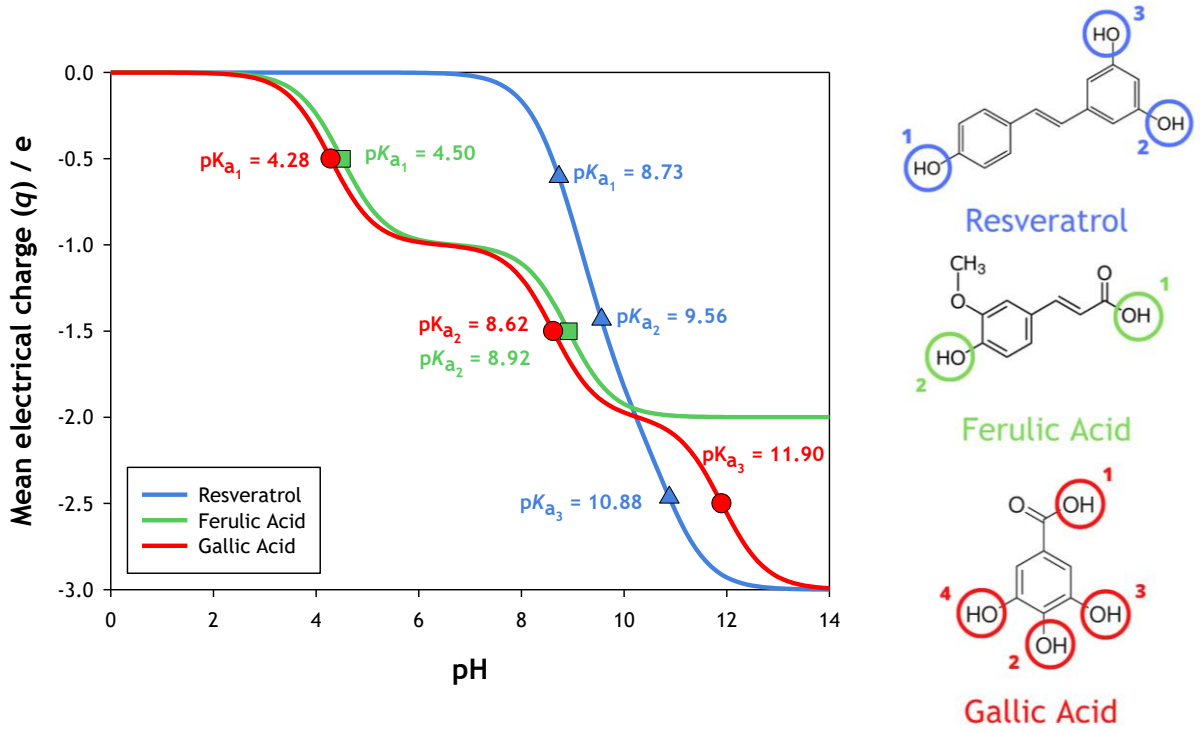


Fig. 9 - Calculated mean electrical charge (q) for resveratrol (triangles), ferulic acid (squares) and gallic acid (circles), expressed in terms of the elementary charge (e), *i.e.*, $1.602 \cdot 10^{-19}\ C$.

In Fig. 10, the UV-Vis absorbance spectra of resveratrol for different normalized pH values can be observed. The results are consistent with the expected behavior since until pH = 7, the spectra is stable, suffering a decrease with the increase of pH. However, three different responses of the spectra are detected for pH > 7, corresponding to the three donated H^+ that result in three differently charged species (monoanion, dianion and trianion)[106]. As the pH changed from the acid to the alkaline side, the UV-Vis absorbance near 306 nm increased and shifted to lower wavelength values, due to the appearance of a new chemical structure.

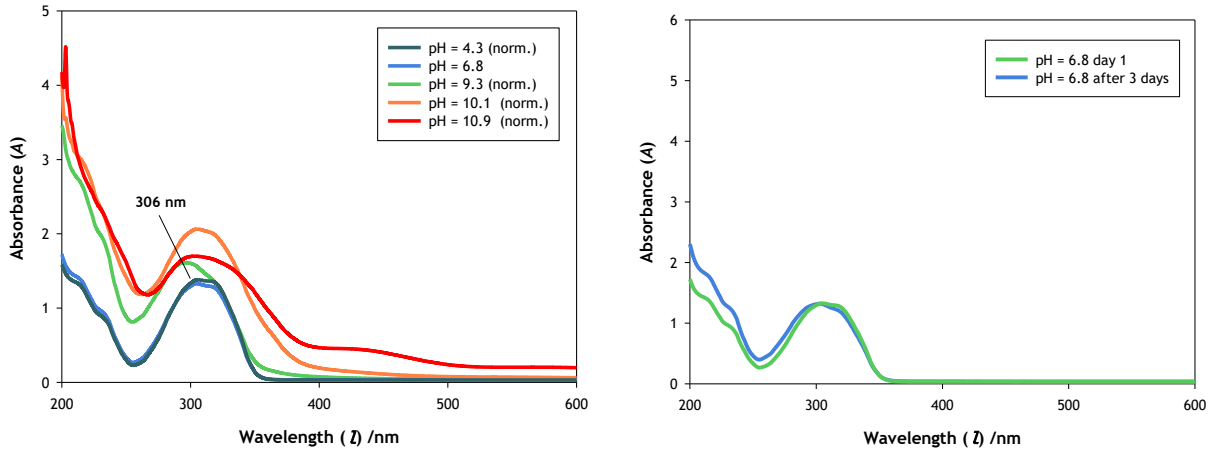


Fig. 10 - Influence of pH on the UV-Vis absorbance spectra of resveratrol ($\sim 9.16 \cdot 10^{-5} g \cdot mL^{-1}$) at 298.15 K and 0.1 MPa (*left*). Study of UV-Vis absorbance spectra stability for resveratrol ($\sim 9.16 \cdot 10^{-5} g \cdot mL^{-1}$) in the moment of preparation and after 3 days of settling for the pH of the ATPS (~ 6.5-7.5) at 298.15 K and 0.1 MPa (*right*).

According to Figs. C1-C4, in Appendix C, at acidic media up to pH 6, resveratrol was shown to be stable. However, there is a rapid degradation in a alkaline medium (for pH = 10.1 and 10.9) due to hydrolysis. So, at pH values close to the one of the studied ATPS (pH = ~ 6.5) the system is still mostly stable[105].

In the case of ferulic acid, whose UV-Vis absorbance spectrum is shown in Fig. 11, the absorbance tends to decrease with larger pH in acidic conditions, although there is a shift in the relative maximum (310 nm, pH = 7.5) in the range of 250-300 nm wavelength due to the donation of a H^+ at pH close to 4.28[101]. Moreover, for higher alkaline pH values (pH = 10.6 and 12.2), the absorbance spectra presented an atypical behavior that was found to be reversible and stable with time, as Figs. C5-C8 show. Thus, ferulic acid was proven to be stable at all studied pH values, as Table 9 shows.

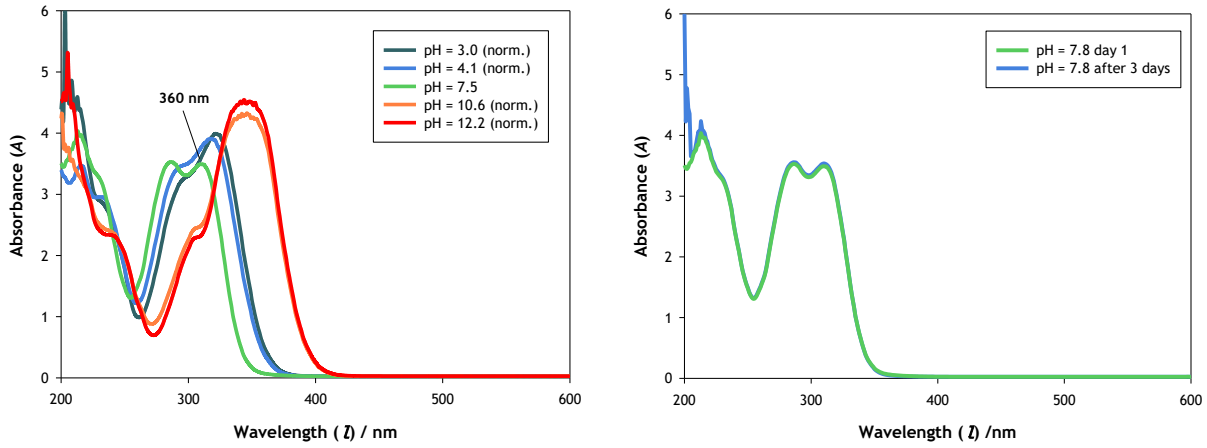


Fig. 11 - Influence of pH on the UV-Vis absorbance spectra of ferulic acid (~ $1.22 \cdot 10^{-4} \mathrm{g} \cdot \mathrm{mL}^{-1}$) at 298.15 K and 0.1 MPa *(left)*. Study of UV-Vis absorbance spectra stability for ferulic acid (~ $1.22 \cdot 10^{-4} \mathrm{g} \cdot \mathrm{mL}^{-1}$) in the moment of preparation and after 3 days of settling for the pH of the ATPS (~ 6.5-7.5) at 298.15 K and 0.1 MPa (*right*).

Additionally, the UV-Vis absorbance spectra of gallic acid was also studied, as shown in Fig. 12. In general, there is a decrease of absorbance with growing pH, with a relative maximum at 260 nm, for a pH of 7.5. However, a shift in the relative maximum in the range of 250-300 nm is proven to be caused not only by the donation of H^+, but also by the changes in chemical conformation[99,100,107]. At acidic conditions (pH = 10.5 and 12.5), a transformation in the spectra is observed due to the presence of differently charged species, caused by the oxidation of gallic acid[99]. Besides, as shown in Figs. C9-C12, in Appendix C, a drastic change in the spectra of pH = 10.5 and 12.5 after 3 days can be observed, supporting the premise of a chemical reaction at high pH values[99].

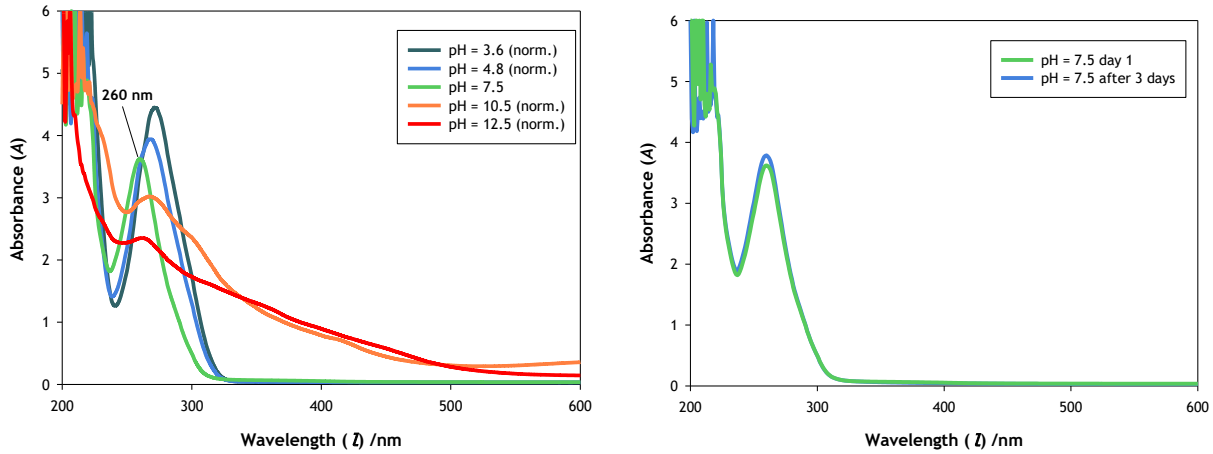


Fig. 12 - Influence of pH on the UV-Vis absorbance spectra of gallic acid (~$2.00 \cdot 10^{-4}$ g · mL^{-1}) at 298.15 K and 0.1 MPa *(left)*. Study of UV-Vis absorbance spectra stability for gallic acid (~$2.00 \cdot 10^{-4}$ g · mL^{-1}) in the moment of preparation and after 3 days of settling for the pH of the ATPS (~ 6.5-7.5) at 298.15 K and 0.1 MPa (*right*).

Previous works reported a pH in the range of 6.5 to 7.5 at 298.15 *K* and 0.1 MPa for the ternary phases of the aqueous two-phase systems: {EL (1) + Na_3Citrate (2) + Water (3)}, {EL (1) + K_3Citrate (2) + Water (3)}, {EL (1) + NaKTartrate (2) + Water (3)} and {EL (1) + Na_2Succinate (2) + Water (3)}. Therefore, and given that at this pH the solutions have mostly stable and reversible absorbance spectra, as reported in Table 8, the stocks of antioxidant used in the partitions were adjusted through addition of an acid (acetic acid) or base (sodium hydroxide), in order to obtain a pH close to the one of the system. Being so, the application of these ternary systems to extract GA, FA and RVT was validated.

Table 8 - Stability of the UV-Vis absorbance spectra of ferulic acid (FA), gallic acid (GA) and resveratrol (RVT) after settling for 3 days at 298.15 K and 0.1 MPa.

	pH									
Antioxidant	**~3.0**	**~4.0**	**~5.0**	**~6.5**	**~7.5**	**~9.0**	**~10.0**	**~11.0**	**~12.0**	**~13.0**
Resveratrol	-	S	-	MS	-	US	US	MS	-	-
Ferulic acid	S	S	-	-	S	-	-	S	S	-
Gallic acid	-	S	S	-	MS	-	-	US	-	US

S – Stable; MS – Mostly stable; US – Unstable.

4.1.3 Calibration curves

The pH value of the solutions used in the determination of the calibration curves were close to the ones available in the literature for the studied ATPS (~ pH = 7), in order to perform and adequate quantification of the antioxidants after phase separation. These were determined at the wavelengths 310, 260 and 306 nm for ferulic acid, gallic acid and resveratrol,

respectively. Solutions with different concentrations of each antioxidant were prepared, by the addition of pure water to the stock solution, in order to obtain the largest range possible of concentrations.

The maximum concentrations for the determinations were established based on the highest solubility of the species in water and on the useful absorbance range of the spectrophotometer. By subtracting the absorbances of pure water and plate, calibration curves were generated at wavelengths corresponding to relative maxima, ensuring that other ATPS species (such as ethyl lactate and salts) and the pH adjuster (sodium hydroxide) did not cause interference. The UV-Vis absorbance calibration curves data of ferulic acid, gallic acid and resveratrol, at 298.15 K and 0.1 MPa, are shown in Table 9 and in Fig. 13.

Comparing the curves obtained for resveratrol with the other two, it is possible to conclude that the range of concentrations in which this antioxidant can be used is limited and corresponds to low values, which is not favorable for large scale extraction.

Table 9 - Calibration curves data for the antioxidants resveratrol, ferulic acid and gallic acid determined at 298.15 K and 0.1 MPa.

Antioxidant	Calibration Equation	R^2
Resveratrol	$A = 2.27 \times 10^4 C_{\mathrm{RVT}} + 0.0115$	0.9985
Ferulic acid	$A = 4.33 \times 10^4 C_{\mathrm{FA}} + 0.0211$	0.9993
Gallic acid	$A = 2.29 \times 10^4 C_{\mathrm{GA}} + 0.0252$	0.9992

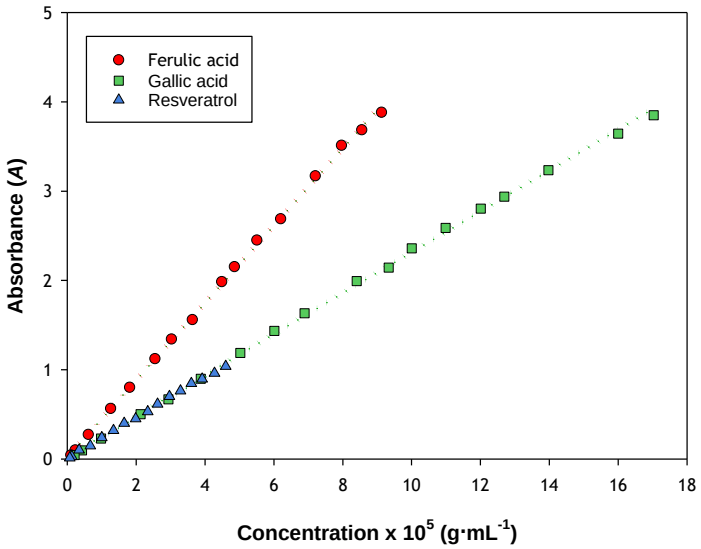


Fig. 13 - UV-Vis absorbance calibration curves for ferulic acid, gallic acid and resveratrol at pH ~ 7, 298.15 K and 0.1 MPa.

Furthermore, the calibration curves were validated through a series of parameters, shown in Tables D.1-D4, in Appendix D.

4.1.4 Liquid-liquid extraction

The potential of the aqueous two-phase systems containing ethyl lactate (EL), water and different salts, such as K_3Citrate, Na_3Citrate, Na_2Succinate and NaKTartrate, for the extraction of antioxidants (ferulic acid, gallic acid and resveratrol) was studied by preparing the partitions of these systems in feed mixtures corresponding to the known tie-line compositions. Since the partition coefficient of the solutes between the two phases is influenced by the feed compositions of the mixture, all partitions were conducted using identical initial compositions, in order to ease comparison.

After equilibrium was reached, mass, pH, density and UV-Vis absorbance of the two phases formed (top and bottom) were measured, and the mass concentrations of antioxidant were calculated through the absorbance values and using the respective calibration curves for each antioxidant.

As shown in Tables E.1-E.4, in Appendix E, the mass losses during phase separation were negligible, which implies that the analytical method used can be considered reliable. In addition, the densities were higher for bottom phases, which is expected according to their relative position. Furthermore, the pH values of the two phases for all the systems were alike and in the range of 6.5 to 7.5, which indicates that the distribution of antioxidant charges in both phases is most probably comparable. Therefore, it is feasible to use a single calibration curve for both phases.

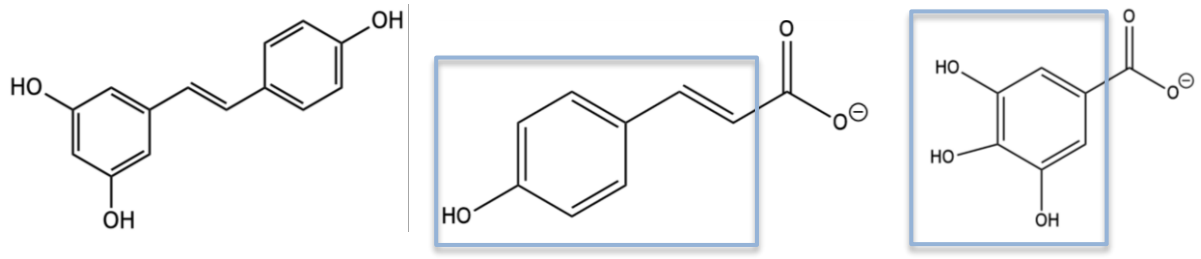
In order to comprehend and correctly compare the behavior of the three studied antioxidants in the different aqueous two-phase systems, different graphical representations were studied and are shown in Appendix E.

With the exception of the partition of gallic acid in the system containing Na_2Succinate, the systems presented higher values of antioxidant concentrations in the top phase, which suggests that the antioxidants had a tendency to diffuse to this phase. This was also confirmed by the values of partition coefficients (K) being higher than unity, as represented in Figs.14-16, and in Tables E.5-E.8, in Appendix E.

The partition coefficient is used to describe how a solute is distributed between two immiscible phases, and refers to the ratio of the concentration of the solute in a phase to the concentration in the second phase when these are at equilibrium. Since ethyl lactate is more abundant in top phases, according to the tie-line data obtained in the literature, it can be inferred that the antioxidants showed more affinity for the ethyl-lactate phase, migrating to the top.

At the pH of the systems, which is close to 7, the chemical structures of the antioxidants in more abundancy in the solution are the ones presented in Fig. 14, in which resveratrol still

presents its neutral form, since the lowest pK_a is higher than the pH of the system, and gallic acid and ferulic acid were deprotonated in the carboxyl group.



(a) (b) (c)

Fig. 14 - Chemical structures of the three studied antioxidants – resveratrol (a), ferulic acid (b) and gallic acid (c) – at the pH of the system (pH ~ 7).

The higher values of extraction efficiency (E) are related to the partitions of resveratrol (RVT) in the different salts, which can be explained by the fact that at the pH of the system this antioxidant is protonated, *i.e.*, there is no group in the form of anion. Therefore, there is more affinity with ethyl lactate, a neutral component, in contrast with the salts that are anions. This leads to a preferable migration of resveratrol to the top phase. It is possible to observe that the best results refer to the partition of RVT in ATPS with tripotassium citrate (K_3Citrate), although the slope related to the system with sodium potassium tartrate (NaKTartrate) is positive and steep. So, by adding EL, the migration to the top is favored. In general, the extraction efficiency increased with longer tie-line length, as shown in Fig. 15, which allows to conclude that more distinct compositions of the phases promote the migration of the solute to the top phase.

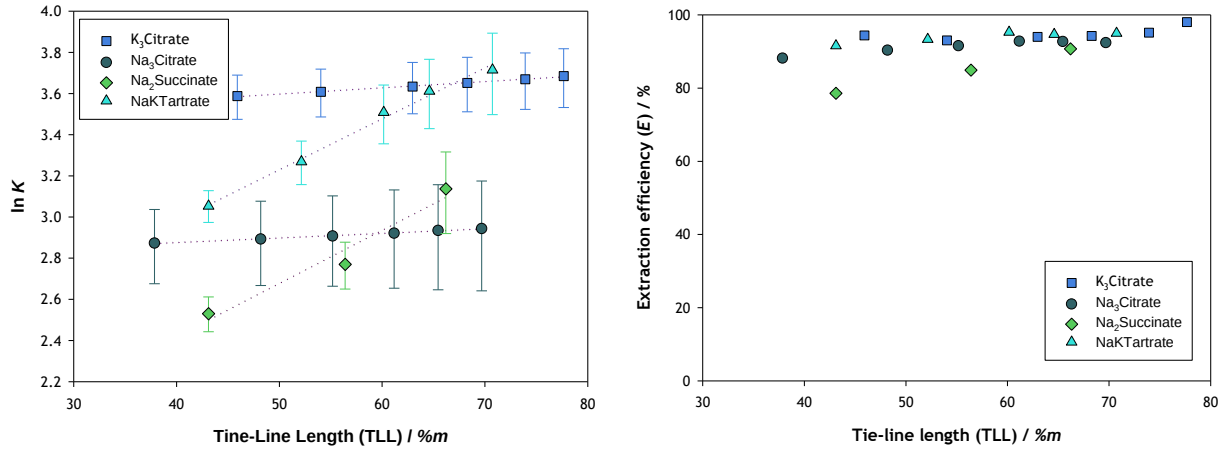


Fig. 15 - Relation between the tie-line lengths (TLL) and the natural logarithms of the experimental partition coefficients (K) (*left*) and extraction efficiencies (E) (*right*) for resveratrol (RVT) in the ATPS containing ethyl lactate, water and salts (K_3Citrate, Na_3Citrate, Na_2Succinate and NaKTartrate) at 298.15 K and 0.1 MPa.

Both ferulic acid (FA) and gallic acid (GA) at pH close to 7 have a deprotonated carboxyl group, so the affinity to ethyl lactate is lower than the one of resveratrol. Comparing the two

antioxidants, gallic acid is more polar because it is composed of three hydroxyl groups (-OH) capable of establishing hydrogen bonds with water, contrary to FA that only has two. Besides, FA has an ether group (-OCH_3) which confers less polarity to the molecule than the phenolic groups. Therefore, this antioxidant has more affinity to organic neutral compounds than to aqueous solutions, and, consequently, migrates preferentially to the EL-rich phase, rather than to the bottom phase.

As shown in Fig.16, ferulic acid has revealed great partition results (high partition coefficients and extraction efficiency values) in all of the salts, although the best results refer to the partition of this antioxidant in citrates, in specific in K_3Citrate. This outcome was expected since these salts present three carboxylate groups (deprotonated carboxyl groups), as shown in Fig. 16, conferring a more polar structure and, therefore, a less polar antioxidant such as FA is more oriented to ethyl lactate, which is less polar than the salt solution. The results obtained in K_3Citrate and Na_3Citrate were similar, although the system containing K_3Citrate presented higher tie-lines length values, which results from larger potential working area of the liquid-liquid equilibria. This can be explained by the lower solubility of this salt in water, contributing to a larger immiscible area.

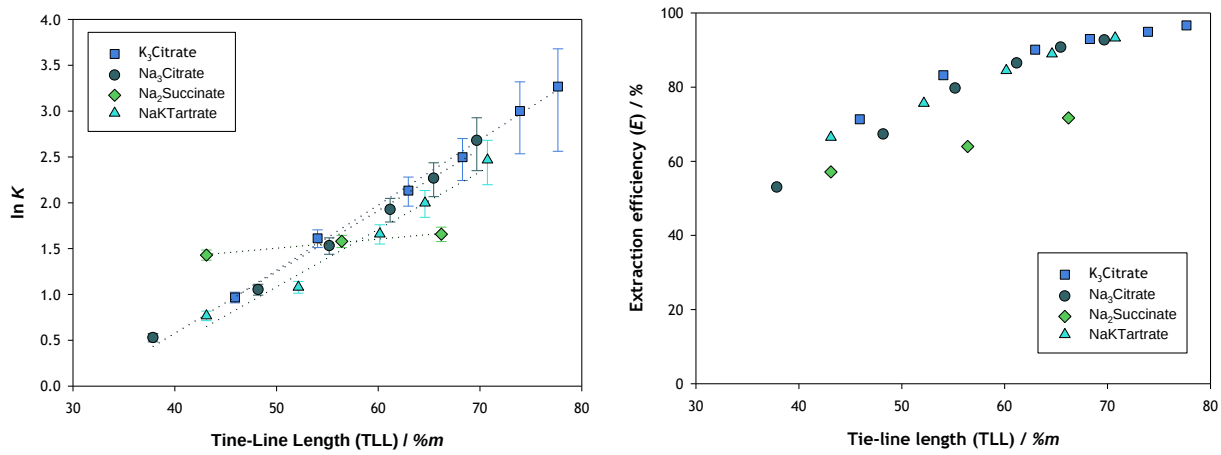


Fig. 16 - Relation between the tie-line lengths (TLL) and the natural logarithms of the experimental partition coefficients (K) (*left*) and extraction efficiencies (E) (*right*) for ferulic acid (FA) in the ATPS containing ethyl lactate, water and salts (K_3Citrate, Na_3Citrate, Na_2Succinate and NaKTartrate) at 298.15 K and 0.1 MPa.

In the partitions of FA in the different salts, except for Na_2Succinate, the slope of the line is positive and steep, which means that the length of the tie-line has influence in the partition, being the top-phase oriented solute migration favored by larger tie-lines. The phase compositions are more distinct, *i.e.*, the top is richer in EL and the bottom is richer in salt, characterized by a steep tie-line. This way, it promotes differences in solvent properties for solute migration, such as polarity, density and dielectric constant.

As shown in Fig. 18, gallic acid (GA) presents similar results in ATPS with K_3Citrate, Na_3Citrate and NaKTartrate, in which the slopes are almost horizontal, inferring that the addition of more EL to the systems does not influence the separation of phases. In the case of the partition of this antioxidant in Na_2Succinate, values of K smaller than unity were observed, decreasing with the addition of EL, resulting in a negative slope for the representation of ln K as a function of the TLL. These results may be explained by the fact that this salt only presents two deprotonated hydroxyl groups, as presented in Fig. 17, and it does not have hydroxyl groups, unlike NaKTartrate, which confers polarity to a molecule. This way, the polarity of this salt may be comparable to the one of ethyl lactate, resulting in a similar distribution of this antioxidant between the two phases. The extraction efficiencies of gallic acid in all the ATPS presents worst results comparing to the other antioxidants, which can be explained by the higher polarity of GA, resulting in more affinity with water, therefore, a distribution less distinct between the top phase, rich in EL and the bottom phase, rich in water and salt.

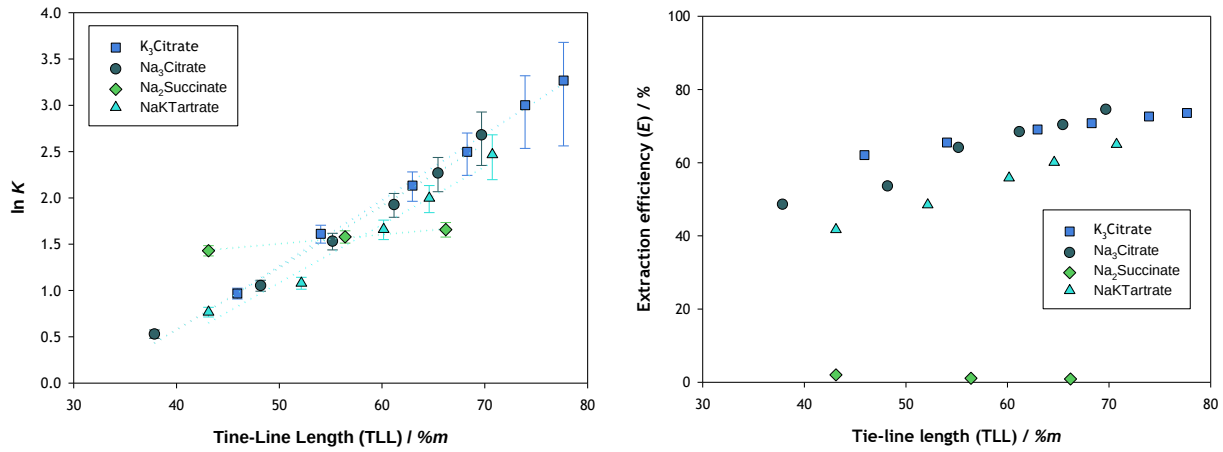


Fig. 17 - Relation between the tie-line lengths (TLL) and the natural logarithms of the experimental partition coefficients (K) (*left*) and extraction efficiencies (E) (*right*) for gallic acid (GA) in the ATPS containing ethyl lactate, water and salts (K_3Citrate, Na_3Citrate, Na_2Succinate or NaKTartrate) at 298.15 K and 0.1 MPa.

The results of the analysis of the *n*-octanol/water partition coefficient ($\log K_{OW}$) values of each antioxidant is in agreement with these results. This variable is a measure of the relative solubility of a compound in octanol compared to water and is often used as an indicator of a compound's hydrophobicity or lipophilicity[108]. A high $\log K_{ow}$ indicates that the substance is more soluble in octanol than water and, therefore, it presents a more lipophilic character. Consequently, it tends to adsorb more readily to organic matter because of their low affinity for water[108]. Resveratrol, ferulic acid and gallic acid have a value of $\log Kow$ of 3.09, 1.58 and 0.89, respectively, so it is possible to conclude that RVT has more affinity to the top phase, with less water content and rich in EL, resulting in greater extraction efficiency results.

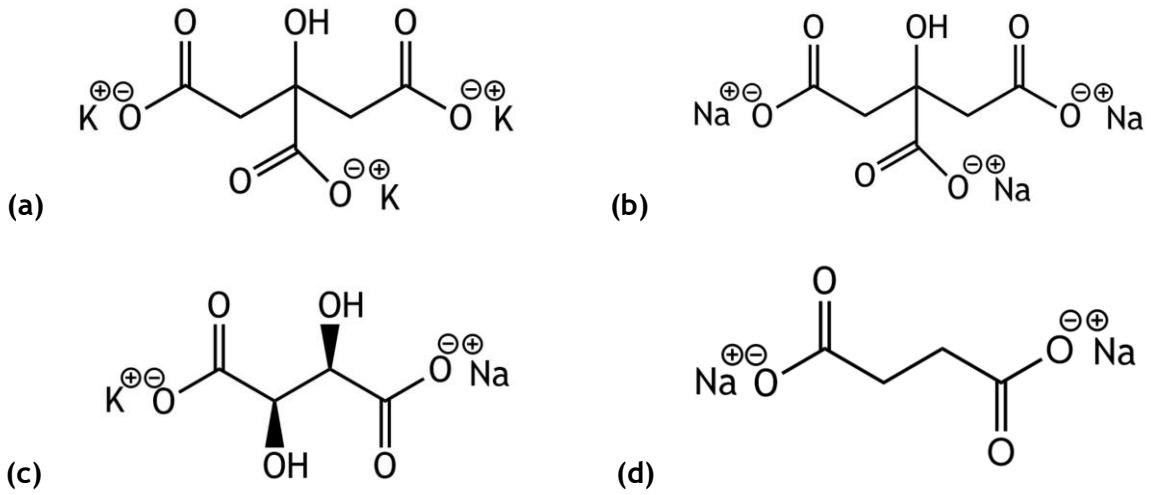


Fig. 18 - Chemical structure of the salts K_3Citrate (a), Na_3Citrate (b), Na_2Succinate (c) and NaKTartrate (d).

In contrast with the other antioxidants, resveratrol (RVT) presented large errors that can be explained by the low UV-Vis absorbance values of this species, even when the concentration of this antioxidant is close to maximum solubility. This way, it can be inferred that the used equipment (UV-Vis absorbance spectrophotometer) may not be the best option to detect with precision this solute. Hence, in order to study the effectiveness of aqueous two-phase systems for the extraction of resveratrol, it would be compelling to test other methods of quantification, such as High-Performance Liquid Chromatography (HPLC).

In the case of gallic acid and resveratrol, taking into account that the studied absorbance value after 3 days of settling at the pH of the system (~ 7) is not stable and is not maintained, the apparent solute losses or errors may be due to oxidation and/or hydrolysis of these antioxidants. Additionally, different tie-line compositions caused different pH values in the phases. Therefore, the study of the distribution of antioxidant stages is crucial to understand the relative abundance of the antioxidant stages and if the tie-line compositions extract the same antioxidant stages, as represented in Fig. 19, 20 and D9, in Appendix D. Since gallic acid and resveratrol are more reactive (chemically unstable), small variances in the pH resulted in disparities in the fraction of the antioxidant stages. These two antioxidants were significantly more affected since these have a $\mathrm{p}K_\mathrm{a}$ near the systems' pH. For ferulic acid, shown in Fig. 19, it was concluded that the tested tie-line compositions yielded the same distribution of electrical charges.

In Fig. 19, 20 and D9, in Appendix D, the superscripts 0, -1, -2, -3 and -4 e refer to the antioxidant stages of the species with the respective electrical charges, and e stands for the elementary charge ($1.602 \cdot 10^{-19}$ C).

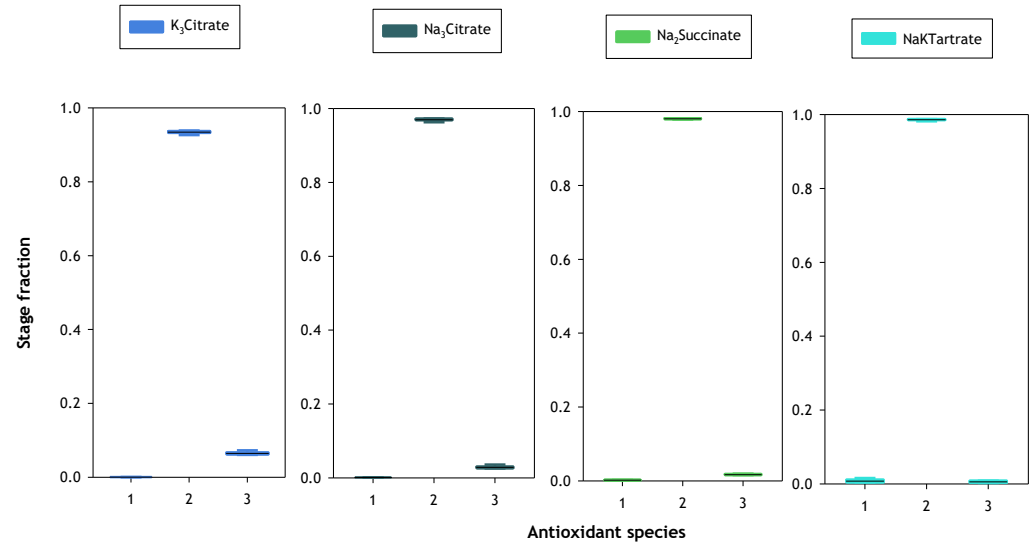


Fig. 19 - Effect of the tie-line compositions in the calculated stage fractions of the antioxidant stages of ferulic acid (FA) in the ATPS containing ethyl lactate, water and different salts (K_3Citrate, Na_3Citrate, Na_2Succinate and NaKTartrate) at 298.15 K and 0.1 MPa.

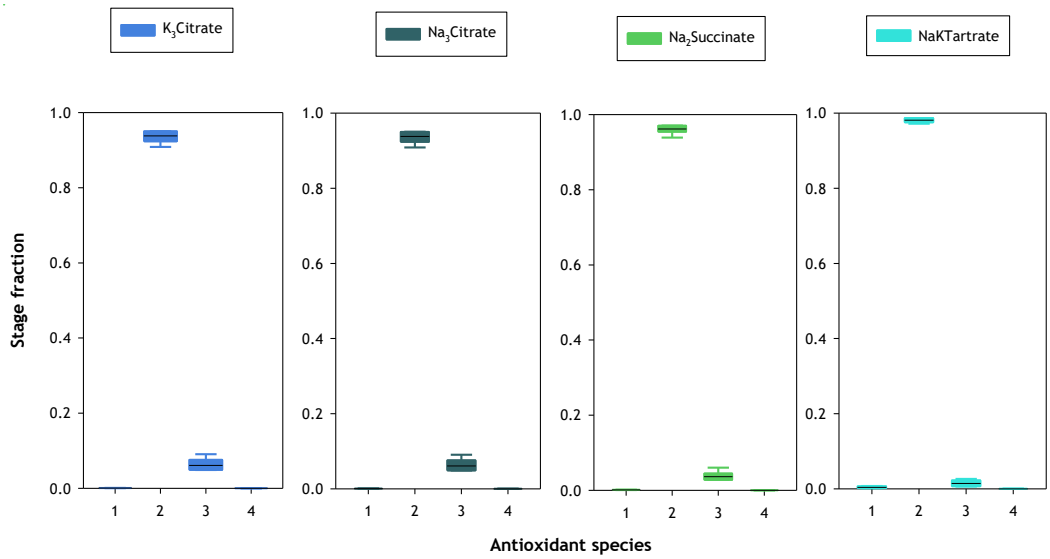


Fig. 20 - Effect of the tie-line compositions in the calculated stage fractions of the antioxidant stages of gallic acid (GA) in the ATPS containing ethyl lactate, water and different salts (K_3Citrate, Na_3Citrate, Na_2Succinate and NaKTartrate) at 298.15 K and 0.1 MPa.

4.1.5 Thermodynamic modeling

As previously mentioned, the electrolyte non-random two-liquid (e-NRTL) model was used to perform the thermodynamic modeling and represent the liquid-liquid equilibria data using MATLAB. Since the long-range interactions were taken into account due to the salt dissociation, the NRTL model combined with a Pitzer-Debye-Hückel (PDH) term was applied. Thus, four species were considered to be present in the system (EL, salt cation, salt anion and water) except for the system with NaKTartrate, in which this salts was considered to dissociate into two cations and one anion. The properties components properties required for the modeling are shown in Annex C and the calculated values are shown in Appendix F.

To ease data interpretation, the standard deviation was calculated according to equation (54) and it was determined for all tested cases.

$$\sigma = \sqrt{\frac{\sum_i^N (x_i^{\mathrm{eNRTL}} - x_i^{\mathrm{exp}})}{N}} \tag{54}$$

The code was applied with two different values of the non-randomness parameter (α_{ij} = 0.2 and 0.3), in order to evaluate the best fit. For $Na_3Citrate$, the smallest deviations were obtained for α_{ij} = 0.2 and for $K_3Citrate$ and NaKTartrate α_{ij} = 0.3 resulted in a better performance. In the case of $Na_2Succinate$, the α_{ij} value did not have much influence in the results. Furthermore, considering the values of the standard deviations obtained, it can be concluded that the modeling results were in good agreement with the liquid-liquid experimental data. Therefore, the e-NRTL model accurately predicts the behavior of the experimental ATPS. The high quality of the correlation is visually evident in Fig. 20, in which the experimental and calculated tie-lines using the e-NRTL model were displayed.

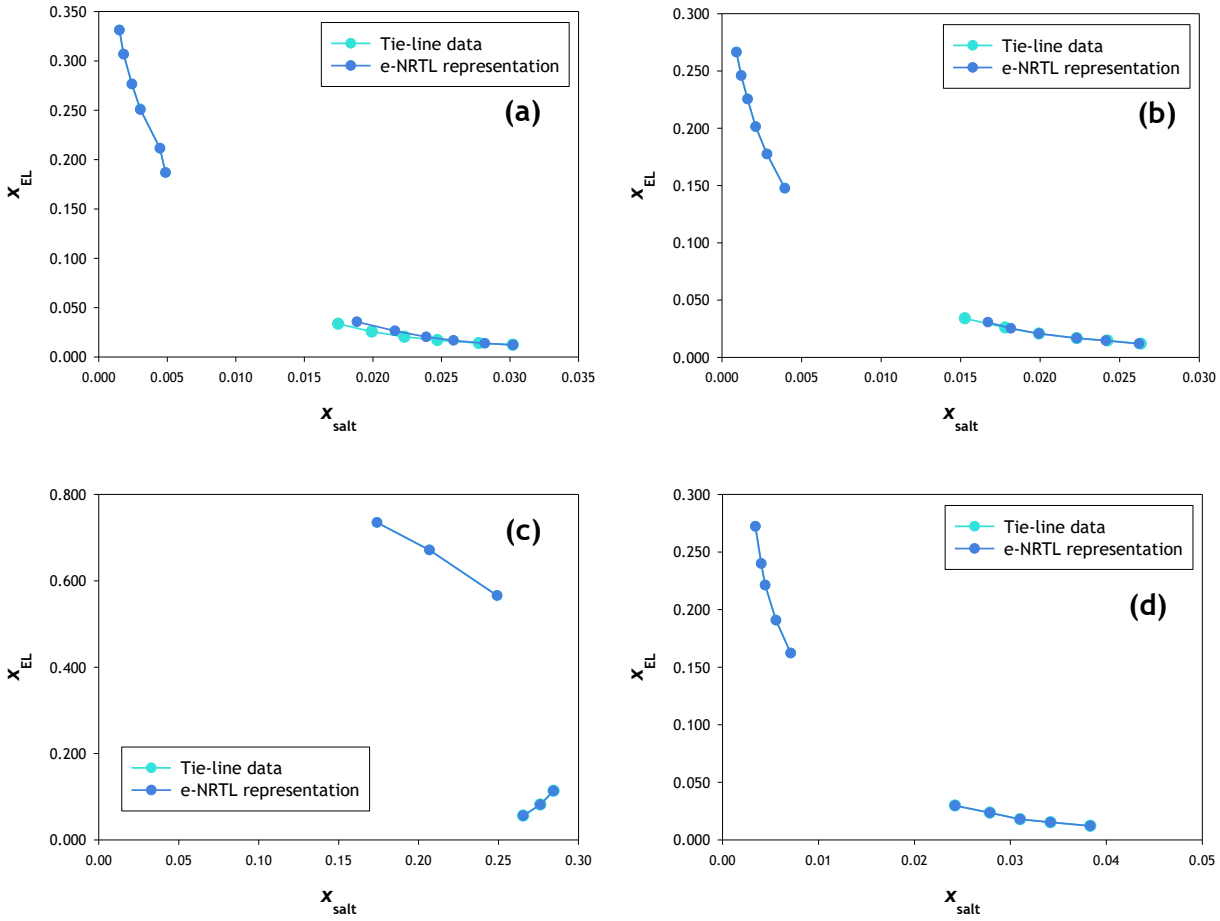


Fig. 21 - Comparison of predicted and experimental liquid-liquid equilibrium data of ATPS containing ethyl lactate, water and different salts (a) $K_3Citrate$, (b) $Na_3Citrate$, (c) $Na_2Succinate$ and (d) NaKTartrate at 298.15 K and 0.1 MPa.

5 Conclusion

The primary purpose of this dissertation was to study the efficiency of extraction of resveratrol (RVT), gallic acid (GA) and ferulic acid (FA), three well-known antioxidants, in green Aqueous Two-Phase Systems (ATPS) containing ethyl lactate, water and different organic salts (trisodium citrate, tripotassium citrate, disodium succinate or sodium potassium tartrate) at 298.15 K and 0.1 MPa, showing favorable separation potential for future application of these antioxidants in food supplements. Generally, the ATPS studied provided partition coefficients (K) larger than unity, which suggested that the antioxidants had a tendency to diffuse to the EL-rich phase (top phase), for which the ATPS were considered successful in the extraction of these species. The results showed that larger tie-lines generally led to an increase of the K and E values and a solute migration to top-phase is favored. The largest values of these parameters were obtained for resveratrol in K_3Citrate ($K = 40 \pm 6,\ E = (98 \pm 1)\ \%$) and in NaKTartrate ($K = 41 \pm 9, E = (95.0 \pm 0.6)\ \%$) for the longest tie-lines (TLL = 77.66 and $70.73\ m\%$, respectively). However, ferulic acid also presented great partition results in all of the salts, in specific in K_3Citrate, with $K = (3 \pm 2) \cdot 10^1, E = (96.7 \pm 0.4)\ \%$ for the longest tie-line (TLL = $45.91\ m\%$).

Additionally, the influence of pH on the UV-Vis absorbance spectra was evaluated for all studied phenolic compounds, to minimize errors in solute quantification, in which RVT, FA and GA were found to be mostly stable under the extractive conditions used. The experimental results had minimal antioxidant mass losses (< 5 %) during quantification, validating the analytical method (UV-Vis spectrometry). However, the UV-Vis absorbance of resveratrol presented low values, conferring a high error to the results and hinting that another analytical method should be tested, such as High-Performance Liquid Chromatography (HPLC).

Moreover, a successful LLE study was performed to the novel ATPS {polyvinylpyrrolidone (1) + sodium potassium tartrate (2) + water (3)} at 298.15 K and 0.1 MPa, for future applications in extractive processes. In order to understand the phase formation process of the ATPS, a solubility curve was determined at 298.15 K and 0.1 MPa, covering the complete region. Moreover, it was fitted by the Merchuk equation, which presented a very good agreement with the experimental data, showing a great potential working area for separation. Additionally, the tie-lines and their respective lengths (TLL) and slopes (STL) were determined. It was possible to conclude that higher concentration of PVP in the feed resulted in higher TLL values, *i.e.*, higher concentration of PVP and salt in the top and bottom phases, respectively, so, in a better phase separation.

Lastly, the studied ternary systems were satisfactorily described using the electrolyte non-random two-liquid (e-NRTL) model, for the first time in the research group. This approach consists of the NRTL model coupled with the Pitzer-Debye-Hückel (PDH) equation and has successfully predicted the behavior of the different ATPS, *i.e.*, the phase distribution of the components, since the results from modeling are in good agreement with the experimental data. Additionally, for the first in the research group, the PDH term was applied to salts with more than one cation or anion, such as sodium potassium tartrate, showing great results.

In conclusion, the ATPS with ethyl-lactate or polyvinylpyrrolidone with organic salts for the separation of resveratrol, gallic acid and ferulic acid may be a promising green approach for the valorization of agricultural by-products, contributing to the circular economy model. The extracted antioxidants could be later implemented in food supplements, having a potentially crucial role in tackling malnutrition in underdeveloped countries.

6 Project assessment

In this concluding chapter, a self-critique of the project will be presented, examining its strengths and weaknesses, as well as providing suggestions for future work.

6.1 Degree of completion

During this dissertation it was possible to perform a successful liquid-liquid equilibria (LLE) study in a novel aqueous two-phase system (ATPS) containing a green polymer (polyvinylpyrrolidone) and an organic salt (sodium potassium tartrate) for future applications in extractive processes, which contributed to fill the gap found in this field, due to scarce information on this sustainable systems.

Additionally, partition studies of important antioxidants (resveratrol, gallic acid and ferulic acid) were positively achieved in green ATPS previously reported in the literature containing ethyl lactate, water and different salts (trisodium citrate, tripotassium citrate, disodium succinate or sodium potassium tartrate), showing favorable separation potential for future application of these species in food supplements.

Furthermore, the behavior of these ternary systems containing electrolytes was predicted using e-NRTL. For that, a MatLab code with the PDH+NRTL model was developed, being necessary to build a database with some properties. The obtained results were compared with experimental data available in the literature and it was shown that the results from modeling are in good agreement with the experimental data. Hence, the objective of testing electrolyte models in ATPS was fully achieved.

In conclusion, all the set objectives were successfully accomplished, and very satisfatory results were obtained.

6.2 Additional work

During the six months of the development of this project, part of the results obtained were integrated in an article published by the research group:

Velho, P.; Rebelo, C.S.; Macedo, E.A. Extraction of Gallic Acid and Ferulic Acid for Application in Hair Supplements. *Molecules* **2023**, *28*, 2369.
DOI: www.doi.org/10.3390/molecules28052369.

Moreover, a new article is currently in preparation:

Rebelo, C.S.; Velho, P.; Macedo, E.A. Partition Studies of Antioxidants in Low Impact ATPS for Food Supplementation. **2023** (under preparation).

Finally, a significant amount of supplementary material, as code sections, plots and figures were created during this project. However, these were not included in the document due to space constraints and lesser importance.

6.3 Future work

Despite the large effort developed in this work and the positive accomplishments, some additional goals were left for future work due to scarceness of time, as, for example, the partition of different antioxidants in the studied liquid-liquid equilibria of the ATPS {PVP (1) + NaKTartrate (2) + Water (3)}.

Second, it would be interesting to test other methods of quantification, such as High-Performance Liquid Chromatography (HPLC) in the extraction efficiency study of resveratrol since this antioxidant presented large errors in all the studied ATPS, using UV-Vis absorbance spectrometry. Even though the research groups' laboratory had an HPLC, this instrument was inoperative during the time of the dissertation.

Additionally, it would be compelling to experiment the complete process of extracting the antioxidants from bio-waste (*e.g.*, grape skins and gallnuts) to produce a purified solid rich in these species and organic salts, for future application in dietary supplements. In order to obtain the final extract, the evaporation of the solvents (ethyl lactate and water) in a vacuum rotary evaporator could be prepared, as already tested in the laboratory.

Lastly, the adaptation of the e-NRTL modeling to be used with polymers should be done, in order to evaluate the LLE experimental data obtained for the system ATPS {PVP (1) + NaKTartrate (2) + Water (3)}.

6.4 Final assessment

The development of this project enabled personal and educational growth through a combination of self-organization and pursuit of excellence, ensuring the achievement of the project objectives and deadlines. Despite the difficulty of self-evaluation in lengthy projects, the deep interest in the subject, intense concentration and unwavering dedication helped maintain a high level of focus throughout the semester, resulting in an outstanding final outcome. This work not only allowed for research in a fascinating field and potential contributions to sustainable antioxidant extraction, but also fostered the development of new laboratory skills and work methods.

7 References

(1) Müller, O.; Krawinkel, M. Malnutrition and health in developing countries. *Can. Med. Assoc. J.* **2005**, *173*, 279-286. DOI: www.doi.org/10.1503/cmaj.050342.

(2) Burchi, F.; Fanzo, J.; Frison, E. The Role of Food and Nutrition System Approaches in Tackling Hidden Hunger. *Int. J. Environ. Res. Public Health* **2011**, *8*, 358-373. DOI: www.doi.org/10.3390/ijerph8020358.

(3) Cencic, A.; Chingwaru, W. The Role of Functional Foods, Nutraceuticals, and Food Supplements in Intestinal Health. *Nutrients* **2010**, *2*, 611-625.

(4) Fibigr, J.; Šatínský, D.; Solich, P. Current trends in the analysis and quality control of food supplements based on plant extracts. *Anal. Chim. Acta* **2018**, *1036*, 1-15. DOI: www.doi.org/10.1016/j.aca.2018.08.017.

(5) Crocker, D. Hunger, capability, and agency-oriented development. In *Ethics of Global Development: Agency, Capability, and Deliberative Democracy*, Cambridge University Press, 2008; pp 255-294.

(6) Fernandes, F.; Gorissen, K.; Delerue-Matos, C.; Grosso, C. Valorisation of Agro-Food By-Products for the Extraction of Phenolic Compounds. *Biol. Life Sci. Forum* **2022**, *18*, 61. DOI: www.doi.org/10.3390/Foods2022-13032.

(7) Conidi, C.; Donato, L.; Algieri, C.; Cassano, A. Valorization of chestnut processing by-products: A membrane-assisted green strategy for purifying valuable compounds from shells. *J. Cleaner Prod.* **2022**, *378*, 134564. DOI: www.doi.org/10.1016/j.jclepro.2022.134564.

(8) Caponio, F.; Piga, A.; Poiana, M. Valorization of Food Processing By-Products. *Foods* **2022**, *11*, 3246. DOI: www.doi.org/10.3390/foods11203246.

(9) Iqbal, M.; Tao, Y.; Xie, S.; Zhu, Y.; Chen, D.; Wang, X.; Huang, L.; Peng, D.; Sattar, A.; Shabbir, M.A.B.; Hussain, H.I.; Ahmed, S.; Yuan, Z. Aqueous two-phase system (ATPS): an overview and advances in its applications. *Biol. Proced. Online* **2016**, *18*, 18. DOI: www.doi.org/10.1186/s12575-016-0048-8.

(10) Titus, A.R.; Madeira, P.P.; Ferreira, L.A.; Chernyak, V.Y.; Uversky, V.N.; Zaslavsky, B.Y. Mechanism of Phase Separation in Aqueous Two-Phase Systems. *Int J Mol Sci* **2022**, *23*. DOI: www.doi.org/10.3390/ijms232214366.

(11) Benavides, J.; Rito-Palomares, M.; Asenjo, J.A. Aqueous Two-Phase Systems. In *Comprehensive Biotechnology*, Moo-Young, M. Ed.; Academic Press, 2011; pp 697-713.

(12) González-Amado, M.; Rodríguez, O.; Soto, A.; Carbonell-Hermida, P.; Olaya, M.d.M.; Marcilla, A. Aqueous Two-Phase Systems: A Correlation Analysis. *Ind. Eng. Chem. Res.* **2020**, *59*, 6318-6328. DOI: www.doi.org/10.1021/acs.iecr.9b06078.

(13) Sosa, F.H.B.; Farias, F.O.; Igarashi-Mafra, L.; Mafra, M.R. Measurement and correlation of aqueous two-phase systems of polyvinylpyrrolidone (PVP) and manganese sulfate: Effects of molecular weight and temperature. *Fluid Phase Equilib.* **2018**, *472*, 204-211. DOI: www.doi.org/10.1016/j.fluid.2018.05.021.

(14) Fedicheva, N.; Ninni, L.; Maurer, G. Aqueous Two-Phase Systems of Poly(vinyl pyrrolidone) and Sodium Sulfate: Experimental Results and Correlation/Prediction. *J. Chem. Eng. Data* **2007**, *52*. DOI: www.doi.org/10.1021/je7002012.

(15) Velho, P.; Marques, L.; Macedo, E.A. Extraction of Polyphenols and Vitamins Using Biodegradable ATPS Based on Ethyl Lactate. *Molecules* **2022**, *27*, 7838. DOI: www.doi.org/10.3390/molecules27227838.

(16) Zafarani-Moattar, M.T.; Seifi-Aghjekohal, P. Liquid–liquid equilibria of aqueous two-phase systems containing polyvinylpyrrolidone and tripotassium phosphate or dipotassium hydrogen phosphate: Experiment and correlation. *Calphad* **2007**, *31*, 553-559. DOI: www.doi.org/10.1016/j.calphad.2007.02.001.

(17) Velho, P.; Oliveira, I.; Gómez, E.; Macedo, E.A. pH Study and Partition of Riboflavin in an Ethyl Lactate-Based Aqueous Two-Phase System with Sodium Citrate. *J. Chem. Eng. Data* **2022**, *67*, 1985-1993. DOI: www.doi.org/10.1021/acs.jced.1c00909.

(18) Requejo, P.F.; Velho, P.; Gómez, E.; Macedo, E.A. Study of Liquid–Liquid Equilibrium of Aqueous Two-Phase Systems Based on Ethyl Lactate and Partitioning of Rutin and Quercetin. *Ind. Eng. Chem. Res.* **2020**, *59*, 21196-21204. DOI: www.doi.org/10.1021/acs.iecr.0c02664.

(19) Kontogeorgis, G.M.; Folas, G.K. Thermodynamic Models for Industrial Applications: From Classical and Advanced Mixing Rules to Association Theories. 2010. DOI: www.doi.org/10.1002/9780470747537.

(20) Boukhalfa, N.; Méniai, A.-H. Thermodynamic Modeling of Aqueous Electrolytes Type 2-1. *Procedia Eng.* **2016**, *148*, 1121-1129. DOI: www.doi.org/10.1016/j.proeng.2016.06.560.

(21) Christov, C. Thermodynamics of Formation of Double Salts and Mixed Crystals from Aqueous Solutions. *J. Chem. Thermodyn.* **2005**, *37*, 1036-1060. DOI: www.doi.org/10.1016/j.jct.2005.01.008.

(22) Chen, C.-C.; Britt, H.I.; Boston, J.F.; Evans, L.B. Local composition model for excess Gibbs energy of electrolyte systems. Part I: Single solvent, single completely dissociated electrolyte systems. *AIChE J.* **1982**, *28*, 588-596. DOI: www.doi.org/10.1002/aic.690280410.

(23) Pisoschi, A.M.; Pop, A. The role of antioxidants in the chemistry of oxidative stress: A review. *Eur. J. Med. Chem.* **2015**, *97*, 55-74. DOI: www.doi.org/10.1016/j.ejmech.2015.04.040.

(24) López-Alarcón, C.; Denicola, A. Evaluating the antioxidant capacity of natural products: A review on chemical and cellular-based assays. *Anal. Chim. Acta* **2013**, *763*, 1-10. DOI: www.doi.org/10.1016/j.aca.2012.11.051.

(25) Poljsak, B.; Šuput, D.; Milisav, I. Achieving the Balance between ROS and Antioxidants: When to Use the Synthetic Antioxidants. *Oxid. Med. Cell. Longevity* **2013**, *2013*, 956792. DOI: www.doi.org/10.1155/2013/956792.

(26) Persson, T.; Popescu, B.O.; Cedazo-Minguez, A. Oxidative Stress in Alzheimer's Disease: Why Did Antioxidant Therapy Fail? *Oxid. Med. Cell. Longevity* **2014**, *2014*, 427318. DOI: www.doi.org/10.1155/2014/427318.

(27) Sindhi, V.; Gupta, V.; Sharma, K.; Bhatnagar, S.; Kumari, R.; Dhaka, N. Potential applications of antioxidants – A review. *J. Pharm. Res.* **2013**, *7*, 828-835. DOI: www.doi.org/10.1016/j.jopr.2013.10.001.

(28) Neha, K.; Haider, M.R.; Pathak, A.; Yar, M.S. Medicinal prospects of antioxidants: A review. *Eur. J. Med. Chem.* **2019**, *178*, 687-704. DOI: www.doi.org/10.1016/j.ejmech.2019.06.010.

(29) Bouayed, J.; Bohn, T. Exogenous antioxidants - Double-edged swords in cellular redox state: Health beneficial effects at physiologic doses versus deleterious effects at high doses. *Oxid. Med. Cell. Longevity* **2010**, *3*, 228-237. DOI: www.doi.org/10.4161/oxim.3.4.12858.

(30) Abbas, M.; Saeed, F.; Anjum, F.M.; Afzaal, M.; Tufail, T.; Bashir, M.S.; Ishtiaq, A.; Hussain, S.; Suleria, H.A.R. Natural polyphenols: An overview. *Int. J. Food Prop.* **2017**, *20*, 1689-1699. DOI: www.doi.org/10.1080/10942912.2016.1220393.

(31) Scalbert, A.; Johnson, I.T.; Saltmarsh, M. Polyphenols: antioxidants and beyond. *Am. J. Clin. Nutr.* **2005**, *81*. DOI: www.doi.org/10.1093/ajcn/81.1.215S.

(32) Bors, W.; Michel, C. Chemistry of the antioxidant effect of polyphenols. *Ann N Y Acad Sci* **2002**, *957*, 57-69. DOI: www.doi.org/10.1111/j.1749-6632.2002.tb02905.x.

(33) Tsioptsias, C.; Tsivintzelis, I. Insights on thermodynamic thermal properties and infrared spectroscopic band assignments of gallic acid. *J. Pharm. Biomed. Anal.* **2022**, *221*, 115065. DOI: www.doi.org/10.1016/j.jpba.2022.115065.

(34) Ow, Y.Y.; Stupans, I. Gallic acid and gallic acid derivatives: effects on drug metabolizing enzymes. *Curr Drug Metab* **2003**, *4*, 241-248. DOI: www.doi.org/10.2174/1389200033489479.

(35) Fernandes, F.H.A.; Salgado, H.R.N. Gallic Acid: Review of the Methods of Determination and Quantification. *Crit. Rev. Anal. Chem.* **2016**, *46*, 257-265. DOI: www.doi.org/10.1080/10408347.2015.1095064.

(36) Graf, E. Antioxidant potential of ferulic acid. *Free Radic. Biol. Med.* **1992**, *13*, 435-448. DOI: www.doi.org/10.1016/0891-5849(92)90184-I.

(37) Ou, S.; Kwok, K.-C. Ferulic acid: pharmaceutical functions, preparation and applications in foods. *J. Sci. Food Agric.* **2004**, *84*, 1261-1269. DOI: www.doi.org/10.1002/jsfa.1873.

(38) Kumar, N.; Pruthi, V. Potential applications of ferulic acid from natural sources. *Biotechnol. Rep.* **2014**, *4*, 86-93. DOI: www.doi.org/10.1016/j.btre.2014.09.002.

(39) Tilay, A.; Bule, M.; Kishenkumar, J.; Annapure, U. Preparation of ferulic acid from agricultural wastes: its improved extraction and purification. *J Agric Food Chem* **2008**, *56*, 7644-7648. DOI: www.doi.org/10.1021/jf801536t.

(40) Frémont, L. Biological effects of resveratrol. *Life Sci.* **2000**, *66*, 663-673. DOI: www.doi.org/10.1016/S0024-3205(99)00410-5.

(41) Kulkarni, S.S.; Cantó, C. The molecular targets of resveratrol. *Biochim. Biophys. Acta, Mol. Basis Dis.* **2015**, *1852*, 1114-1123. DOI: www.doi.org/10.1016/j.bbadis.2014.10.005.

(42) Szkudelska, K.; Szkudelski, T. Resveratrol, obesity and diabetes. *Eur. J. Pharmacol.* **2010**, *635*, 1-8. DOI: www.doi.org/10.1016/j.ejphar.2010.02.054.

(43) Bhat, K.P.L.; Kosmeder, J.W.; Pezzuto, J.M. Biological Effects of Resveratrol. *Antioxid. Redox Signaling* **2001**, *3*, 1041-1064. DOI: www.doi.org/10.1089/152308601317203567.

(44) Wang, D.-G.; Liu, W.-Y.; Chen, G.-T. A simple method for the isolation and purification of resveratrol from Polygonum cuspidatum. *J. Pharm. Anal.* **2013**, *3*, 241-247. DOI: www.doi.org/10.1016/j.jpha.2012.12.001.

(45) Jovanović, A.; Petrović, P.; Djordjevic, V.; Zdunić, G.; Savikin, K.; Bugarski, B. Polyphenols Extraction From Plant Sources. *Lek. Sirovine* **2017**, *37*, 34-39. DOI: www.doi.org/10.5937/leksir1737037J.

(46) Sridhar, A.; Ponnuchamy, M.; Kumar, P.S.; Kapoor, A.; Vo, D.N.; Prabhakar, S. Techniques and modeling of polyphenol extraction from food: a review. *Environ. Chem. Lett.* **2021**, *19*, 3409-3443. DOI: www.doi.org/10.1007/s10311-021-01217-8.

(47) Alara, O.R.; Abdurahman, N.H.; Ukaegbu, C.I. Extraction of phenolic compounds: A review. *Curr. Res. Food Sci.* **2021**, *4*, 200-214. DOI: www.doi.org/10.1016/j.crfs.2021.03.011.

(48) Hidalgo, G.I.; Almajano, M.P. Red Fruits: Extraction of Antioxidants, Phenolic Content, and Radical Scavenging Determination: A Review. *Antioxidants* **2017**, *6*, 7. DOI: www.doi.org/10.3390/antiox6010007.

(49) Selvamuthukumaran, M.; Shi, J. Recent advances in extraction of antioxidants from plant by-products processing industries. *Food Qual. Saf.* **2017**, *1*, 61-81. DOI: www.doi.org/10.1093/fqsafe/fyx004.

(50) Brglez Mojzer, E.; Knez Hrnčič, M.; Škerget, M.; Knez, Ž.; Bren, U. Polyphenols: Extraction Methods, Antioxidative Action, Bioavailability and Anticarcinogenic Effects. *Molecules* **2016**, *21*, 901. DOI: www.doi.org/10.3390/molecules21070901.

(51) Urkude, R.; Dhurvey, V.; Kochhar, S. Pesticide Residues in Beverages. In *Quality Control in the Beverage Industry*, Grumezescu, A.M., Holban, A.M. Eds.; Academic Press, 2019; pp 529-560.

(52) Kyle, P.B. Toxicology: GCMS. In *Mass Spectrometry for the Clinical Laboratory*, Nair, H., Clarke, W. Eds.; Academic Press, 2017; pp 131-163.

(53) Ignat, I.; Volf, I.; Popa, V.I. A critical review of methods for characterisation of polyphenolic compounds in fruits and vegetables. *Food Chem* **2011**, *126*, 1821-1835. DOI: www.doi.org/10.1016/j.foodchem.2010.12.026.

(54) Baughman, D.R.; Liu, Y.A. Development of Expert Networks: A Hybrid System of Expert Systems and Neural Networks. In *Neural Networks in Bioprocessing and Chemical Engineering*, Baughman, D.R., Liu, Y.A. Eds.; Academic Press, 1995; pp 365-433.

(55) Yau, Y.K.; Ooi, C.W.; Ng, E.-P.; Lan, J.C.-W.; Ling, T.C.; Show, P.L. Current applications of different type of aqueous two-phase systems. *BIOB* **2015**, *2*, 49. DOI: www.doi.org/10.1186/s40643-015-0078-0.

(56) Chao, Y.; Shum, H.C. Emerging aqueous two-phase systems: From fundamentals of interfaces to biomedical applications. *Chem. Soc. Rev.* **2019**, *49*, 114-142. DOI: www.doi.org/10.1039/C9CS00466A.

(57) Patel, N.; Bracewell, D.; Sorensen, E. Dynamic Simulation of a Batch Aqueous Two-Phase Extraction Process for α-Amylase. In *Computer Aided Chemical Engineering*, Vol. 37; Elsevier, 2015; pp 713-718.

(58) Mukherjee, S. Isolation and Purification of Industrial Enzymes: Advances in Enzyme Technology. In *Advances in Enzyme Technology*, Singh, R.S., Singhania, R.R., Pandey, A., Larroche, C. Eds.; Elsevier, 2019; pp 41-70.

(59) Hatti-Kaul, R. Aqueous two-phase systems. A general overview. *Mol Biotechnol* **2001**, *19*, 269-277. DOI: www.doi.org/10.1385/mb:19:3:269.

(60) Pereira, J.F.B.; Coutinho, J.A.P. Aqueous Two-Phase Systems. In *Liquid-Phase Extraction*, Poole, C.F. Ed.; Elsevier, 2020; pp 157-182.

(61) Aparicio, S.; Alcalde, R. The green solvent ethyl lactate: an experimental and theoretical characterization. *Green Chem.* **2009**, *11*, 65-78. DOI: www.doi.org/10.1039/B811909K.

(62) Kamalanathan, I.; Petrovski, Z.; Branco, L.C.; Najdanovic-Visak, V. Novel aqueous biphasic system based on ethyl lactate for sustainable separations: Phase splitting mechanism. *J. Mol. Liq.* **2018**, *262*, 37-45. DOI: www.doi.org/10.1016/j.molliq.2018.03.119.

(63) Pereira, C.S.M.; Silva, V.M.T.M.; Rodrigues, A.E. Ethyl lactate as a solvent: Properties, applications and production processes – a review. *Green Chem.* **2011**, *13*, 2658-2671. DOI: www.doi.org/10.1039/C1GC15523G.

(64) Velho, P.; Rebelo, C.S.; Macedo, E.A. Extraction of Gallic Acid and Ferulic Acid for Application in Hair Supplements. *Molecules* **2023**, *28*, 2369. DOI: www.doi.org/10.3390/molecules28052369.

(65) Silva, M.; Lidon, F. An Overview on Applications and Side Effects of Antioxidant Food Additives. *EJFA* **2016**, *28*. DOI: www.doi.org/10.9755/ejfa.2016-07-806.

(66) Colosqui, C.E. Thermodynamics, Dynamics, and Kinetics at Liquid–Fluid and Fluid–Solid Interfaces. In *Encyclopedia of Interfacial Chemistry*, Elsevier, 2018; pp 654-667.

(67) Duroudier, J.-P. 1 - A Logical Presentation of Thermodynamics. In *Thermodynamics*, Duroudier, J. Ed.; Elsevier, 2016; pp 1-49.

(68) Chaves, I.D.G.; López, J.R.G.; Zapata, J.L.G.; Robayo, A.L.; Niño, G.R. Thermodynamic and Property Models. In *Process Analysis and Simulation in Chemical Engineering*, Springer International Publishing, 2016; pp 53-102.

(69) Velho, P.; Liang, X.; Macedo, E.A.; Gómez, E.; Kontogeorgis, G.M. Towards a predictive Cubic Plus Association equation of state. *Fluid Phase Equilib.* **2021**, *540*, 113045. DOI: www.doi.org/10.1016/j.fluid.2021.113045.

(70) Mayer, C.; Wallek, T. A Discrete Modeling Approach for Excess Gibbs-energy Models Combined with Molecular Sampling. In *Computer Aided Chemical Engineering*, Vol. 48; Elsevier, 2020; pp 169-174.

(71) Velho, P.; Lopes, C.; Rebello de A. Macedo, M.E. Predicting the ionicity of ionic liquids in binary mixtures based on solubility data: II. *Fluid Phase Equilib.* **2023**, *569*, 113766. DOI: www.doi.org/10.1016/j.fluid.2023.113766.

(72) Laar, J.J.v. Über Dampfspannungen von binären Gemischen. *Zeitschrift für Physikalische Chemie* **1910**, *72U* (1), 723-751. DOI: www.doi.org/10.1515/zpch-1910-7236.

(73) Zhao, Y.H.; Abraham, M.H.; Zissimos, A.M. Fast Calculation of van der Waals Volume as a Sum of Atomic and Bond Contributions and Its Application to Drug Compounds. *J. Org. Chem.* **2003**, *68*, 7368-7373. DOI: www.doi.org/10.1021/jo034808o.

(74) Wilson, G.M. Vapor-Liquid Equilibrium. XI. A New Expression for the Excess Free Energy of Mixing. *J. Am. Chem. Soc.* **1964**, *86*, 127-130. DOI: www.doi.org/10.1021/ja01056a002.

(75) Assael, M.J.; Trusler, J.P.M.; Tsolakis, T.F. Activity Coefficient Models. In *Thermophysical Properties of Fluids*, 1996; pp 161-206.

(76) Abrams, D.S.; Prausnitz, J.M. Statistical thermodynamics of liquid mixtures: A new expression for the excess Gibbs energy of partly or completely miscible systems. *AIChE Journal* **1975**, *21*, 116-128. DOI: www.doi.org/10.1002/aic.690210115.

(77) Fredenslund, A.; Jones, R.L.; Prausnitz, J.M. Group-contribution estimation of activity coefficients in nonideal liquid mixtures. *AIChE Journal* **1975**, *21*, 1086-1099. DOI: www.doi.org/10.1002/aic.690210607.

(78) Renon, H.; Prausnitz, J.M. Local compositions in thermodynamic excess functions for liquid mixtures. *AIChE Journal* **1968**, *14*, 135-144. DOI: www.doi.org/10.1002/aic.690140124.

(79) Dadmohammadi, Y.; Gebreyohannes, S.; Neely, B.J.; Gasem, K.A.M. Multicomponent phase behavior predictions using QSPR-generalized NRTL and UNIQUAC models. *Fluid Phase Equilib.* **2016**, *409*, 318-326. DOI: www.doi.org/10.1016/j.fluid.2015.10.009.

(80) Chang, C.-K.; Lin, S.-T. Extended Pitzer–Debye–Hückel Model for Long-Range Interactions in Ionic Liquids. *J. Chem. Eng. Data* **2020**, *65*, 1019-1027. DOI: www.doi.org/10.1021/acs.jced.9b00368.

(81) Pitzer, K.S. *Activity Coefficients in Electrolyte Solutions*; CRC Press, 1991. DOI: www.doi.org/10.1201/9781351069472.

(82) Oster, G. The Dielectric Properties of Liquid Mixtures1. *J. Am. Chem. Soc.* **1946**, *68*, 2036-2041. DOI: www.doi.org/10.1021/ja01214a050.

(83) Velho, P.; Gómez, E.; Macedo, E.A. Calculating the closest approach parameter for ethyl lactate-based ATPS. *Fluid Phase Equilibria* **2022**, *556*, 113389. DOI: www.doi.org/10.1016/j.fluid.2022.113389.

(84) Pitzer, K.S. Thermodynamics of electrolytes. I. Theoretical basis and general equations. *J. Phys. Chem.* **1973**, *77*, 268-277. DOI: www.doi.org/10.1021/j100621a026.

(85) Bondi, A. van der Waals Volumes and Radii. *J. Phys. Chem.* **1964**, *68* (3), 441-451. DOI: www.doi.org/10.1021/j100785a001.

(86) Chang, Y.A.; Chen, S.; Zhang, F.; Yan, X.; Xie, F.; Schmid-Fetzer, R.; Oates, W.A. Phase diagram calculation: past, present and future. *Prog. Mater. Sci.* **2004**, *49*, 313-345. DOI: www.doi.org/10.1016/S0079-6425(03)00025-2.

(87) Gómez, E.; Requejo, P.F.; Tojo, E.; Macedo, E.A. Recovery of flavonoids using novel biodegradable choline amino acids ionic liquids based ATPS. *Fluid Phase Equilib.* **2019**, *493*, 1-9. DOI: www.doi.org/10.1016/j.fluid.2019.03.024.

(88) Arce, A.; Arce, A., Jr.; Rodriguez, O. Revising Concepts on Liquid–Liquid Extraction: Data Treatment and Data Reliability. *J. Chem. Eng. Data* **2022**, *67* (1), 286-296. DOI: www.doi.org/10.1021/acs.jced.1c00778.

(89) Velho, P.; Requejo, P.F.; Gómez, E.; Macedo, E.A. Novel ethyl lactate based ATPS for the purification of rutin and quercetin. *Sep. Purif. Technol.* **2020**, *252*, 117447. DOI: www.doi.org/10.1016/j.seppur.2020.117447.

(90) Velho, P.; Requejo, P.F.; Gómez, E.; Macedo, E.A. Thermodynamic study of ATPS involving ethyl lactate and different inorganic salts. *Sep. Purif. Technol.* **2021**, *275*, 119155. DOI: www.doi.org/10.1016/j.seppur.2021.119155.

(91) Han, J.; Wang, Y.; Yu, C.; Li, Y.; Kang, W.; Yan, Y. (Liquid+liquid) equilibrium of (imidazolium ionic liquids+organic salts) aqueous two-phase systems at T=298.15K and the influence of salts and ionic liquids on the phase separation. *J. Chem. Thermodyn.* **2012**, *45*, 59-67. DOI: www.doi.org/10.1016/j.jct.2011.09.004.

(92) Merchuk, J.C.; Andrews, B.A.; Asenjo, J.A. Aqueous two-phase systems for protein separation: Studies on phase inversion. *J. Chromatogr. B: Biomed. Sci. Appl.* **1998**, *711*, 285-293. DOI: www.doi.org/10.1016/S0378-4347(97)00594-X.

(93) Hu, M.; Zhai, Q.; Jiang, Y.; Jin, L.; Liu, Z. Liquid−Liquid and Liquid−Liquid−Solid Equilibrium in PEG + Cs2SO4 + H2O. *J. Chem. Eng. Data* **2004**, *49*, 1440-1443. DOI: www.doi.org/10.1021/je0498558.

(94) Jayapal, M.; Regupathi, I.; Murugesan, T. Liquid−Liquid Equilibrium of Poly(ethylene glycol) 2000 + Potassium Citrate + Water at (25, 35, and 45) °C. *J. Chem. Eng. Data* **2007**, *52*, 56-59. DOI: www.doi.org/10.1021/je060209d.

(95) Silvério, S.C.; Rodríguez, O.; Teixeira, J.A.; Macedo, E.A. The Effect of Salts on the Liquid–Liquid Phase Equilibria of PEG600 + Salt Aqueous Two-Phase Systems. *J. Chem. Eng. Data* **2013**, *58* (12), 3528-3535. DOI: www.doi.org/10.1021/je400825w.

(96) Othmer, D.F.; Tobias, P.E. Liquid -Liquid Extraction Data -Toluene and Acetaldehyde Systems. *Ind. Eng. Chem.* **1942**, *34*, 690-692. DOI: www.doi.org/10.1021/ie50390a011.

(97) Tubío, G.; Pellegrini, L.; Nerli, B.B.; Picó, G.A. Liquid−Liquid Equilibria of Aqueous Two-Phase Systems Containing Poly(ethylene glycols) of Different Molecular Weight and Sodium Citrate. *J. Chem. Eng. Data* **2006**, *51*, 209-212. DOI: www.doi.org/10.1021/je050332p.

(98) Chapter 13 - Acid-Base Equilibria in Wine. In *Enological Chemistry*, Moreno, J., Peinado, R. Eds.; Academic Press, 2012; pp 195-221.

(99) Fink, D.W.; Stong, J.D. The electronic spectral properties of gallic acid. *Spectrochim. Acta, Part A* **1982**, *38*, 1295-1298. DOI: www.doi.org/10.1016/0584-8539(82)80127-X.

(100) Eslami, A.C.; Pasanphan, W.; Wagner, B.A.; Buettner, G.R. Free radicals produced by the oxidation of gallic acid: An electron paramagnetic resonance study. *Chem. Cent. J.* **2010**, *4*, 15. DOI: www.doi.org/10.1186/1752-153X-4-15.

(101) Borges, F.; Lima, J.L.F.C.; Pinto, I.; Reis, S.; Siquet, C. Application of a Potentiometric System with Data-Analysis Computer Programs to the Quantification of Metal-Chelating Activity of Two Natural Antioxidants: Caffeic Acid and Ferulic Acid. *Helv. Chim. Acta* **2003**, *86*, 3081-3087. DOI: www.doi.org/10.1002/hlca.200390250.

(102) Brittes, J.; Lúcio, M.; Nunes, C.; Lima, J.L.; Reis, S. Effects of resveratrol on membrane biophysical properties: relevance for its pharmacological effects. *Chem Phys Lipids* **2010**, *163*, 747-754. DOI: www.doi.org/10.1016/j.chemphyslip.2010.07.004.

(103) Speight, J.G. Molecular Interactions, Partitioning, and Thermodynamics. In *Reaction Mechanisms in Environmental Engineering*, Speight, J.G. Ed.; Butterworth-Heinemann, 2018; pp 307-336.

(104) Li, Z.; Mumford, K.A.; Smith, K.H.; Chen, J.; Wang, Y.; Stevens, G.W. Solution Structure of Isoactivity Equations for Liquid–Liquid Equilibrium Calculations Using the Nonrandom Two-Liquid Model. *Ind. Eng. Chem. Res.* **2016**, *55*, 2852-2859. DOI: www.doi.org/10.1021/acs.iecr.5b04469.

(105) Robinson, K.; Mock, C.; Liang, D. Pre-formulation studies of resveratrol. *Drug Dev Ind Pharm* **2015**, *41*, 1464-1469. DOI: www.doi.org/10.3109/03639045.2014.958753.

(106) Zimányi, L.; Thekkan, S.; Eckert, B.; Condren, A.R.; Dmitrenko, O.; Kuhn, L.R.; Alabugin, I.V.; Saltiel, J. Determination of the pKa Values of trans-Resveratrol, a Triphenolic Stilbene, by Singular Value Decomposition. Comparison with Theory. *J. Phys. Chem. A* **2020**, *124*, 6294-6302. DOI: www.doi.org/10.1021/acs.jpca.0c04792.

(107) Ramaiah, N.A.; Chaturvedi, R.K. Potentiometric studies on the dissociation of gallic acid. *Proc. Indian Acad. Sci.* **1960**, *51*, 177-188. DOI: www.doi.org/10.1007/BF03045780.

(108) Miller, M.M.; Wasik, S.P.; Huang, G.L.; Shiu, W.Y.; Mackay, D. Relationships between octanol-water partition coefficient and aqueous solubility. *Environ. Sci. Technol.* **1985**, *19*, 522-529. DOI: www.doi.org/10.1021/es00136a007.

(109) Lix, L.M.; Keselman, J.C.; Keselman, H.J. Consequences of Assumption Violations Revisited: A Quantitative Review of Alternatives to the One-Way Analysis of Variance F Test. *Rev. Educ. Res.* **1996**, *66*, 579-619. DOI: www.doi.org/10.3102/00346543066004579.

Appendices and annexes

Annex A - Physicochemical properties

Table AA.1 - Physicochemical properties of the compounds used in the liquid-liquid equilibria study and in the extraction of antioxidants.

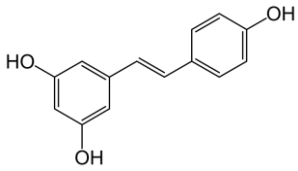
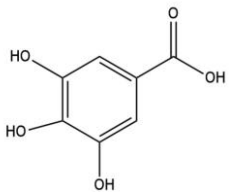
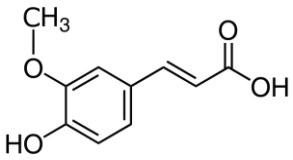
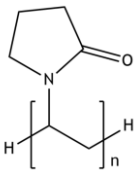
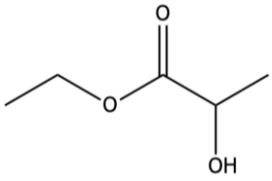
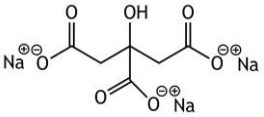
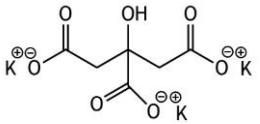
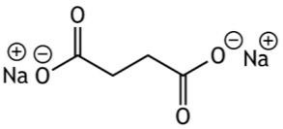
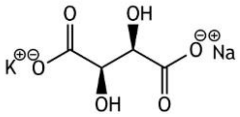
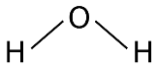
Compound	Resveratrol	**Molecular formula**	$C_{14}H_{12}O_3$
Chemical structure		**Solubility in water** (at 25 ºC)	0.05 $mg \cdot mL^{-1}$ [1]
		Molecular mass	228.24 $g \cdot mol^{-1}$
		log K_{ow}	3.09 [2]
Compound	Gallic acid	**Molecular formula**	$C_7H_6O_5$
Chemical structure		**Solubility in water** (at 25 ºC)	14.7 $g \cdot L^{-1}$ [3]
		Molecular mass	170.12 $g \cdot mol^{-1}$
		log K_{ow}	0.89 [4]
		Anion (-1 e):	- 0.46[5]
Compound	Ferulic acid	**Molecular formula**	$C_{10}H_{10}O_4$
Chemical structure		**Solubility in water** (at 25 ºC)	0.78 $g \cdot L^{-1}$ [3]
		Molecular mass	194.18 $g \cdot mol^{-1}$
		log K_{ow}	1.58 [6]
Compound	Polyvinylpyrrolidone	**Molecular formula**	$(C_6H_9NO)_n$
Chemical structure		**Solubility in water** (at 25 ºC)	Very soluble [7]
		Molecular mass	111.14 $g \cdot mol^{-1}$
		log K_{ow}	-
Compound	Ethyl lactate	**Molecular formula**	$C_5H_{10}O_3$
Chemical structure		**Solubility in water** (at 25 ºC)	Miscible [8]
		Molecular mass	118.13 $g \cdot mol^{-1}$
		log K_{ow}	0.06 [8]
Density (at 25 ºC)	1.03 $g \cdot cm^{-3}$ [8]	**Boiling point** (at 1 atm)	153.00 ºC [8]

Table AA.1 – *Cont.*

Compound	Trisodium Citrate	**Chemical structure**	
Molecular formula	$Na_3C_6H_5O_7$		
Molecular mass	258.06 g·mol^{-1}		
Compound	Tripotassium Citrate	**Chemical structure**	
Molecular formula	$K_3C_6H_5O_7$		
Molecular mass	306.40 g·mol^{-1}		
Compound	Disodium Succinate	**Chemical structure**	
Molecular formula	$Na_2C_4H_4O_4$		
Molecular mass	162.05 g·mol^{-1}		
Compound	Sodium Potassium Tartrate	**Chemical structure**	
Molecular formula	$Na_2C_4H_4O_4$		
Molecular mass	282.1 g·mol^{-1}		
Compound	Water	**Molecular formula**	H_2O
		Molecular mass	18.0 g·mol^{-1}
Chemical structure		**Boiling point**	100 ºC [9] (at 1 atm)
		Density (at 25 ºC)	0.997 g·cm^{-3} [10]

Annex B - Liquid-liquid equilibria

In this annex, the liquid-liquid equilibria data taken from previous works of the research group are shown.

Table BB.1 - Liquid-liquid equilibria data for the ternary systems containing ethyl lactate, water and different salts ($Na_3Citrate$[89], $K_3Citrate$[89], NaKTartrate[18], $Na_2Succinate$[62]), at 298.15 K and 0.1 MPa.

No. TL	Feed		Top phase			Bottom phase			TLL
	$w_{EL,feed}$	$w_{salt,feed}$	$w_{EL,top}$	$w_{salt,top}$	pH	$w_{EL,bot}$	$w_{salt,bot}$	pH	/ *m*%
{EL (1) + $Na_3Citrate$ (2) + Water (3)}[11]									
TL1	0.300	0.110	0.517	0.030	7.00	0.160	0.157	6.98	37.58
TL2	0.320	0.114	0.575	0.020	6.98	0.123	0.185	6.96	48.18
TL3	0.343	0.117	0.615	0.014	6.98	0.098	0.207	6.97	55.17
TL4	0.365	0.121	0.650	0.010	7.00	0.079	0.230	7.00	61.17
Tl5	0.385	0.123	0.677	0.007	6.98	0.068	0.247	6.97	65.44
TL6	0.406	0.126	0.701	0.005	6.98	0.055	0.266	7.00	69.68
{EL (1) + $K_3Citrate$ (2) + Water (3)}[11]									
TL1	0.355	0.126	0.579	0.039	7.21	0.150	0.203	7.39	45.91
TL2	0.375	0.130	0.619	0.034	7.22	0.115	0.232	7.41	54.02
TL3	0.392	0.135	0.674	0.021	7.19	0.091	0.258	7.37	62.96
TL4	0.411	0.139	0.704	0.016	7.23	0.075	0.282	7.41	68.28
Tl5	0.430	0.143	0.736	0.011	7.12	0.060	0.310	7.39	73.92
TL6	0.446	0.148	0.758	0.009	7.22	0.052	0.331	7.43	77.66
{EL (1) + NaKTartrate (2) + Water (3)}[12]									
TL1	0.320	0.130	0.538	0.042	6.62	0.137	0.200	6.61	43.10
TL2	0.343	0.133	0.590	0.031	6.71	0.108	0.229	6.56	52.13
TL3	0.365	0.137	0.637	0.023	6.64	0.082	0.255	6.56	60.15
TL4	0.385	0.139	0.662	0.020	6.65	0.069	0.277	6.56	64.59
TL5	0.414	0.142	0.700	0.016	6.61	0.054	0.305	6.56	70.73
{EL (1) + $Na_2Succinate$ (2) + Water (3)}[13]									
TL1	0.280	0.126	0.602	0.030	7.25	0.189	0.153	7.25	43.10
TL2	0.300	0.130	0.687	0.019	7.45	0.145	0.174	7.37	56.40
TL3	0.320	0.135	0.742	0.014	7.37	0.106	0.196	7.34	66.20

Annex C - Pure compound parameters

Table CC.1 - Molar density, molecular mass and dielectric constants of the solvents, ethyl lactate (EL) and water (H_2O) of the ATPS with different salts (K_3Citrate, Na_3Citrate, Na_2Succinate and NaKTartrate).

	EL	**H_2O**
Molar density (ρ_x) / $\mathbf{g \cdot cm^{-3}}$	1.03 [8]	1.00 [10]
Molecular mass (M) / $\mathbf{g \cdot mol^{-1}}$	118.13	18.02
Dielectric constant (ε)	15.7 [14]	78.5 [15]

Table CC.2 - Molecular mass, charge, radius, van de Waals radius and volume of the sodium and potassium ions.

	Na^+	**K^+**
Molecular mass (M) / $\mathbf{g \cdot mol^{-1}}$	22.99	39.1
Charge (q) / e	$+1$	$+1$
van der Walls radius (r_w) / Å	2.27	2.75
van der Walls volume (V_w) / $\mathbf{cm^3 \cdot mol^{-1}}$	$4.90 \cdot 10^{-10}$	$8.71 \cdot 10^{-10}$

Table CC.3 - Molecular mass and charge of ions present in the studied with different salts (K_3Citrate, Na_3Citrate, Na_2Succinate and NaKTartrate).

	$Citrate^{3-}$	**$Succinate^{2-}$**	**$Tartrate^{2-}$**
Molecular mass (M) / $\mathbf{g \cdot mol^{-1}}$	189.10	118.09	150.087
Charge (q) / e	-3	-2	-2

Appendix A. Experimental apparatus

During the experimental procedure, some pictures were taken, which will be presented in this appendix, with the aim to visually demonstrate the procedures.

Figs. A.1-A.2 show the evolution of the color of the antioxidant stocks in the day of preparation and after settling for three days.

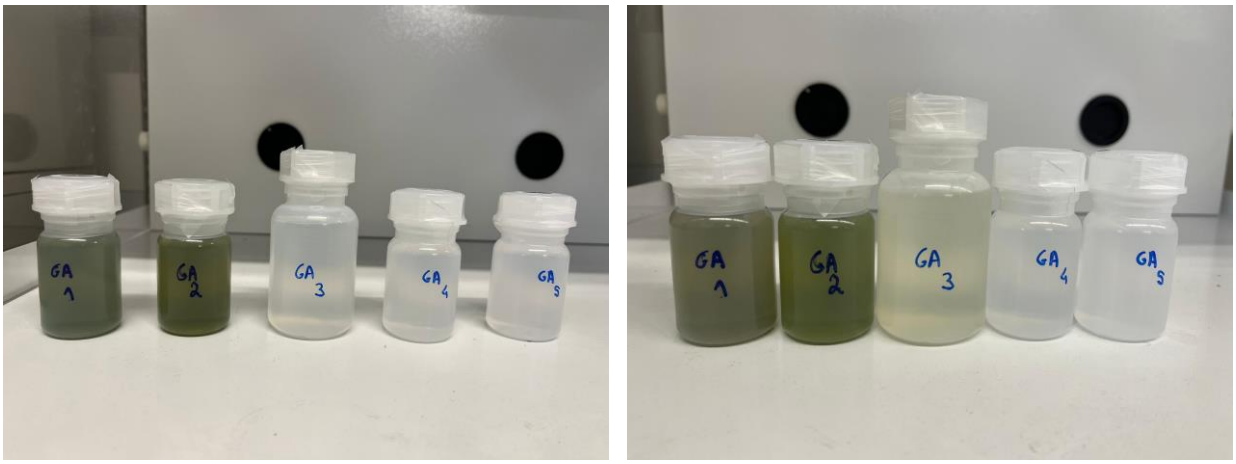


Fig. A.1 - Stock solutions of gallic acid (~$2.00 \cdot 10^{-4}\ \mathrm{g \cdot mL^{-1}}$) at different pH values in the moment of preparation (*left*) and after 3 days of settling (*right*).

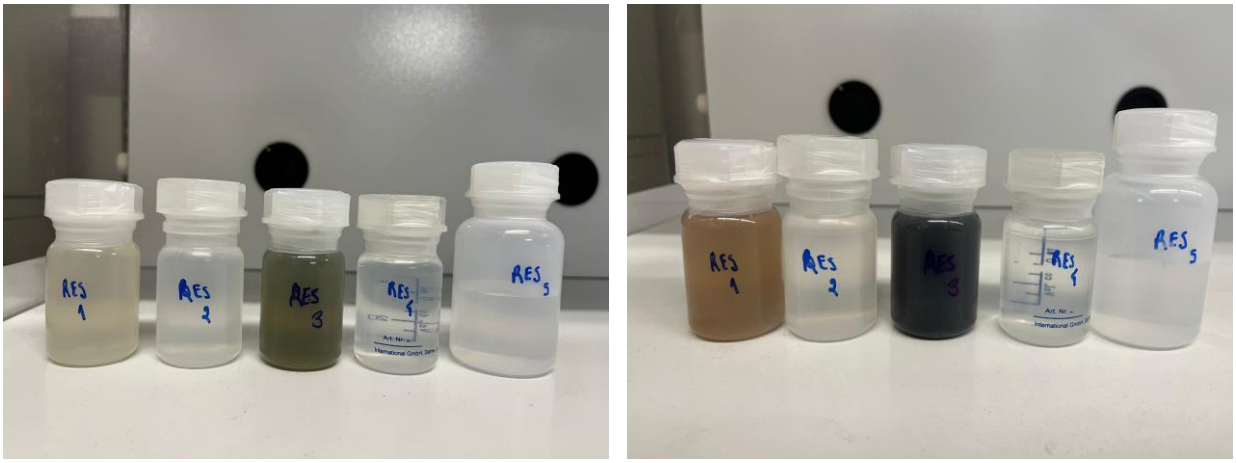


Fig. A.2 - Stock solutions of resveratrol ($\sim 9.16 \cdot 10^{-5}\ g \cdot mL^{-1}$) at different pH values in the moment of preparation *(left)* and after 3 days of settling *(right)*.

Fig. A.3 is a demonstration of the behavior of a partition after agitation and settling for a few moments. It is possible to observe the division of the mixture in two phases (the top and bottom phases).

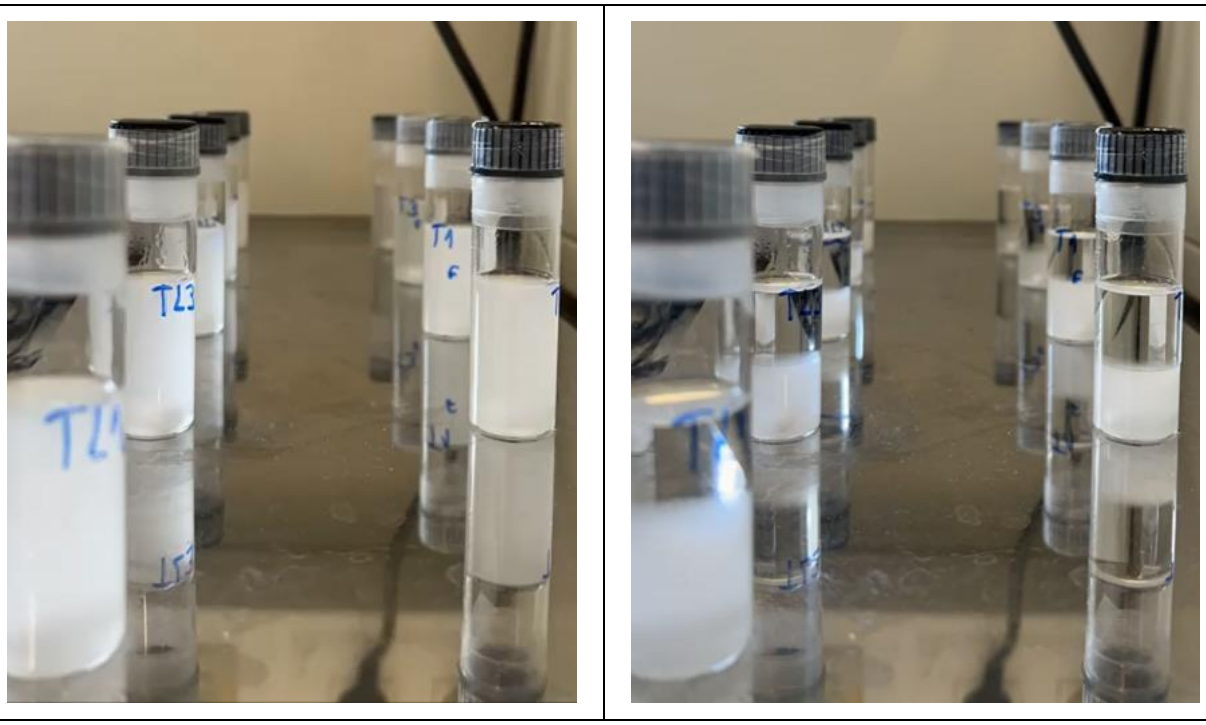


Fig. A.3 - Blanks and partition of ferulic acid (FA) for ATPS {EL (1) + NaKTartrate (2) + Water (3)} while stirring (*left*) and after settling for one minute (*right*).

Appendix B. Liquid-liquid equilibria

In Figs. B.1-B.4, it is possible to observe the fit of the different equations (Han[91], Merchuk[92], Hu[93] and Jayapal[94]) to the experimental cloud-point data for the ATPS {PVP (1) + NaKTartrate (2) + Water (3)}. The data points represented in these figures are shown in Table B.1.

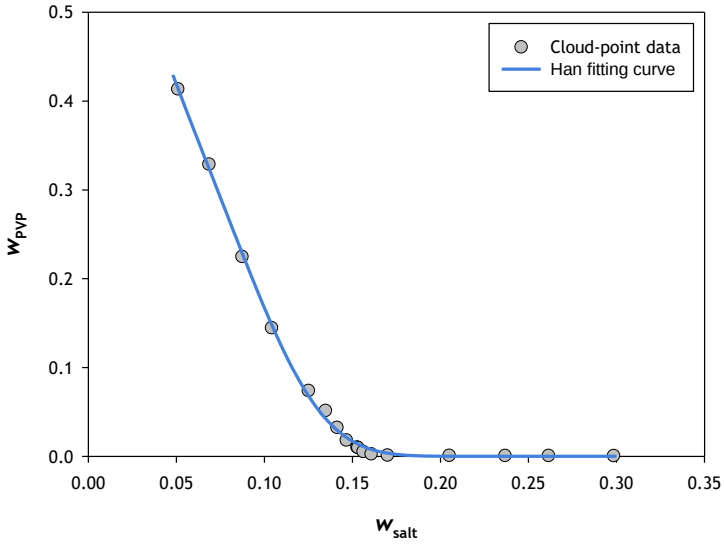


Fig. B.1 - Cloud-point data and solubility curve fitting data according to Han's equation[91].

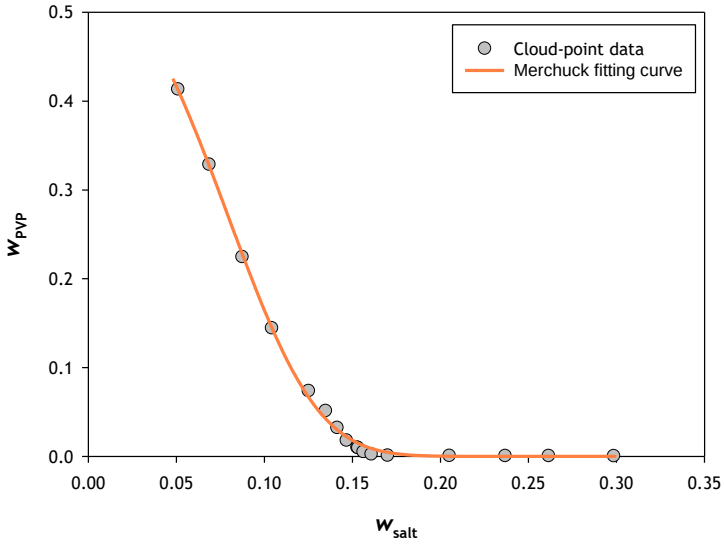


Fig. B.2 - Cloud-point data and solubility curve fitting data according to Merchuk's equation[92].

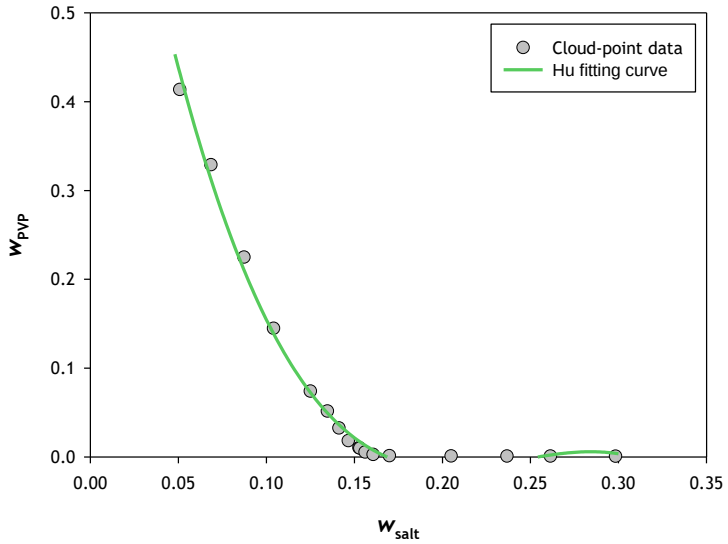


Fig. B.3 - Cloud-point data and solubility curve fitting data according to Hu's equation[93].

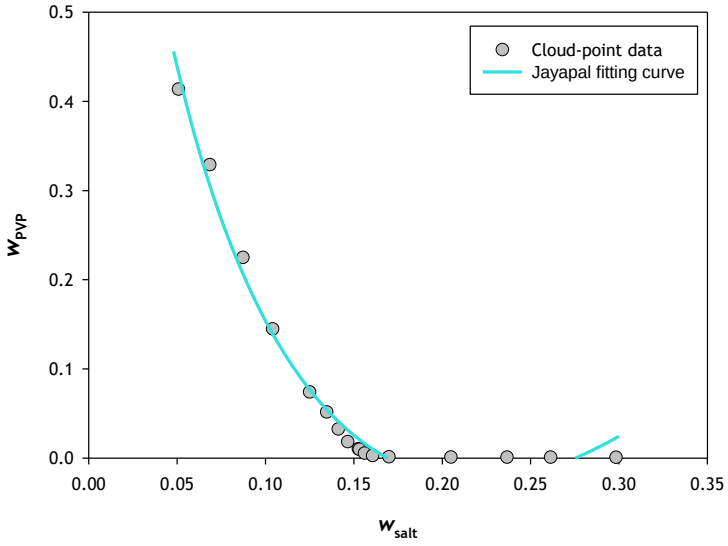


Fig. B.4 - Cloud-point data and solubility curve fitting data according to Jayapal's equation[94].

Table B.1 – Cloud-point compositions for the ATPS {PVP (1) + NaKTartrate (2) + Water (3)} and calculated PVP mass fraction using fitting equations Han[91], Merchuk[92], Hu[93] and Jayapal[94].

Solubility curve		Fitting equations							
		Han		Merchuk		Hu		Jayapal	
w_{salt}	w_{PVP}	w_{PVP}	σ	w_{PVP}	σ	w_{PVP}	σ	w_{PVP}	σ
0.051	0.414	0.415	$3.2 \cdot 10^{-4}$	0.413	$1.1 \cdot 10^{-17}$	0.433	$4.6 \cdot 10^{-3}$	0.433	$1.6 \cdot 10^{-4}$
0.068	0.329	0.324	$1.1 \cdot 10^{-3}$	0.328	$3.5 \cdot 10^{-15}$	0.313	$4.0 \cdot 10^{-3}$	0.306	$3.9 \cdot 10^{-5}$
0.087	0.225	0.229	$1.0 \cdot 10^{-3}$	0.229	$6.2 \cdot 10^{-13}$	0.210	$3.6 \cdot 10^{-3}$	0.206	$8.1 \cdot 10^{-6}$
0.104	0.145	0.148	$8.8 \cdot 10^{-4}$	0.145	$6.9 \cdot 10^{-16}$	0.139	$1.5 \cdot 10^{-3}$	0.139	$1.7 \cdot 10^{-6}$
0.125	0.074	0.068	$1.4 \cdot 10^{-3}$	0.067	$8.4 \cdot 10^{-12}$	0.073	$3.5 \cdot 10^{-4}$	0.077	$1.5 \cdot 10^{-7}$
0.135	0.052	0.043	$2.1 \cdot 10^{-3}$	0.043	$2.2 \cdot 10^{-11}$	0.049	$5.0 \cdot 10^{-4}$	0.054	$3.9 \cdot 10^{-8}$
0.141	0.032	0.030	$6.6 \cdot 10^{-4}$	0.030	$7.4 \cdot 10^{-14}$	0.036	$9.5 \cdot 10^{-4}$	0.041	$1.3 \cdot 10^{-8}$
0.147	0.018	0.021	$7.5 \cdot 10^{-4}$	0.022	$9.2 \cdot 10^{-13}$	0.027	$2.1 \cdot 10^{-3}$	0.031	$4.3 \cdot 10^{-9}$
0.153	0.010	0.014	$9.6 \cdot 10^{-4}$	0.016	$2.4 \cdot 10^{-12}$	0.018	$1.8 \cdot 10^{-3}$	0.022	$9.6 \cdot 10^{-10}$
0.153	0.010	0.014	$9.9 \cdot 10^{-4}$	0.015	$2.6 \cdot 10^{-12}$	0.017	$1.8 \cdot 10^{-3}$	0.021	$8.2 \cdot 10^{-10}$
0.156	0.005	0.010	$1.4 \cdot 10^{-3}$	0.012	$8.1 \cdot 10^{-12}$	0.013	$1.9 \cdot 10^{-3}$	0.016	$3.2 \cdot 10^{-10}$
0.161	0.003	0.008	$1.2 \cdot 10^{-3}$	0.009	$5.4 \cdot 10^{-12}$	0.008	$1.2 \cdot 10^{-3}$	0.010	$4.7 \cdot 10^{-11}$
0.170	0.001	0.004	$5.5 \cdot 10^{-4}$	0.005	$3.6 \cdot 10^{-13}$	−0.00	$5.8 \cdot 10^{-4}$	−0.00	$1.8 \cdot 10^{-15}$
0.205	0.001	0	$2.4 \cdot 10^{-4}$	0	$2.0 \cdot 10^{-15}$	−0.01	$3.4 \cdot 10^{-3}$	−0.02	$1.3 \cdot 10^{-9}$
0.237	0.001	0	$2.3 \cdot 10^{-4}$	0	$2.9 \cdot 10^{-15}$	−0.00	$1.7 \cdot 10^{-3}$	−0.02	$1.1 \cdot 10^{-9}$
0.261	0.001	0	$2.1 \cdot 10^{-4}$	0	$1.9 \cdot 10^{-15}$	0.002	$3.2 \cdot 10^{-4}$	−0.01	$5.2 \cdot 10^{-11}$
0.298	0.001	0	$2.0 \cdot 10^{-4}$	0	$1.7 \cdot 10^{-15}$	0.004	$7.8 \cdot 10^{-4}$	0.023	$1.2 \cdot 10^{-9}$
		Sum	$1.4 \cdot 10^{-2}$	**Sum**	$5.1 \cdot 10^{-11}$	**Sum**	$3.1 \cdot 10^{-2}$	**Sum**	$2.0 \cdot 10^{-4}$

In Table B.2, the experimentally measured values of the physical properties (density and conductivity), as well as the calculated values through the fitting equation, for the system {PVP (1) + NaKTartrate (2) + Water (3)} are shown.

Table B.2 - Density and conductivity obtained experimentally and calculated through the fitting equation for different compositions of salt and PVP in the homogeneous zone for the ATPS {PVP (1) + NaKTartrate (2) + Water (3)}.

w_{salt}	w_{PVP}	ρ_{exp} $(kg \cdot m^{-3})$	ρ'_{calc} $(kg \cdot m^{-3})$	μ_{exp} $(mS \cdot cm^{-1})$	μ'_{calc} $(mS \cdot cm^{-1})$
0	0	1.00	1.00	1.88	2.29
0.008	0.197	1.04	1.04	3.95	4.07
0.008	0.099	1.02	1.02	5.55	4.94
0.008	0.350	1.08	1.08	1.97	1.93
0.008	0.050	1.01	1.01	6.16	5.91
0.008	0.021	1.01	1.01	6.47	6.74
0.008	0.253	1.06	1.06	3.32	3.83
0.009	0.152	1.03	1.03	4.97	4.95
0.009	0.297	1.07	1.07	3.26	3.49
0.039	0.301	1.09	1.09	9.43	8.66
0.040	0.329	1.10	1.10	6.30	6.60
0.040	0.200	1.07	1.07	14.85	14.87
0.040	0.050	1.03	1.03	24.22	23.51
0.041	0.022	1.03	1.03	26.55	25.86
0.042	0.099	1.05	1.04	21.76	21.11
0.043	0.148	1.06	1.06	18.99	18.76
0.045	0.248	1.08	1.08	13.35	13.40
0.078	0.021	1.05	1.05	44.30	44.79
0.079	0.103	1.07	1.07	35.10	35.84
0.079	0.054	1.06	1.06	40.80	41.50
0.080	0.152	1.08	1.08	30.70	30.89
0.081	0.201	1.09	1.10	25.67	25.21
0.118	0	1.08	1.08	63.25	64.51
0.119	0.020	1.08	1.08	60.70	61.32
0.121	0.051	1.09	1.09	55.75	56.56
0.160	0.001	1.11	1.11	75.90	75.82
0.169	0	1.12	1.11	79.40	77.22
0.204	0	1.14	1.14	81.25	78.49
0.239	0	1.16	1.16	68.70	72.35
0.277	0	1.20	1.19	56.95	55.98

In Table B.3, the *F*-tests applied to the isolines of the two physical properties studied (density and conductivity) for the ATPS {PVP (1) + NaKTartrate (2) + Water (3)} are shown. The results were obtained using the function *F-Test Two-Sample for Variances* using Microsoft Excel. F is the ratio of variance of the first data points to variance of the second data points.

Since F is higher than F Critical for both physical properties (density and conductivity), it is possible to conclude that the null hypothesis is observed, *i.e.*, the variances of the two data points are equal[109].

Table B.3 – F-test results for the isolines of two physical properties – density and conductivity.

	Density		**Conductivity**	
Properties	ρ	ρ'	μ	μ'
Mean	1.07	1.07	29.71	29.71
Variance	0	0	697.54	696.43
Observations	30.00	30.00	30.00	30.00
Df	29.00	29.00	29.00	29.00
F	1.00		1.00	
P (F<=f) one-tail	0.50		0.50	
F Critical one-tail	1.86		1.86	
	F Critical > F		F Critical > F	

Appendix C. pH study

In Figs. C.1-C.12, the study of UV-Vis absorbance spectra stability for the three antioxidants (resveratrol, ferulic acid and gallic acid) is shown. This study consisted in the measurement of the UV-Vis absorbance spectra in the moment of preparation of the stocks solutions at different pH values and after settling for 3 days.

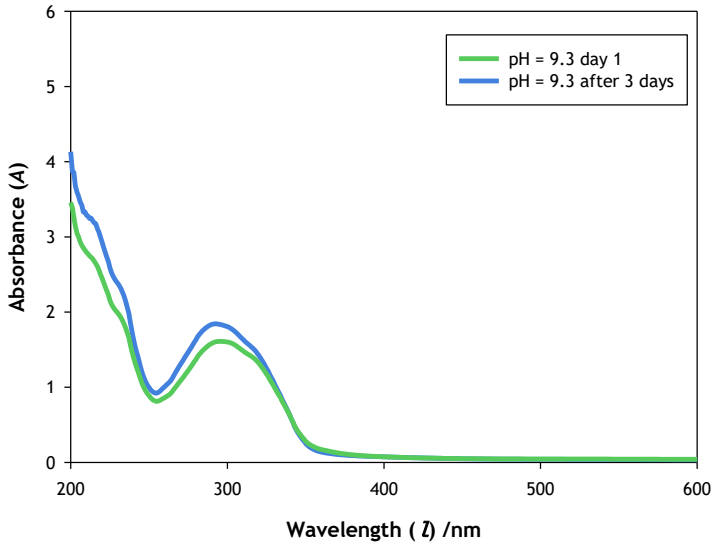


Fig. C.1 - Study of UV-Vis absorbance spectra stability for resveratrol ($\sim 9.16 \cdot 10^{-5}$ g·mL^{-1}) in the moment of preparation and after 3 days of settling for pH = 9.3 at 298.15 K and 0.1 MPa.

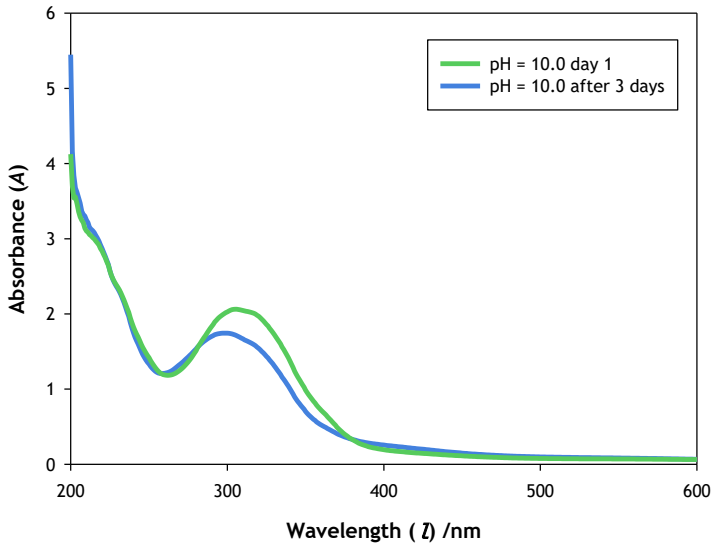


Fig. C.2 - Study of UV-Vis absorbance spectra stability for resveratrol ($\sim 9.16 \cdot 10^{-5}$ g·mL^{-1}) in the moment of preparation and after 3 days of settling for pH = 10.0 at 298.15 K and 0.1 MPa.

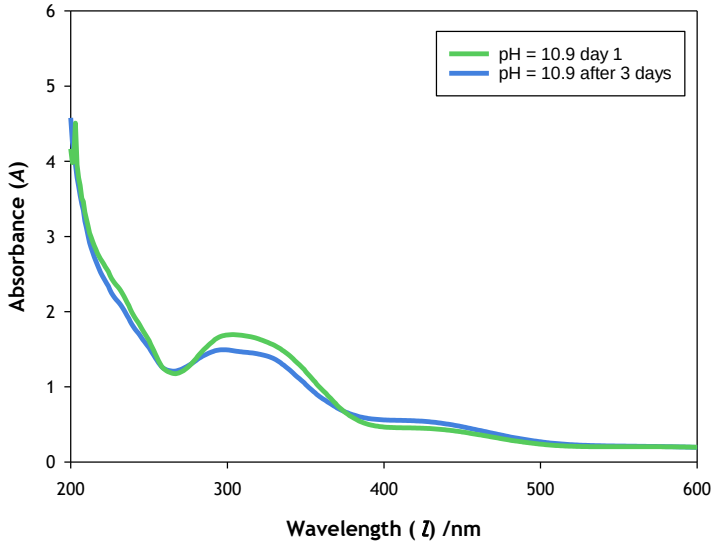


Fig. C.3 - Study of UV-Vis absorbance spectra stability for resveratrol ($\sim 9.16 \cdot 10^{-5}$ g·mL^{-1}) in the moment of preparation and after 3 days of settling for pH = 10.9 at 298.15 K and 0.1 MPa.

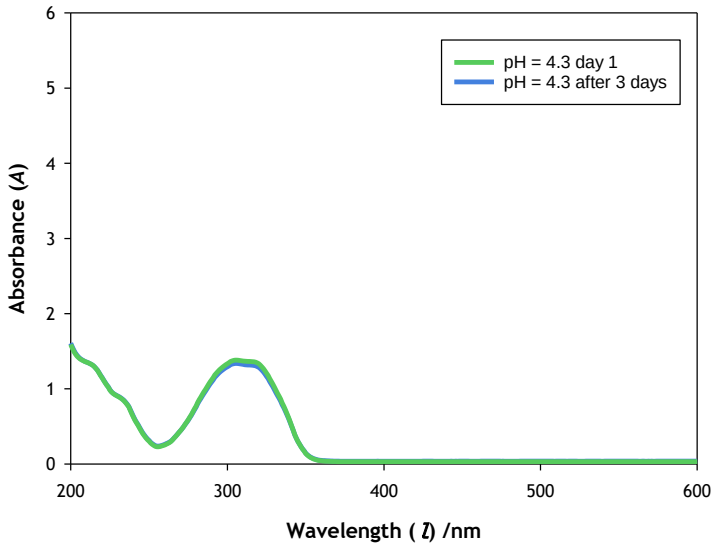


Fig. C.4 - Study of UV-Vis absorbance spectra stability for resveratrol ($\sim 9.16 \cdot 10^{-5}$ g·mL^{-1}) in the moment of preparation and after 3 days of settling for pH = 4.3 at 298.15 K and 0.1 MPa.

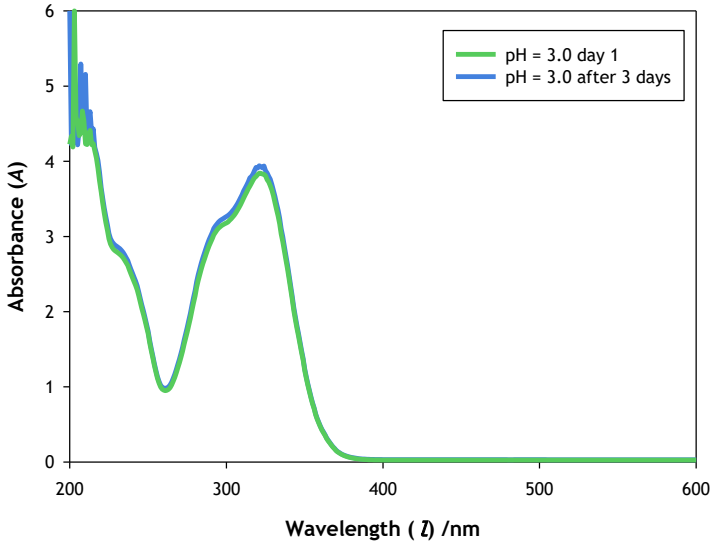


Fig. C.5 - Study of UV-Vis absorbance spectra stability for ferulic acid ($\sim 1.22 \cdot 10^{-4}$ g·mL^{-1}) in the moment of preparation and after 3 days of settling for pH = 3.0 at 298.15 K and 0.1 MPa.

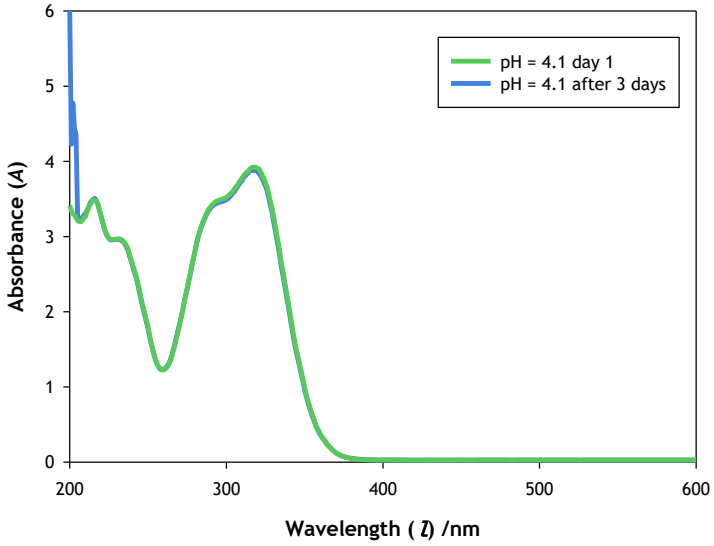


Fig. C.6 - Study of UV-Vis absorbance spectra stability for ferulic acid ($\sim 1.22 \cdot 10^{-4}$ g·mL^{-1})in the moment of preparation and after 3 days of settling for pH = 4.1 at 298.15 K and 0.1 MPa.

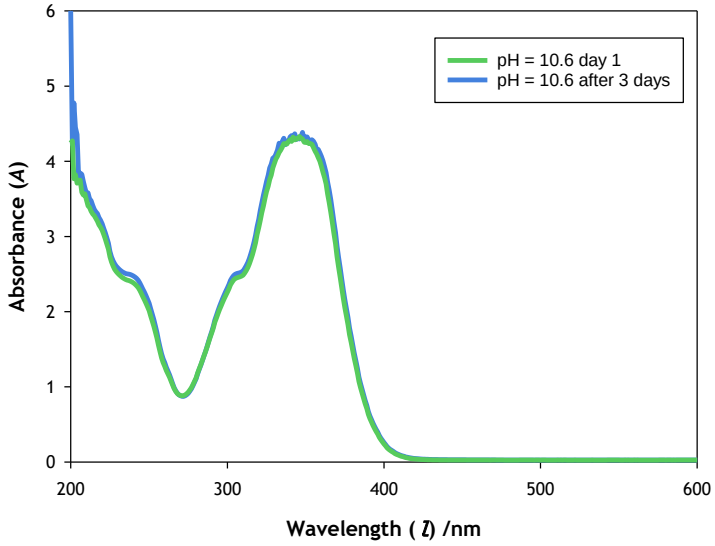


Fig. C.7 - Study of UV-Vis absorbance spectra stability for ferulic acid ($\sim 1.22 \cdot 10^{-4}$ g·mL^{-1}) in the moment of preparation and after 3 days of settling for pH = 10.6 at 298.15 K and 0.1 MPa.

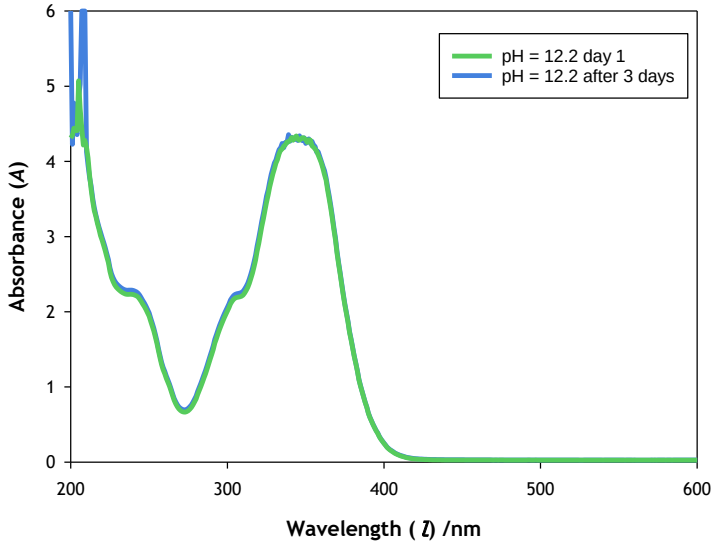


Fig. C.8 - Study of UV-Vis absorbance spectra stability for ferulic acid ($\sim 1.22 \cdot 10^{-4}$ g·mL^{-1}) in the moment of preparation and after 3 days of settling for pH = 12.2 at 298.15 K and 0.1 MPa.

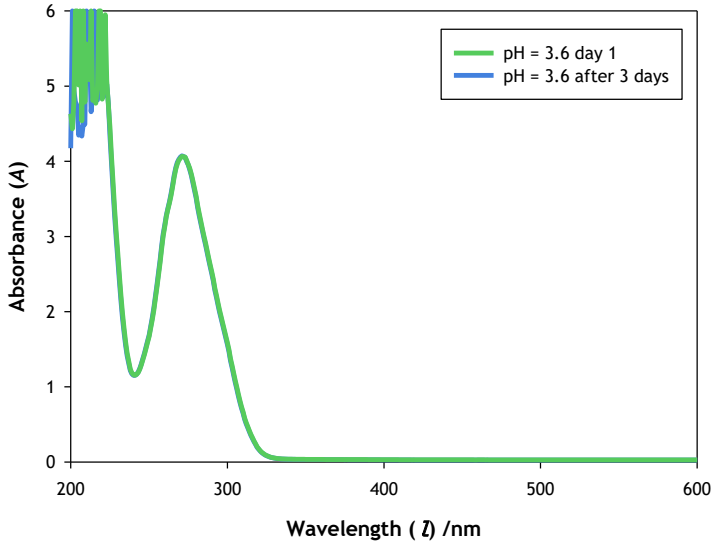


Fig. C.9 - Study of UV-Vis absorbance spectra stability for gallic acid ($\sim 2.00 \cdot 10^{-4}$ g·mL^{-1}) in the moment of preparation and after 3 days of settling for pH = 3.6 at 298.15 K and 0.1 MPa.

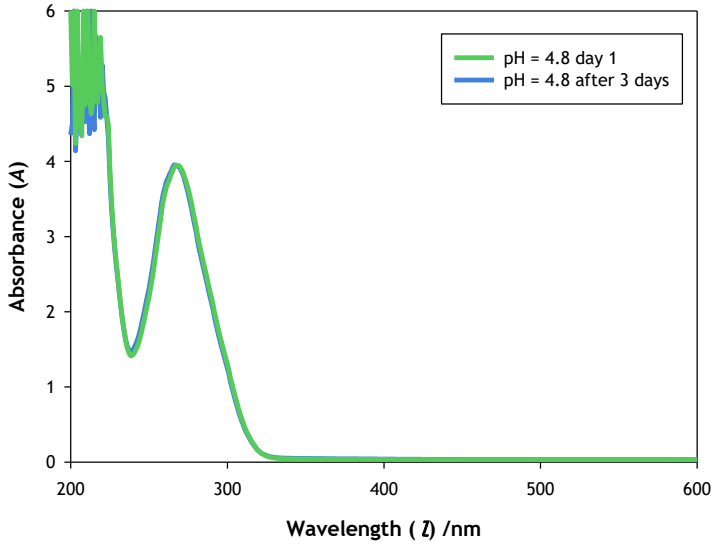


Fig. C.10 - Study of UV-Vis absorbance spectra stability for gallic acid ($\sim 2.00 \cdot 10^{-4}$ g·mL^{-1}) in the moment of preparation and after 3 days of settling for pH = 4.8 at 298.15 K and 0.1 MPa.

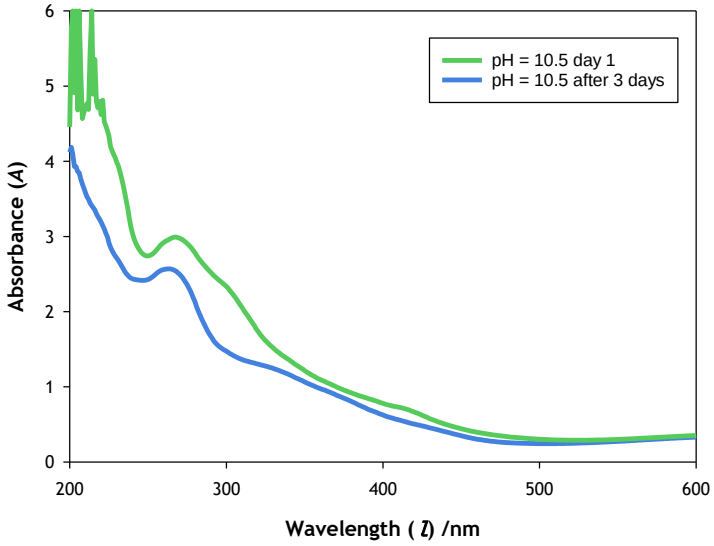


Fig. C.11 - Study of UV-Vis absorbance spectra stability for gallic acid (~$2.00 \cdot 10^{-4}$ g·mL^{-1}) in the moment of preparation and after 3 days of settling for pH = 10.5 at 298.15 K and 0.1 MPa.

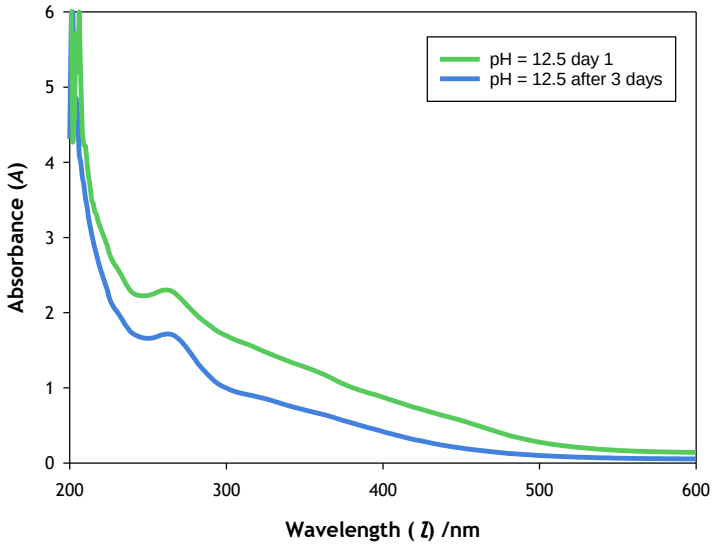


Fig. C.12 - Study of UV-Vis absorbance spectra stability for gallic acid (~$2.00 \cdot 10^{-4}$ g·mL^{-1}) in the moment of preparation and after 3 days of settling for pH = 12.5 at 298.15 K and 0.1 MPa.

Table C.1 shows the study of distribution of charges according to the $\mathrm{p}K_\mathrm{a}$ values of gallic acid, where x_{GA^0}, $x_{\mathrm{GA}^{-1}}$, $x_{\mathrm{GA}^{-2}}$, $x_{\mathrm{GA}^{-3}}$ are the antioxidant stage fractions of electrical charges equal to 0, -1, -2 and -3 e, respectively. e stands for the elementary charge ($1.602 \cdot 10^{-19}$ C).

Table C.1 – Calculated stage fraction of each antioxidant and mean electrical charge (q) at different pH values for gallic acid (GA).

pH	x_{GA^0}	$x_{\mathrm{GA}^{-1}}$	$x_{\mathrm{GA}^{-2}}$	$x_{\mathrm{GA}^{-3}}$	q / e
0.00	1.00	0.00	0.00	0.00	0.00
0.25	1.00	0.00	0.00	0.00	0.00
0.50	1.00	0.00	0.00	0.00	0.00
0.75	1.00	0.00	0.00	0.00	0.00
1.00	1.00	0.00	0.00	0.00	0.00
1.25	1.00	0.00	0.00	0.00	0.00
1.50	1.00	0.00	0.00	0.00	0.00
1.75	1.00	0.00	0.00	0.00	0.00
2.00	0.99	0.01	0.00	0.00	-0.01
2.25	0.99	0.01	0.00	0.00	-0.01
2.50	0.98	0.02	0.00	0.00	-0.02
2.75	0.97	0.03	0.00	0.00	-0.03
3.00	0.95	0.05	0.00	0.00	-0.05
3.25	0.91	0.09	0.00	0.00	-0.09
3.50	0.86	0.14	0.00	0.00	-0.14
3.75	0.77	0.23	0.00	0.00	-0.23
4.00	0.66	0.34	0.00	0.00	-0.34
4.25	0.52	0.48	0.00	0.00	-0.48
4.50	0.38	0.62	0.00	0.00	-0.62
4.75	0.25	0.75	0.00	0.00	-0.75
5.00	0.16	0.84	0.00	0.00	-0.84
5.25	0.10	0.90	0.00	0.00	-0.90
5.50	0.06	0.94	0.00	0.00	-0.94
5.75	0.03	0.97	0.00	0.00	-0.97
6.00	0.02	0.98	0.00	0.00	-0.98
6.25	0.01	0.99	0.00	0.00	-0.99
6.5	0.01	0.99	0.01	0.00	-1.00
6.75	0.00	0.98	0.01	0.00	-1.01
7.00	0.00	0.97	0.02	0.00	-1.02
7.25	0.00	0.96	0.04	0.00	-1.04
7.5	0.00	0.93	0.07	0.00	-1.07
7.75	0.00	0.88	0.12	0.00	-1.12
8.00	0.00	0.81	0.19	0.00	-1.19
8.25	0.00	0.70	0.30	0.00	-1.30
8.5	0.00	0.57	0.43	0.00	-1.43
8.75	0.00	0.43	0.57	0.00	-1.57
9.00	0.00	0.29	0.71	0.00	-1.71
9.25	0.00	0.19	0.81	0.00	-1.81
9.50	0.00	0.12	0.88	0.00	-1.89
9.75	0.00	0.07	0.92	0.01	-1.94
10.00	0.00	0.04	0.95	0.01	-1.97
10.25	0.00	0.02	0.96	0.02	-2.00
10.5	0.00	0.01	0.95	0.04	-2.03
10.75	0.00	0.01	0.93	0.07	-2.06
11.00	0.00	0.00	0.88	0.11	-2.11
11.25	0.00	0.00	0.82	0.18	-2.18
11.50	0.00	0.00	0.71	0.28	-2.28
11.75	0.00	0.00	0.59	0.41	-2.41
12.00	0.00	0.00	0.44	0.56	-2.56
12.25	0.00	0.00	0.31	0.69	-2.69
12.50	0.00	0.00	0.20	0.80	-2.80
12.75	0.00	0.00	0.12	0.88	-2.88
13.00	0.00	0.00	0.07	0.93	-2.93
13.25	0.00	0.00	0.04	0.96	-2.96
13.50	0.00	0.00	0.02	0.98	-2.98
13.75	0.00	0.00	0.01	0.99	-2.99
14.00	0.00	0.00	0.01	0.99	-2.99

Table C.2 shows the study of distribution of charges according to the pK_a values of ferulic acid, where x_{FA^0}, $x_{FA^{-1}}$ and $x_{FA^{-2}}$ are the antioxidant stage fractions of electrical charges equal to 0, -1 and -2 e, respectively. e stands for the elementary charge ($1.60 \cdot 10^{-19}$ C).

Table C.2 - Calculated stage fraction of each antioxidant and mean electrical charge (q) at different pH values for ferulic acid (FA).

pH	x_{FA^0}	$x_{FA^{-1}}$	$x_{FA^{-2}}$	q / e
0.00	1.00	0.00	0.00	0.00
0.25	1.00	0.00	0.00	0.00
0.50	1.00	0.00	0.00	0.00
0.75	1.00	0.00	0.00	0.00
1.00	1.00	0.00	0.00	0.00
1.25	1.00	0.00	0.00	0.00
1.50	1.00	0.00	0.00	0.00
1.75	1.00	0.00	0.00	0.00
2.00	1.00	0.00	0.00	0.00
2.25	0.99	0.01	0.00	-0.01
2.50	0.99	0.01	0.00	-0.01
2.75	0.98	0.02	0.00	-0.02
3.00	0.97	0.03	0.00	-0.03
3.25	0.95	0.05	0.00	-0.05
3.50	0.91	0.09	0.00	-0.09
3.75	0.85	0.15	0.00	-0.15
4.00	0.76	0.24	0.00	-0.24
4.25	0.64	0.36	0.00	-0.36
4.50	0.50	0.50	0.00	-0.50
4.75	0.36	0.64	0.00	-0.64
5.00	0.24	0.76	0.00	-0.76
5.25	0.15	0.85	0.00	-0.85
5.50	0.09	0.91	0.00	-0.91
5.75	0.05	0.95	0.00	-0.95
6.00	0.03	0.97	0.00	-0.97
6.25	0.02	0.98	0.00	-0.98
6.5	0.01	0.99	0.00	-0.99
6.75	0.01	0.99	0.01	-1.00
7.00	0.00	0.99	0.01	-1.01
7.25	0.00	0.98	0.02	-1.02
7.5	0.00	0.96	0.04	-1.04
7.75	0.00	0.94	0.06	-1.06
8.00	0.00	0.89	0.11	-1.11
8.25	0.00	0.82	0.18	-1.18
8.5	0.00	0.72	0.28	-1.28
8.75	0.00	0.60	0.40	-1.40
9.00	0.00	0.45	0.55	-1.55
9.25	0.00	0.32	0.68	-1.68
9.50	0.00	0.21	0.79	-1.79
9.75	0.00	0.13	0.87	-1.87
10.00	0.00	0.08	0.92	-1.92
10.25	0.00	0.04	0.96	-1.96
10.5	0.00	0.03	0.97	-1.97
10.75	0.00	0.01	0.99	-1.99
11.00	0.00	0.01	0.99	-1.99
11.25	0.00	0.00	1.00	-2.00
11.50	0.00	0.00	1.00	-2.00
11.75	0.00	0.00	1.00	-2.00
12.00	0.00	0.00	1.00	-2.00
12.25	0.00	0.00	1.00	-2.00
12.50	0.00	0.00	1.00	-2.00
12.75	0.00	0.00	1.00	-2.00
13.00	0.00	0.00	1.00	-2.00
13.25	0.00	0.00	1.00	-2.00
13.50	0.00	0.00	1.00	-2.00
13.75	0.00	0.00	1.00	-2.00
14.00	0.00	0.00	1.00	-2.00

Table C.3 shows the study of distribution of charges according to the $\mathrm{p}K_\mathrm{a}$ values of RVT, where x_{RVT^0}, $x_{\mathrm{RVT}^{-1}}$, $x_{\mathrm{RVT}^{-2}}$, $x_{\mathrm{RVY}^{-3}}$ are the antioxidant stage fractions of electrical charges equal to 0, -1, -2 and -3 e, respectively. e stands for the elementary charge ($1.602 \cdot 10^{-19}$ C).

Table C.3 - Calculated stage fraction of each antioxidant and mean electrical charge (q) at different pH values for resveratrol (RVT).

pH	x_{RVT^0}	$x_{\mathrm{RVT}^{-1}}$	$x_{\mathrm{RVT}^{-2}}$	$x_{\mathrm{RVT}^{-3}}$	q / e
0	1.00	0.00	0.00	0.00	0.00
0.25	1.00	0.00	0.00	0.00	0.00
0.5	1.00	0.00	0.00	0.00	0.00
0.75	1.00	0.00	0.00	0.00	0.00
1	1.00	0.00	0.00	0.00	0.00
1.25	1.00	0.00	0.00	0.00	0.00
1.5	1.00	0.00	0.00	0.00	0.00
1.75	1.00	0.00	0.00	0.00	0.00
2	1.00	0.00	0.00	0.00	0.00
2.25	1.00	0.00	0.00	0.00	0.00
2.5	1.00	0.00	0.00	0.00	0.00
2.75	1.00	0.00	0.00	0.00	0.00
3	1.00	0.00	0.00	0.00	0.00
3.25	1.00	0.00	0.00	0.00	0.00
3.5	1.00	0.00	0.00	0.00	0.00
3.75	1.00	0.00	0.00	0.00	0.00
4	1.00	0.00	0.00	0.00	0.00
4.25	1.00	0.00	0.00	0.00	0.00
4.5	1.00	0.00	0.00	0.00	0.00
4.75	1.00	0.00	0.00	0.00	0.00
5	1.00	0.00	0.00	0.00	0.00
5.25	1.00	0.00	0.00	0.00	0.00
5.5	1.00	0.00	0.00	0.00	0.00
5.75	1.00	0.00	0.00	0.00	0.00
6	1.00	0.00	0.00	0.00	0.00
6.25	1.00	0.00	0.00	0.00	0.00
6.5	0.99	0.01	0.00	0.00	-0.01
6.75	0.99	0.01	0.00	0.00	-0.01
7	0.98	0.02	0.00	0.00	-0.02
7.25	0.97	0.03	0.00	0.00	-0.03
7.5	0.94	0.06	0.00	0.00	-0.06
7.75	0.90	0.09	0.00	0.00	-0.10
8	0.84	0.16	0.00	0.00	-0.16
8.25	0.74	0.25	0.01	0.00	-0.27
8.5	0.61	0.36	0.03	0.00	-0.42
8.75	0.45	0.47	0.07	0.00	-0.62
9	0.30	0.55	0.15	0.00	-0.86
9.25	0.17	0.55	0.27	0.01	-1.12
9.5	0.08	0.48	0.42	0.02	-1.37
9.75	0.03	0.36	0.56	0.04	-1.61
10	0.01	0.24	0.66	0.09	-1.82
10.25	0.00	0.14	0.69	0.16	-2.01
10.5	0.00	0.07	0.65	0.27	-2.19
10.75	0.00	0.04	0.55	0.41	-2.37
11	0.00	0.02	0.42	0.56	-2.54
11.25	0.00	0.01	0.30	0.70	-2.69
11.5	0.00	0.00	0.19	0.80	-2.80
11.75	0.00	0.00	0.12	0.88	-2.88
12	0.00	0.00	0.07	0.93	-2.93
12.25	0.00	0.00	0.04	0.96	-2.96
12.5	0.00	0.00	0.02	0.98	-2.98
12.75	0.00	0.00	0.01	0.99	-2.99
13	0.00	0.00	0.01	0.99	-2.99
13.25	0.00	0.00	0.00	1.00	-3.00
13.5	0.00	0.00	0.00	1.00	-3.00
13.75	0.00	0.00	0.00	1.00	-3.00
14	0.00	0.00	0.00	1.00	-3.00

Appendix D. Calibration curves

In order to study the validity of the calibration curves of the three antioxidants (ferulic acid, gallic acid and resveratrol), a series of parameters were taken into account and are shown in Tables D.1-D.4.

Table D.1 - Parameters of validation of the calibration curve for gallic acid.

Parameter	Requisite	Experimental	Validity
Reference points	5	18	✓
Concentration range (linearity interval)	Factor of 10 or superior	Factor of 80	✓
Correlation coefficient	≥ 0.9950	0.9996	✓
Standard deviation related to the slope	$< 5\ \%$	$0.70\ \%$	✓
y-intercept	Contains the intercept $\beta - S_\beta < 0 < \beta + S_\beta$	$\beta - S_\beta = 1.04 \cdot 10^{-2}$ $\beta + S_\beta = 4.01 \cdot 10^{-2}$	✗

Table D.2 – Parameters of validation of the calibration curve for ferulic acid.

Parameter	Requisite	Experimental	Validity
Reference points	5	16	✓
Concentration range (linearity interval)	Factor of 10 or superior	Factor of 90	✓
Correlation coefficient	≥ 0.9950	0.9996	✓
Standard deviation related to the slope	$< 5\ \%$	$0.72\ \%$	✓
y-intercept	Contains the intercept $\beta - S_\beta < 0 < b + S_\beta$	$\beta - S_\beta = 5.19 \cdot 10^{-3}$ $\beta + S_\beta = 3.70 \cdot 10^{-2}$	✗

Table D.3 - Parameters of validation of the calibration curve for resveratrol.

Parameter	Requisite	Experimental	Validity
Reference points	5	16	✓
Concentration range (linearity interval)	Factor of 10 or superior	Factor of 70	✓
Correlation coefficient	≥ 0.9950	0.9992	✓
Standard deviation related to the slope	$< 5\ \%$	$1.04\ \%$	✓
y-intercept	Contains the intercept $\beta - S_\beta < 0 < \beta + S_\beta$	$\beta - S_\beta = 5.37 \cdot 10^{-3}$ $\beta + S_\beta = 1.77 \cdot 10^{-2}$	✗

Table D.4 – Parameters of the calibration curves for ferulic acid, gallic acid and resveratrol.

Parameter	Ferulic acid	Gallic acid	Resveratrol
Sensibility	43 253.26	22 917.26	22 711.51
Detection limit (A)	$6.89 \cdot 10^{-2}$	$6.99 \cdot 10^{-2}$	$3.01 \cdot 10^{-2}$
Detection limit (C)	$7.36 \cdot 10^{-7}$	$1.30 \cdot 10^{-6}$	$5.44 \cdot 10^{-7}$
Quantification limit (A)	$1.80 \cdot 10^{-1}$	$1.74 \cdot 10^{-1}$	$7.34 \cdot 10^{-2}$
Quantification limit (C)	$3.68 \cdot 10^{-6}$	$6.50 \cdot 10^{-6}$	$2.72 \cdot 10^{-6}$

Appendix E. Extraction of antioxidants

This appendix presents the data related to the extraction of the three antioxidants (ferulic acid, gallic acid and resveratrol) in the different ATPS studied {ethyl lactate (1) + K_3Citrate or Na_3Citrate or Na_2Succinate or NaKTartrate (2) + Water (3)}.

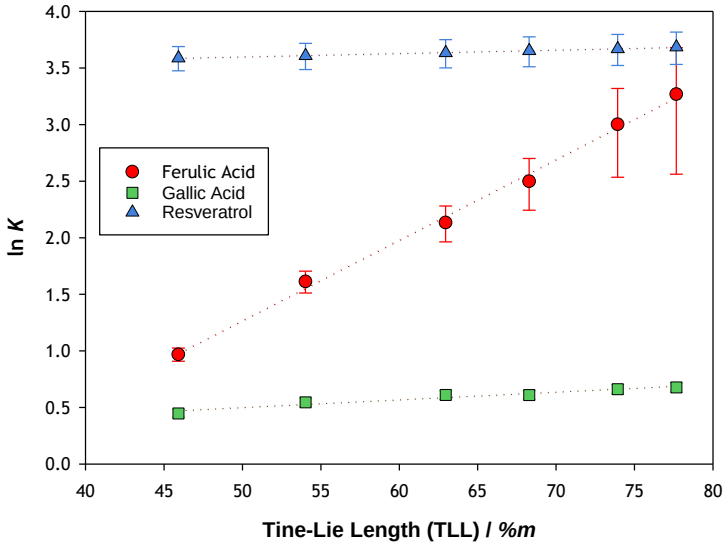


Fig. E.1. - Relation between the natural logarithms of the experimental partition coefficients (*K*) and the tie-line lengths (TLL) for ferulic acid (FA), gallic acid (GA) and resveratrol (RVT) in the ATPS {ethyl lactate (1) + K_3Citrate (2) + water (3)} at 298.15 K and 0.1 MPa.

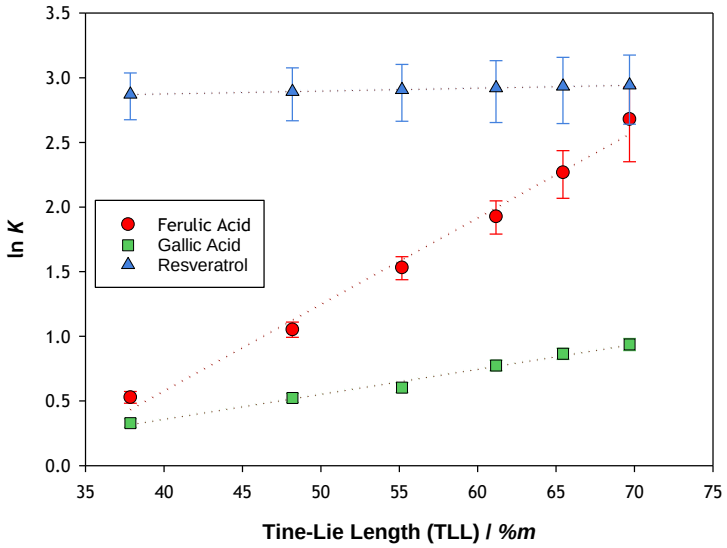


Fig. E.2 - Relation between the natural logarithms of the experimental partition coefficients (*K*) and the tie-line lengths (TLL) for ferulic acid (FA), gallic acid (GA) and resveratrol (RVT) in the ATPS {ethyl lactate (1) + Na_3Citrate (2) + water (3)} at 298.15 K and 0.1 MPa.

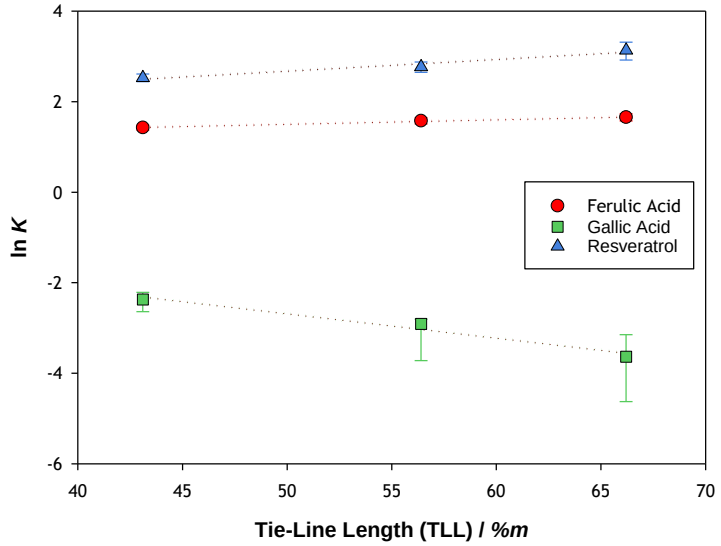


Fig. E.3 - Relation between the natural logarithms of the experimental partition coefficients (*K*) and the tie-line lengths (TLL) for ferulic acid (FA), gallic acid (GA) and resveratrol (RVT) in the ATPS {ethyl lactate (1) + Na_2Succinate (2) + water (3)} at 298.15 K and 0.1 MPa.

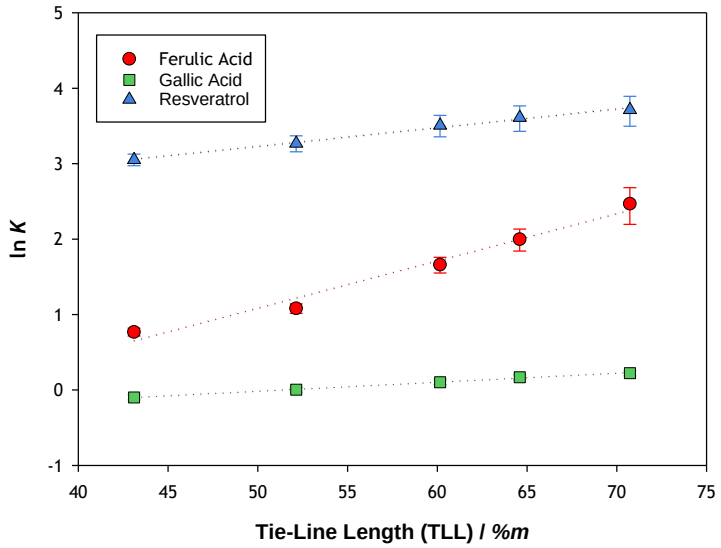


Fig. E.4 - Relation between the natural logarithms of the experimental partition coefficients (*K*) and the tie-line lengths (TLL) for ferulic acid (FA), gallic acid (GA) and resveratrol (RVT) in the ATPS {ethyl lactate (1) + NaKTartrate (2) + water (3)} at 298.15 K and 0.1 MPa.

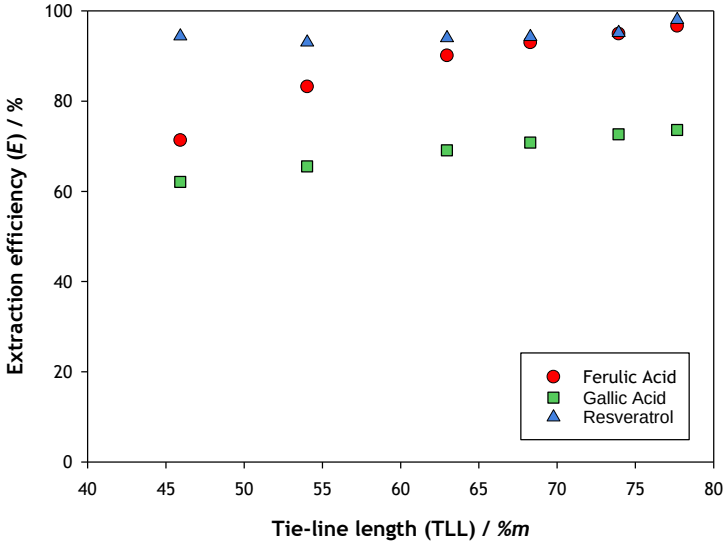


Fig. E.5 - Relation between the extraction efficiencies (*E*) and the tie-line lengths (TLL) for ferulic acid (FA) gallic acid (GA) and resveratrol (RVT) in the ATPS {ethyl lactate (1) + K_3Citrate (2) and water (3)} at 298.15 K and 0.1 MPa.

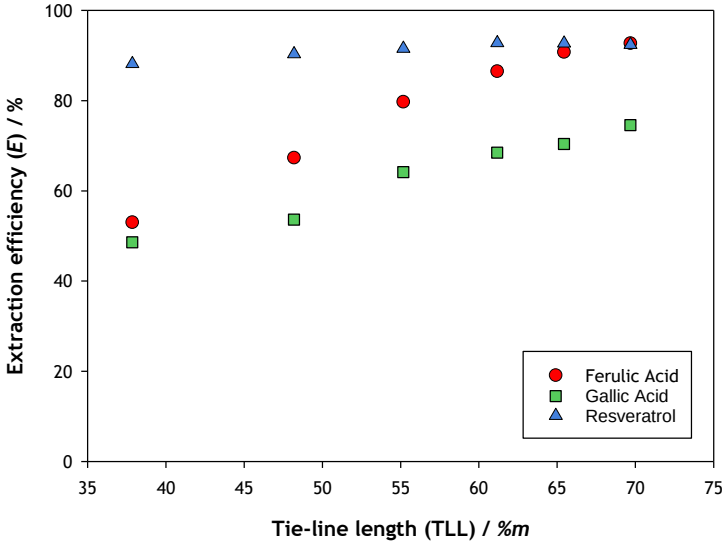


Fig. E.6 - Relation between the extraction efficiencies (*E*) and the tie-line lengths (TLL) for ferulic acid (FA) gallic acid (GA) and resveratrol (RVT) in the ATPS {ethyl lactate (1) + Na_3Citrate (2) and water (3)} at 298.15 K and 0.1 MPa.

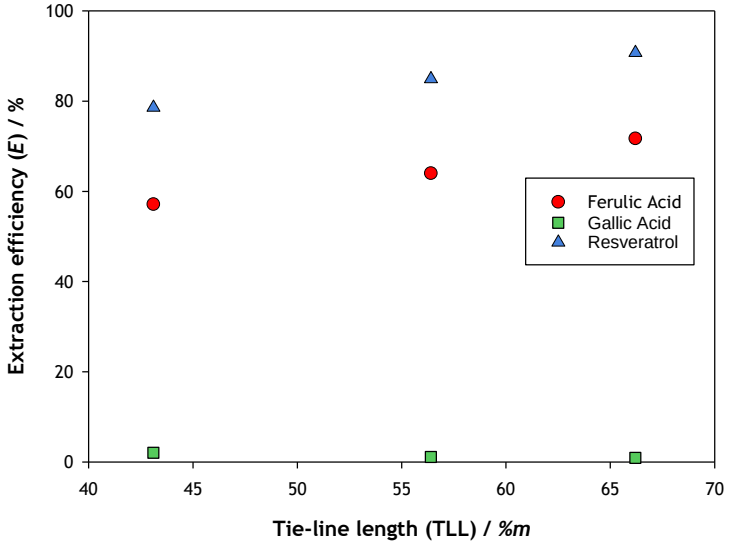


Fig. E.7 - Relation between the extraction efficiencies (*E*) and the tie-line lengths (TLL) for ferulic acid (FA) gallic acid (GA) and resveratrol (RVT) in the ATPS {ethyl lactate (1) + Na_2Succinate (2) and water (3)} at 298.15 K and 0.1 MPa.

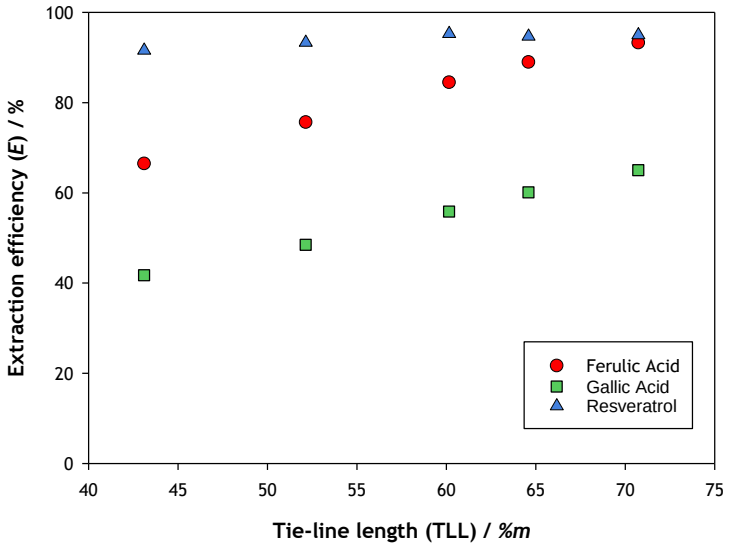


Fig. E.8 - Relation between the extraction efficiencies (*E*) and the tie-line lengths (TLL) for ferulic acid (FA), gallic acid (GA) and resveratrol (RVT) in the ATPS {ethyl lactate (1) + NaKTartrate (2) and water (3)} at 298.15 K and 0.1 MPa.

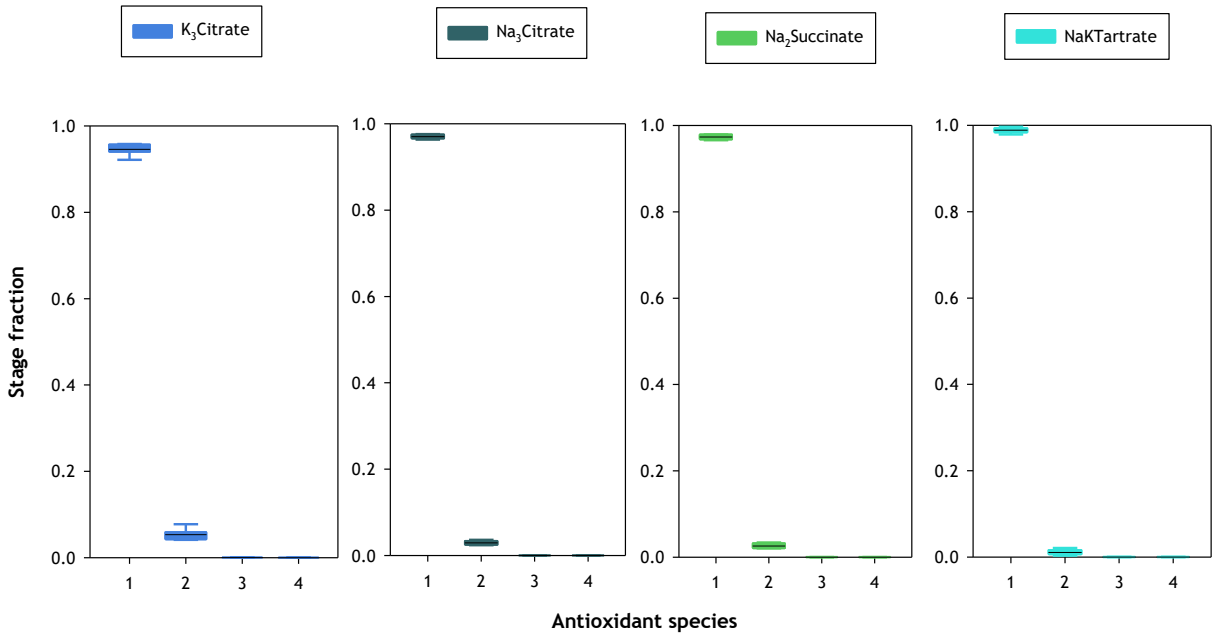


Fig. E.9 - Effect of the tie-line compositions in the calculated stage fractions of the antioxidant stages of resveratrol (RVT) in the ATPS containing ethyl lactate, water and different salts (K_3Citrate, Na_3Citrate, Na_2Succinate and NaKTartrate) at 298.15 K and 0.1 MPa.

Table E.1 - Experimental phase mass (m), antioxidant mass losses (L_m), antioxidant concentration (C), phase density (ρ) and phase pH for the top and bottom phases in the extraction of gallic acid, ferulic acid and resveratrol in the ATPS {ethyl lactate (1) + trisodium citrate (2) + water (3)} at 298.15 K and 0.1 MPa.

Tie-Line	Phase	m / g	L_m / %	C / g · mL^{-1}	ρ / g · mL^{-1}	pH
Gallic acid in {EL (1) + Na_3Citrate (2) + Water (3)}						
1	Top	3.9712	−0.52	$8.11 \cdot 10^{-5}$	1.05717	7.36
	Bottom	6.0217		$5.83 \cdot 10^{-5}$	1.12267	7.33
2	Top	3.9556	−0.25	$8.90 \cdot 10^{-5}$	1.04894	7.33
	Bottom	6.0885		$5.27 \cdot 10^{-5}$	1.13875	7.33
3	Top	4.7830	−0.69	$8.77 \cdot 10^{-5}$	1.04395	7.35
	Bottom	5.2566		$4.79 \cdot 10^{-5}$	1.15652	7.36
4	Top	4.7938	−1.12	$9.34 \cdot 10^{-5}$	1.04385	7.36
	Bottom	5.1479		$4.30 \cdot 10^{-5}$	1.17005	7.56
5	Top	4.8096	−0.66	$9.56 \cdot 10^{-5}$	1.04291	7.39
	Bottom	5.2244		$4.02 \cdot 10^{-5}$	1.17719	7.62
6	Top	5.1917	−0.49	$9.38 \cdot 10^{-5}$	1.04110	7.44
	Bottom	4.8698		$3.67 \cdot 10^{-5}$	1.19781	7.62
Ferulic acid in {EL (1) + Na_3Citrate (2) + Water (3)}						
1	Top	4.0326	−0.41	$3.82 \cdot 10^{-5}$	1.06631	7.49
	Bottom	5.9923		$2.25 \cdot 10^{-5}$	1.09589	7.50
2	Top	4.2842	−0.20	$4.56 \cdot 10^{-5}$	1.06154	7.36
	Bottom	5.7625		$1.59 \cdot 10^{-5}$	1.11329	7.37
3	Top	4.8229	−0.50	$4.74 \cdot 10^{-5}$	1.05130	7.34
	Bottom	5.2068		$1.02 \cdot 10^{-5}$	1.13350	7.39
4	Top	5.0262	−0.49	$4.92 \cdot 10^{-5}$	1.04683	7.34
	Bottom	4.9886		$7.15 \cdot 10^{-6}$	1.14866	7.36
5	Top	5.3019	−0.36	$4.84 \cdot 10^{-5}$	1.04361	7.38
	Bottom	4.6933		$5.00 \cdot 10^{-6}$	1.16247	7.35
6	Top	5.5474	−0.21	$4.75 \cdot 10^{-5}$	1.04404	7.42
	Bottom	4.5557		$3.36 \cdot 10^{-6}$	1.17527	7.36
Resveratrol in {EL (1) + Na_3Citrate (2) + Water (3)}						
1	Top	3.7449	−0.84	$1.71 \cdot 10^{-5}$	1.05031	7.14
	Bottom	6.2275		$9.62 \cdot 10^{-7}$	1.12571	7.11
2	Top	4.2547	−0.76	$1.53 \cdot 10^{-5}$	1.04615	7.20
	Bottom	5.7364		$8.51 \cdot 10^{-7}$	1.1388	7.13
3	Top	4.5240	−0.66	$1.46 \cdot 10^{-5}$	1.04382	7.20
	Bottom	5.4766		$7.95 \cdot 10^{-7}$	1.15492	7.15
4	Top	4.8996	−0.93	$1.36 \cdot 10^{-5}$	1.04259	7.23
	Bottom	5.0818		$7.33 \cdot 10^{-7}$	1.16688	7.32
5	Top	5.1535	−0.40	$1.29 \cdot 10^{-5}$	1.04126	7.22
	Bottom	4.8613		$6.88 \cdot 10^{-7}$	1.17741	7.28
6	Top	5.2745	−0.85	$1.25 \cdot 10^{-5}$	1.03611	7.29
	Bottom	4.7184		$6.60 \cdot 10^{-7}$	1.19608	7.24

Table E.2 - Experimental phase mass (m), antioxidant mass losses (L_m), antioxidant concentration (C), phase density (ρ) and phase pH for the top and bottom phases in the extraction of gallic acid, ferulic acid and resveratrol in the ATPS {ethyl lactate (1) + tripotassium citrate (2) + water (3)} at 298.15 K and 0.1 MPa.

Tie-Line	Phase	m / g	L_m / %	C / g · mL^{-1}	ρ / g · mL^{-1}	pH
Gallic acid in {EL (1) + K_3Citrate (2) + Water (3)}						
1	Top	5.0341	−0.67	$8.29 \cdot 10^{-5}$	1.06598	7.56
	Bottom	4.9839		$5.27 \cdot 10^{-5}$	1.13952	7.68
2	Top	5.1521	−0.51	$8.58 \cdot 10^{-5}$	1.06438	7.56
	Bottom	4.8572		$4.94 \cdot 10^{-5}$	1.14674	7.70
3	Top	5.3737	−0.42	$8.58 \cdot 10^{-5}$	1.05704	7.58
	Bottom	4.6898		$4.63 \cdot 10^{-5}$	1.16473	7.70
4	Top	5.4942	−0.40	$8.54 \cdot 10^{-5}$	1.05212	7.59
	Bottom	4.5353		$4.61 \cdot 10^{-5}$	1.18149	7.82
5	Top	5.5606	−0.50	$8.65 \cdot 10^{-5}$	1.04930	7.61
	Bottom	4.4468		$4.44 \cdot 10^{-5}$	1.19981	7.78
6	Top	5.5914	−0.60	$8.61 \cdot 10^{-5}$	1.04942	7.65
	Bottom	4.3850		$4.35 \cdot 10^{-5}$	1.21668	7.93
Ferulic acid in {EL (1) + K_3Citrate (2) + Water (3)}						
1	Top	4.8465	−0.52	$8.29 \cdot 10^{-5}$	1.07341	7.75
	Bottom	5.1568		$5.27 \cdot 10^{-5}$	1.13804	7.73
2	Top	5.0310	−0.34	$8.58 \cdot 10^{-5}$	1.05944	7.75
	Bottom	4.9931		$4.94 \cdot 10^{-5}$	1.16013	7.74
3	Top	5.2857	−0.40	$8.58 \cdot 10^{-5}$	1.05433	7.73
	Bottom	4.7126		$4.63 \cdot 10^{-5}$	1.17877	7.76
4	Top	5.3688	−0.47	$8.54 \cdot 10^{-5}$	1.04734	7.75
	Bottom	4.6258		$4.61 \cdot 10^{-5}$	1.19250	7.78
5	Top	5.5171	−0.67	$8.65 \cdot 10^{-5}$	1.04685	7.75
	Bottom	4.4224		$4.44 \cdot 10^{-5}$	1.21242	7.81
6	Top	5.7985	−0.61	$8.61 \cdot 10^{-5}$	1.04685	7.75
	Bottom	4.3484		$4.35 \cdot 10^{-5}$	1.21885	7.82
Resveratrol in {EL (1) + K_3Citrate (2) + Water (3)}						
1	Top	4.7376	−0.68	$1.50 \cdot 10^{-5}$	1.09061	7.37
	Bottom	5.2458		$4.14 \cdot 10^{-7}$	1.15041	7.38
2	Top	4.8898	−0.66	$1.41 \cdot 10^{-5}$	1.07885	7.36
	Bottom	5.0966		$3.83 \cdot 10^{-7}$	1.15923	7.42
3	Top	5.1701	−0.50	$1.35 \cdot 10^{-5}$	1.07774	7.39
	Bottom	5.1705		$3.57 \cdot 10^{-7}$	1.16745	7.43
4	Top	5.3554	−0.82	$1.30 \cdot 10^{-5}$	1.07437	7.51
	Bottom	4.6205		$3.37 \cdot 10^{-7}$	1.19500	7.51
5	Top	5.4847	−0.98	$1.27 \cdot 10^{-5}$	1.06902	7.50
	Bottom	4.4542		$3.25 \cdot 10^{-7}$	1.21203	7.58
6	Top	5.7583	−0.86	$1.24 \cdot 10^{-5}$	1.06030	7.53
	Bottom	4.3781		$3.12 \cdot 10^{-7}$	1.21984	7.68

Table E.3 - Experimental phase mass (m), antioxidant mass losses (L_m), antioxidant concentration (C), phase density (ρ) and phase pH for the top and bottom phases in the extraction of gallic acid, ferulic acid and resveratrol in the ATPS {ethyl lactate (1) + disodium succinate (2) + water (3)} at 298.15 K and 0.1 MPa.

Tie-Line	Phase	m / g	L_m / %	C / g · mL^{-1}	ρ / g · mL^{-1}	pH
Gallic acid in {EL (1) + Na_2Succinate (2) + Water (3)}						
1	Top	2.5343	−0.59	$7.94 \cdot 10^{-6}$	1.05331	7.43
	Bottom	7.4560		$8.80 \cdot 10^{-5}$	1.13187	7.09
2	Top	2.7734	−0.88	$3.89 \cdot 10^{-6}$	1.05094	7.18
	Bottom	7.1883		$9.20 \cdot 10^{-5}$	1.13823	7.08
3	Top	3.3147	−0.78	$2.66 \cdot 10^{-6}$	1.04685	7.23
	Bottom	6.7511		$1.01 \cdot 10^{-4}$	1.14673	7.10
Ferulic acid in {EL (1) + Na_2Succinate (2) + Water (3)}						
1	Top	2.3664	−0.51	$6.91 \cdot 10^{-5}$	1.05065	7.13
	Bottom	7.6460		$1.65 \cdot 10^{-5}$	1.12142	7.17
2	Top	2.7637	−0.54	$6.62 \cdot 10^{-5}$	1.04976	7.13
	Bottom	7.2318		$1.36 \cdot 10^{-5}$	1.11646	7.13
3	Top	3.3355	−0.80	$6.13 \cdot 10^{-5}$	1.04637	7.18
	Bottom	6.6332		$1.17 \cdot 10^{-5}$	1.14317	7.22
Resveratrol in {EL (1) + Na_2Succinate (2) + Water (3)}						
1	Top	2.4170	−0.82	$4.87 \cdot 10^{-5}$	1.05609	7.24
	Bottom	7.5530		$3.88 \cdot 10^{-6}$	1.12070	7.07
2	Top	2.7324	−0.76	$4.63 \cdot 10^{-5}$	1.04922	7.16
	Bottom	7.2495		$2.90 \cdot 10^{-6}$	1.11748	7.05
3	Top	3.4559	−0.83	$3.89 \cdot 10^{-5}$	1.04408	7.28
	Bottom	6.5689		$1.69 \cdot 10^{-6}$	1.14185	7.13

Table E.4 - Experimental phase mass (m), antioxidant mass losses (L_m), antioxidant concentration (C), phase density (ρ) and phase pH for the top and bottom phases in the extraction of gallic acid, ferulic acid and resveratrol in the ATPS {ethyl lactate (1) + sodium potassium tartrate (2) + water (3)} at 298.15 K and 0.1 MPa.

Tie-Line	Phase	m / g	L_m / %	C / g · mL^{-1}	ρ / g · mL^{-1}	pH
Gallic acid in {EL (1) + NaKTartrate (2) + Water (3)}						
1	Top	4.5732	−0.56	$6.49 \cdot 10^{-5}$	1.12251	6.42
	Bottom	5.3971		$7.16 \cdot 10^{-5}$	1.12078	6.62
2	Top	4.9212	−0.49	$6.83 \cdot 10^{-5}$	1.09480	6.40
	Bottom	5.0654		$6.80 \cdot 10^{-5}$	1.13146	6.75
3	Top	5.3427	−0.39	$7.12 \cdot 10^{-5}$	1.07553	6.71
	Bottom	4.6558		$6.42 \cdot 10^{-5}$	1.14649	6.95
4	Top	5.5257	−0.85	$7.33 \cdot 10^{-5}$	1.06218	6.49
	Bottom	4.4420		$6.19 \cdot 10^{-5}$	1.16764	7.04
5	Top	5.7553	−0.60	$7.55 \cdot 10^{-5}$	1.05683	6.84
	Bottom	4.2334		$6.04 \cdot 10^{-5}$	1.19553	7.06
Ferulic acid in {EL (1) + NaKTartrate (2) + Water (3)}						
1	Top	4.8238	−0.72	$4.02 \cdot 10^{-5}$	1.06950	6.28
	Bottom	5.1533		$1.87 \cdot 10^{-5}$	1.11754	6.77
2	Top	5.0839	−0.82	$4.32 \cdot 10^{-5}$	1.06436	6.38
	Bottom	4.8760		$1.47 \cdot 10^{-5}$	1.13020	6.70
3	Top	5.2756	−0.79	$4.60 \cdot 10^{-5}$	1.05445	6.47
	Bottom	4.6844		$8.75 \cdot 10^{-6}$	1.14582	6.85
4	Top	5.4829	−0.68	$4.65 \cdot 10^{-5}$	1.05114	6.60
	Bottom	4.4941		$6.30 \cdot 10^{-6}$	1.15990	6.84
5	Top	5.8762	−0.67	$4.54 \cdot 10^{-5}$	1.04784	6.70
	Bottom	4.0933		$3.84 \cdot 10^{-6}$	1.18348	6.86
Resveratrol in {EL (1) + NaKTartrate (2) + Water (3)}						
1	Top	4.4691	−0.62	$2.14 \cdot 10^{-5}$	1.08840	6.23
	Bottom	5.4936		$1.01 \cdot 10^{-6}$	1.15408	6.60
2	Top	4.9191	−0.54	$1.95 \cdot 10^{-5}$	1.07267	6.43
	Bottom	5.0616		$7.41 \cdot 10^{-5}$	1.15707	6.71
3	Top	5.3141	−0.76	$1.84 \cdot 10^{-5}$	1.06839	6.66
	Bottom	4.6596		$5.50 \cdot 10^{-7}$	1.15888	6.82
4	Top	5.5428	−0.64	$1.73 \cdot 10^{-5}$	1.06146	6.76
	Bottom	4.4430		$4.68 \cdot 10^{-7}$	1.16755	6.93
5	Top	5.8594	−0.72	$1.64 \cdot 10^{-5}$	1.05784	6.93
	Bottom	4.1162		$4.00 \cdot 10^{-7}$	1.17314	7.08

Table E.5 - Calculated solute losses (L_s), extraction efficiency (*E*) intervals, partition coefficients (*K*) and literature-based tie-line lengths (TLL) for the extraction of gallic acid, ferulic acid and resveratrol in the ATPS {ethyl lactate (1) + trisodium citrate (2) + water (3)} at 298.15 K and 0.1 MPa.

TL	L_s / %	E / %	K	TLL / m%
Gallic acid in {EL (1) + Na_3Citrate (2) + Water (3)}				
1	-1.47	48.62 ± 0.07	1.39 ± 0.05	37.85
2	-1.32	53.64 ± 0.08	1.69 ± 0.06	48.18
3	-1.05	64.16 ± 0.09	1.83 ± 0.07	55.17
4	-1.28	68.49 ± 0.1	2.17 ± 0.09	61.17
5	-1.06	65.44 ± 0.1	2.4 ± 0.2	65.44
6	-1.62	69.68 ± 0.2	2.6 ± 0.2	69.68
Ferulic acid in {EL (1) + Na_3Citrate (2) + Water (3)}				
1	-1.79	53.0 ± 0.3	1.70 ± 0.08	37.85
2	-2.50	67.4 ± 0.3	2.9 ± 0.2	48.18
3	-2.98	79.7 ± 0.4	4.6 ± 0.5	55.17
4	-2.09	86.5 ± 0.4	6.9 ± 0.9	61.17
5	-1.77	90.8 ± 0.4	10 ± 2	65.44
6	-2.63	92.7 ± 0.4	15 ± 5	69.68
Resveratrol in {EL (1) + Na_3Citrate (2) + Water (3)}				
1	-4.07	88.2 ± 0.9	18 ± 4	37.85
2	-3.44	90.4 ± 0.9	18 ± 4	48.18
3	-2.96	91.6 ± 0.9	18 ± 4	55.17
4	-2.56	93 ± 1	19 ± 5	61.17
5	-3.16	93 ± 1	19 ± 5	65.44
6	-3.79	92 ± 1	19 ± 5	69.68

Table E.6 - Calculated solute losses (L_s), extraction efficiency (*E*) intervals, partition coefficients (*K*) and literature-based tie-line lengths (TLL) for the extraction of gallic acid, ferulic acid and resveratrol in the ATPS {ethyl lactate (1) + tripotassium citrate (2) + water (3)} at 298.15 K and 0.1 MPa.

TL	L_s / %	E / %	K	TLL / m%
Gallic acid in {EL (1) + K_3Citrate (2) + Water (3)}				
1	-1.15	62.10 ± 0.09	1.56 ± 0.06	45.91
2	-1.21	65.57 ± 0.09	1.73 ± 0.07	54.02
3	-1.16	69.1 ± 0.1	1.84 ± 0.08	62.96
4	-0.90	70.8 ± 0.1	1.84 ± 0.08	68.28
5	-1.15	72.7 ± 0.1	1.94 ± 0.08	73.92
6	-1.10	73.6 ± 0.1	1.97 ± 0.09	77.66
Ferulic acid in {EL (1) + K_3Citrate (2) + Water (3)}				
1	-1.43	71.4 ± 0.3	2.6 ± 0.2	45.91
2	-1.71	83.2 ± 0.4	5.0 ± 0.5	54.02
3	-1.38	90.1 ± 0.4	8 ± 2	62.96
4	-1.21	93.0 ± 0.4	12 ± 3	68.28
5	-1.77	95.0 ± 0.4	20 ± 8	73.92
6	-0.94	96.7 ± 0.4	$(3 \pm 2) \cdot 10^1$	45.91
Resveratrol in {EL (1) + K_3Citrate (2) + Water (3)}				
1	-2.84	94 ± 1	36 ± 4	45.91
2	-4.48	93 ± 1	37 ± 5	54.02
3	-3.66	94 ± 1	38 ± 5	62.96
4	-3.83	94 ± 1	39 ± 6	68.28
5	-3.06	95 ± 1	40 ± 6	73.92
6	-031	98 ± 1	40 ± 6	45.91

Table E.7 - Calculated solute losses (L_s), extraction efficiency (*E*) intervals, partition coefficients (*K*) and literature-based tie-line lengths (TLL) for the extraction of gallic acid, ferulic acid and resveratrol in the ATPS {ethyl lactate (1) + disodium succinate (2) + water (3)} at 298.15 K and 0.1 MPa.

TL	L_s / %	E / %	K	TLL / m%
Gallic acid in {EL (1) + Na_2Succinate (2) + Water (3)}				
1	-3.62	3.182 ± 0.004	0.09 ± 0.02	43.10
2	-2.33	2.179 ± 0.003	0.05 ± 0.02	56.40
3	-3.52	1.352 ± 0.002	0.03 ± 0.02	66.20
Ferulic acid in {EL (1) + Na_2Succinate (2) + Water (3)}				
1	-1.44	57.2 ± 0.3	4.2 ± 0.3	43.10
2	-3.52	64.0 ± 0.3	4.9 ± 0.4	56.40
3	-3.38	71.7 ± 0.3	5.3 ± 0.5	66.20
Resveratrol in {EL (1) + Na_2Succinate (2) + Water (3)}				
1	-3.47	77.5 ± 0.5	12 ± 2	43.10
2	-3.89	82.56 ± 0.01	15 ± 2	56.40
3	-2.32	89.90 ± 0.01	20 ± 5	66.20

Table E.8 - Calculated solute losses (L_s), extraction efficiency (*E*) intervals, partition coefficients (*K*) and literature-based tie-line lengths (TLL) for the extraction of gallic acid, ferulic acid and resveratrol in the ATPS {ethyl lactate (1) + sodium potassium tartrate (2) + water (3)} at 298.15 K and 0.1 MPa.

TL	$L_s/\%$	$E/\%$	K	TL
Gallic acid in {EL (1) + NaKTartrate (2) + Water (3)}				
1	-3.81	41.74 ± 0.06	0.91 ± 0.03	43.10
2	-3.41	48.50 ± 0.07	1.00 ± 0.04	52.13
3	-2.92	55.88 ± 0.08	1.11 ± 0.04	60.15
4	-2.72	60.14 ± 0.08	1.18 ± 0.04	64.59
5	-1.09	65.06 ± 0.09	1.25 ± 0.05	70.73
Ferulic acid in {EL (1) + NaKTartrate (2) + Water (3)}				
1	-1.94	66.5 ± 0.3	2.2 ± 0.2	43.10
2	-1.08	75.7 ± 0.3	2.9 ± 0.2	52.13
3	-2.34	84.5 ± 0.4	5.3 ± 0.6	60.15
4	-2.03	89.0 ± 0.4	7 ± 2	64.59
5	-1.83	93.3 ± 0.4	12 ± 3	70.73
Resveratrol in {EL (1) + NaKTartrate (2) + Water (3)}				
1	-3.39	91.6 ± 0.6	21 ± 2	43.10
2	-3.27	93.4 ± 0.6	27 ± 3	52.13
3	-2.39	95.3 ± 0.6	33 ± 4	60.15
4	-3.42	94.7 ± 0.6	37 ± 7	64.59
5	-3.52	95.0 ± 0.6	41 ± 9	70.73

Appendix F. Thermodynamic modeling

In this appendix, the calculated parameters necessary for the execution of the MatLab code are shown, as well as the data calculated through the electrolyte non-random two-liquid (e-NRTL) model.

Table F.1 – Calculated values of radii for the ions presented in the systems.

	Na^+	K^+	$Citrate^{3-}$	$Succinate^{2-}$	$Tartrate^{2-}$
Calculated radii (r)	1.945	3.458	5.104	3.353	4.413

Table F.2 – Calculated values of van der Waals radii for ions presented in the systems using the Bondi method[85].

	$Citrate^{3-}$	$Succinate^{2-}$	$Tartrate^{2-}$
van der Waals radius (r_w) / cm	$1.29 \cdot 10^{-28}$	$8.45 \cdot 10^{-29}$	$1.11 \cdot 10^{-28}$
van der Waals volume (V_w) / $cm^3 \cdot mol^{-1}$	$3.13 \cdot 10^{-10}$	$2.72 \cdot 10^{-10}$	$2.98 \cdot 10^{-10}$

Table F.3 - Values of non-randomness parameter, standard deviation and optimized τ_{ij} values obtained for the ATPS {EL (1) + $Na_3Citrate$ (2) + H_2O (3)}.

Non-randomness parameter		**Standard deviation**		
0.2		$1.57 \cdot 10^{-3}$		
Calculated τ_{ij}				
i/j	**1**	**2**	**3**	**4**
1	0	-11.81	-18.30	1.24
2	7.51	0	-3.37	1.05
3	-16.04	5.18	0	0.39
4	-4.53	7.39	8.59	0

Table F.4 - Initial values of each component in each phase in molar fraction of the ATPS {EL (1) + Na_3Citrate (2) + H_2O (3)}.

Top phase				Bottom phase			
x_1	x_2	x_3	x_4	x_1	x_2	x_3	x_4
0.1460	0.0116	0.0039	0.8385	0.0325	0.0438	0.0146	0.9091
0.1760	0.0084	0.0028	0.8128	0.0246	0.0508	0.0169	0.9076
0.2001	0.0063	0.0021	0.7915	0.0195	0.0565	0.0188	0.9052
0.2244	0.0047	0.0016	0.7683	0.0157	0.0628	0.0209	0.9006
0.2452	0.0035	0.0012	0.7502	0.0136	0.0677	0.0226	0.8962
0.2658	0.0026	0.0009	0.7307	0.0110	0.0732	0.0244	0.8914

Table F.5 - Calculated values of the ionic strength, Debye-Hückel parameter and the closest approach parameter for the ATPS {EL (1) + Na_3Citrate (2) + H_2O (3)}.

Top phase			Bottom phase		
I_x	$A_{DH,x}$	ρ	I_x	$A_{DH,x}$	ρ
0.0233	0.2463	0.2273	0.0960	0.7377	0.8787
0.0168	0.2075	0.1902	0.1039	0.7902	1.0066
0.0125	0.1841	0.1682	0.1128	0.8262	1.1423
0.0095	0.1651	0.1506	0.1252	0.8310	1.2711
0.0070	0.1518	0.1382	0.1349	0.8174	1.3496
0.0052	0.1404	0.1277	0.1456	0.8001	1.4681

Table F.6 - Calculated values of each component in each phase in molar fraction of the ATPS {EL (1) + Na_3Citrate (2) + H_2O (3)}.

Top phase				Bottom phase			
x_1	x_2	x_3	x_4	x_1	x_2	x_3	x_4
0.1459	0.0116	0.0039	0.8386	0.0292	0.0491	0.0159	0.9058
0.1760	0.0084	0.0028	0.8128	0.0239	0.0528	0.0172	0.9060
0.2001	0.0063	0.0021	0.7915	0.0195	0.0565	0.0188	0.9053
0.2244	0.0047	0.0016	0.7693	0.0157	0.0627	0.0209	0.9007
0.2452	0.0035	0.0012	0.7502	0.0136	0.0676	0.0225	0.8964
0.2658	0.0026	0.0009	0.7307	0.0110	0.0730	0.0243	0.8917

Table F.7 - Values of non-randomness parameter, standard deviation and optimized τ_{ij} values obtained for the ATPS {EL (1) + K_3Citrate (2) + H_2O (3)}.

Non-randomness parameter			Standard deviation	
0.3			$1.06 \cdot 10^{-3}$	
Calculated τ_{ij}				
i/j	**1**	**2**	**3**	**4**
1	0	-4.85	-19.41	-6.32
2	12.84	0	1.54	-6.36
3	-14.38	-12.22	0	-6.25
4	8.78	3.05	13.06	0

Table F.8 - Initial values of each component in each phase in molar fraction of the ATPS {EL (1) + K_3Citrate (2) + H_2O (3)}.

Top phase				Bottom phase			
x_1	x_2	x_3	x_4	x_1	x_2	x_3	x_4
0.1842	0.0144	0.0048	0.7967	0.0319	0.0499	0.0166	0.9016
0.2086	0.0133	0.0044	0.7736	0.0242	0.0565	0.0188	0.9005
0.2491	0.0090	0.0030	0.7389	0.0191	0.0627	0.0209	0.8972
0.2745	0.0072	0.0024	0.7158	0.0159	0.0690	0.0230	0.8921
0.3052	0.0053	0.0018	0.6878	0.0129	0.0768	0.0256	0.8847
0.3297	0.0045	0.0015	0.6643	0.0113	0.0831	0.0277	0.8779

Table F.9 - Calculated values of the ionic strength, Debye-Hückel parameter and the closest approach parameter for the ATPS {EL (1) + K_3Citrate (2) + H_2O (3)}.

Top phase			Bottom phase		
I_x	$A_{\mathrm{DH},x}$	ρ	I_x	$A_{\mathrm{DH},x}$	ρ
0.0287	0.1946	0.1954	0.1052	0.6430	0.8289
0.0266	0.1729	0.1731	0.1198	0.7067	1.0147
0.0180	0.1471	0.1465	0.1320	0.7426	1.1894
0.0144	0.1343	0.1334	0.1430	0.7454	1.3083
0.0106	0.1215	0.1205	0.1557	0.7306	1.4223
0.0091	0.1127	0.1117	0.1665	0.7034	1.4701

Table F.10 - Calculated values of each component in each phase in molar fraction of the ATPS {EL (1) + K_3Citrate (2) + H_2O (3)}.

Top phase				Bottom phase			
x_1	x_2	x_3	x_4	x_1	x_2	x_3	x_4
0.1842	0.0144	0.0048	0.7967	0.0338	0.0496	0.0179	0.8987
0.2086	0.0133	0.0044	0.7736	0.0249	0.0561	0.0204	0.8986
0.2481	0.0090	0.0030	0.7389	0.0190	0.0626	0.0224	0.8961
0.2745	0.0072	0.0024	0.7158	0.0156	0.0691	0.0241	0.8912
0.3052	0.0053	0.0018	0.6878	0.0127	0.0771	0.0260	0.8842
0.3297	0.0045	0.0015	0.6643	0.0112	0.0836	0.0277	0.8776

Table F.11 - Values of non-randomness parameter, standard deviation and optimized τ_{ij} values obtained for the ATPS {EL (1) + Na_2Succinate (2) + H_2O (3)}.

Non-randomness parameter			Standard deviation	
0.3			$9.46 \cdot 10^{-17}$	
Calculated τ_{ij}				
i/j	**1**	**2**	**3**	**4**
1	0	18.68	-18.49	17.7
2	-16.80	0	-11.76	16.57
3	18.46	-18.46	0	-18.78
4	-18.97	-18.46	17.61	0

Table F.12 - Initial values of each component in each phase in molar fraction of the ATPS {EL (1) + Na_2Succinate (2) + H_2O (3)}.

Top phase				Bottom phase			
x_1	x_2	x_3	x_4	x_1	x_2	x_3	x_4
0.3778	0.3325	0.1663	0.1234	0.0723	0.3626	0.1813	0.3838
0.4749	0.2927	0.1463	0.0861	0.0526	0.2557	0.1779	0.4138
0.5453	0.2582	0.1291	0.0674	0.0366	0.2468	0.1734	0.4433

Table F.13 - Calculated values of the ionic strength, Debye-Hückel parameter and the closest approach parameter for the ATPS {EL (1) + Na_2Succinate (2) + H_2O (3)}.

Top phase			Bottom phase		
I_x	$A_{DH,x}$	ρ	I_x	$A_{DH,x}$	ρ
0.4988	0.0331	0.0329	0.5439	0.0553	0.0983
0.4290	0.0329	0.0327	0.5336	0.0597	0.1190
0.3873	0.0334	0.0320	0.5201	0.0643	0.1453

Table F.14 - Calculated values of each component in each phase in molar fraction of the ATPS {EL (1) + Na_2Succinate (2) + H_2O (3)}.

Top phase				Bottom phase			
x_1	x_2	x_3	x_4	x_1	x_2	x_3	x_4
0.3778	0.3325	0.1663	0.1234	0.0723	0.3626	0.1813	0.3838
0.4749	0.2927	0.1463	0.0861	0.0526	0.3557	0.1779	0.4138
0.5453	0.2582	0.1291	0.0674	0.0366	0.3468	0.1734	0.4433

Table F.15 - Values of non-randomness parameter, standard deviation and optimized τ_{ij} values obtained for the ATPS {EL (1) + NaKTartrate (2) + H_2O (3)}.

Non-randomness parameter			Standard deviation		
0.3			$9.46 \cdot 10^{-17}$		
Calculated τ_{ij}					
i/j	**1**	**2**	**3**	**4**	**5**
1	0	-7.31	-7.25	-6.90	19.38
2	-9.93	0	-8.26	-6.45	-13.68
3	-11.13	-7.97	0	-6.23	-13.64
4	-11.28	-10.83	-11.06	0	-13.13
5	10.41	3.87	3.79	8.96	0

Table F.16 - Initial values of each component in each phase in molar fraction of the ATPS {EL (1) + NaKTartrate (2) + H_2O (3)}.

Top phase					Bottom phase				
x_1	x_2	x_3	x_4	x_5	x_1	x_2	x_3	x_4	x_5
0.1600	0.0070	0.0070	0.0070	0.8191	0.0284	0.0231	0.0231	0.0231	0.9022
0.1887	0.0055	0.0055	0.0055	0.7947	0.0223	0.0264	0.0264	0.0264	0.8986
0.2193	0.0044	0.0044	0.0044	0.7674	0.0169	0.0292	0.0292	0.0292	0.8954
0.2381	0.0040	0.0040	0.0040	0.7499	0.0143	0.0320	0.0320	0.0320	0.8897
0.2704	0.0034	0.0034	0.0034	0.7192	0.0113	0.0356	0.0356	0.0356	0.8818

Table F.17 - Calculated values of the ionic strength, Debye-Hückel parameter and the closest approach parameter for the ATPS {EL (1) + NaKTartrate (2) + H_2O (3)}.

Top phase				Bottom phase			
I_x	$A_{\mathrm{DH},x}$	ρ_1	ρ_2	I_x	$A_{\mathrm{DH},x}$	ρ_1	ρ_2
0.0209	0.2194	0.8742	0.9540	0.0693	0.6259	1.3296	1.4510
0.0166	0.1897	0.8119	0.8861	0.0791	0.6349	1.3997	1.5276
0.0132	0.1654	0.7575	0.8267	0.0877	0.6366	1.4808	1.6161
0.0120	0.1531	0.7285	0.7951	0.0960	0.6087	1.5070	1.6447
0.0103	0.1356	0.6855	0.7482	0.1069	0.5665	1.5354	1.6757

Table F.18 - Calculated values of each component in each phase in molar fraction of the ATPS {EL (1) + NaKTartrate (2) + H_2O (3)}.

Top phase					Bottom phase				
x_1	x_2	x_3	x_4	x_5	x_1	x_2	x_3	x_4	x_5
0.2704	0.0034	0.0034	0.0034	0.7192	0.0113	0.0356	0.0356	0.0356	0.8818
0.2381	0.0040	0.0040	0.0040	0.7499	0.0143	0.0320	0.0320	0.0320	0.8897
0.2193	0.0044	0.0044	0.0044	0.7674	0.0169	0.0292	0.0292	0.0292	0.8954
0.1887	0.0055	0.0055	0.0055	0.7947	0.0223	0.0264	0.0264	0.0264	0.8986
0.1600	0.0070	0.0070	0.0070	0.8191	0.0284	0.0231	0.0231	0.0231	0.9022

References

(1) Robinson, K.; Mock, C.; Liang, D. Pre-formulation studies of resveratrol. *Drug Dev Ind Pharm* **2015**, 41, 1464-1469. DOI: www.doi.org/10.3109/03639045.2014.958753.

(2) Yang, S.-C.; Tseng, C.-H.; Wang, P.-W.; Lu, P.-L.; Weng, Y.-H.; Yen, F.-L.; Fang, J.-Y. Pterostilbene, a Methoxylated Resveratrol Derivative, Efficiently Eradicates Planktonic, Biofilm, and Intracellular MRSA by Topical Application. *Front Microbiol* **2017**, 8, 1103. DOI: www.doi.org/10.3389/fmicb.2017.01103.

(3) Mota, F.L.; Queimada, A.J.; Pinho, S.P.; Macedo, E.A. Aqueous Solubility of Some Natural Phenolic Compounds. Ind. Eng. Chem. Res. **2008**, 47, 5182-5189. DOI: www.doi.org/10.1021/ie071452o.

(4) Locatelli, C.; Rosso, R.; Santos-Silva, M.C.; Souza, C.; Licínio, M.; Leal, P.; Bazzo, M.L.; Yunes, R.; Creczynski-Pasa, t. Ester derivatives of gallic acid with potential toxicity toward L1210 leukemia cells. *Bioorg. Med. Chem.* **2008**, 16, 3791-3799. DOI: www.doi.org/10.1016/j.bmc.2008.01.049.

(5) Delfanian, M.; Sahari, M.A.; Barzegar, M.; Ahmadi Gavlighi, H. Structure–antioxidant activity relationships of gallic acid and phloroglucinol. *J. Food Meas. Charact.* **2021**, 15, 5036-5046. DOI: www.doi.org/10.1007/s11694-021-01045-y.

(6) Raj, N.D.; Singh, D. A critical appraisal on ferulic acid: Biological profile, biopharmaceutical challenges and nano formulations. *Health Sci. J.* **2022**, 5, 100063. DOI: www.doi.org/10.1016/j.hsr.2022.100063.

(7) Jirgensons, B. Solubility and fractionation of polyvinylpyrrolidone. *J. Polym. Sci.* **1952**, 8, 519-527. DOI: www.doi.org/10.1002/pol.1952.120080508.

(8) Dolzhenko, A.V. Ethyl lactate and its aqueous solutions as sustainable media for organic synthesis. *Sustainable Chem. Pharm.* **2020**, 18, 100322. DOI: www.doi.org/10.1016/j.scp.2020.100322.

(9) Feuer, H. Solubilities of Inorganic and Organic Compounds: A Compilation of Solubility Data from the Periodical Literature. *Science* **1954**, 119, 902-902. DOI: www.doi.org/10.1126/science.119.3104.902.b.

(10) Chang, H. When water does not boil at the boiling point. *Endeavour* **2007**, 31, 7-11. DOI: www.doi.org/10.1016/j.endeavour.2007.01.005.

(11) Lemmon, E.W.; McLinden, M.O.F., D. G. Thermophysical properties of fluids systems. CRC, CRC, CO: **1998**.

(12) Velho, P.; Marques, L.; Macedo, E.A. Extraction of Polyphenols and Vitamins Using Biodegradable ATPS Based on Ethyl Lactate. *Molecules* **2022**, 27, 7838. DOI: www.doi.org/10.3390/molecules27227838.

(13) Requejo, P.F.; Velho, P.; Gómez, E.; Macedo, E.A. Study of Liquid–Liquid Equilibrium of Aqueous Two-Phase Systems Based on Ethyl Lactate and Partitioning of Rutin and Quercetin. *Ind. Eng. Chem. Res.* **2020**, 59, 21196-21204. DOI: www.doi.org/10.1021/acs.iecr.0c02664.

(14) Kamalanathan, I.; Petrovski, Z.; Branco, L.C.; Najdanovic-Visak, V. Novel aqueous biphasic system based on ethyl lactate for sustainable separations: Phase splitting mechanism. *J. Mol. Liq.* **2018**, 262, 37-45. DOI: www.doi.org/10.1016/j.molliq.2018.03.119.

(15) Aparicio, S.; Alcalde, R. The green solvent ethyl lactate: an experimental and theoretical characterization. *Green Chem.* **2009**, 11, 65-78. DOI: www.doi.org/10.1039/B811909K.

(16) Maryott, A.A.; Smith, E.R. Table of Dielectric Constants of Pure Liquids; **1951**.

(17) Mantina, M.; Chamberlin, A.C.; Valero, R.; Cramer, C.J.; Truhlar, D.G. Consistent van der Waals Radii for the Whole Main Group. *J. Phys. Chem. A* **2009**, 113, 5806-5812. DOI: www.doi.org/10.1021/jp8111556.